NASA TECHNICAL MEMORANDUM

NASA TM X-2529

NASA TM X-2529

EXPLORATORY INVESTIGATION OF LIFT INDUCED ON A SWEPT WING BY A TWO-DIMENSIONAL PARTIAL-SPAN DEFLECTED JET AT MACH NUMBERS FROM 0.20 TO 1.30

by Francis J. Capone

Langley Research Center
Hampton, Va. 23365

NATIONAL AERONAUTICS AND SPACE ADMINISTRATION • WASHINGTON, D. C. • APRIL 1972

1. Report No.	2. Government Accession No.	3. Recipient's Catalog No.
NASA TM X-2529		

4. Title and Subtitle	5. Report Date
EXPLORATORY INVESTIGATION OF LIFT INDUCED ON A SWEPT WING BY A TWO-DIMENSIONAL PARTIAL-SPAN DEFLECTED JET AT MACH NUMBERS FROM 0.20 TO 1.30	April 1972
	6. Performing Organization Code
7. Author(s)	8. Performing Organization Report No.
Francis J. Capone	L-8177
	10. Work Unit No.
9. Performing Organization Name and Address	764-74-02-01
NASA Langley Research Center Hampton, Va. 23365	11. Contract or Grant No.
	13. Type of Report and Period Covered
12. Sponsoring Agency Name and Address	Technical Memorandum
National Aeronautics and Space Administration Washington, D.C. 20546	14. Sponsoring Agency Code

15. Supplementary Notes

16. Abstract

An exploratory investigation has been conducted in the Langley 16-foot transonic tunnel at Mach numbers from 0.20 to 1.30 to determine the induced lift characteristics of a body and swept-wing configuration having a partial-span two-dimensional propulsive nozzle with exhaust exit in the notch of the swept-wing trailing edge. The Reynolds number per meter varied from 4.90×10^6 to 14.03×10^6. The effects on wing-body characteristics of deflecting the propulsive jet in the flap mode at nominal exhaust-nozzle deflection angles of 0^o and 30^o have been studied for two nozzle designs with different geometry and wing spans.

17. Key Words (Suggested by Author(s))	18. Distribution Statement
Jet flap Induced lift Subsonic Transonic	Unclassified – Unlimited

19. Security Classif. (of this report)	20. Security Classif. (of this page)	21. No. of Pages	22. Price*
Unclassified	Unclassified	78	$3.00

*For sale by the National Technical Information Service, Springfield, Virginia 22151

EXPLORATORY INVESTIGATION OF LIFT INDUCED ON A SWEPT WING BY A TWO-DIMENSIONAL PARTIAL-SPAN DEFLECTED JET AT MACH NUMBERS FROM 0.20 TO 1.30

By Francis J. Capone
Langley Research Center

SUMMARY

An exploratory investigation has been conducted in the Langley 16-foot transonic tunnel at Mach numbers from 0.20 to 1.30 to determine the induced lift characteristics of a body and swept-wing configuration having a partial-span two-dimensional propulsive nozzle with exhaust exit in the notch of the swept-wing trailing edge. The Reynolds number per meter varied from 4.90×10^6 to 14.03×10^6. The effects on wing-body characteristics of deflecting the propulsive jet in the flap mode at nominal exhaust-nozzle deflection angles of 0^o and 30^o have been studied for two nozzle designs with different geometry and wing spans. Experimental results for one of the models tested over a range of jet deflection angles are reported in NASA TM X-2309.

Results indicated that deflecting the jet induced a flow field which resulted in an increase in lift by an amount up to three times the magnitude of the lift component of the exhaust-nozzle gross thrust. At subsonic speeds, the body-alone configuration developed about one-half as much induced lift as developed on the wing and body combined.

INTRODUCTION

The design of high-speed V/STOL aircraft is usually complicated by such constraints as excessive weight, requirement for special lift engines, complexity of mechanical or gas ducting systems, and severe trim changes related to the lift augmentation. For example, requirement for special lift engines can be accompanied by an increase in frontal area and decrease in fineness ratio which usually results in an increase in drag at transonic and supersonic speeds.

In an attempt to alleviate some of the deficiencies associated with high-speed V/STOL aircraft, a research program has been initiated to develop a high-speed aircraft configuration having STOL properties and a highly sweptback wing with a jet flap located in the wing trailing-edge notch. The span of the jet flap would be much less than the wing span. This configuration would be powered with centrally located turbojet or

turbofan engines. The deflected jet would serve two purposes: (1) to obtain an increase in lift at cruise conditions due to the induced flow field associated with the deflected jet with possibly no increase in cruise drag and (2) to function as a transonic maneuver device to produce high lift. The experimental results presented herein were obtained in an exploratory investigation of the foregoing concept which was conducted as much as possible with existing hardware. Consequently, the model configuration was not intended to represent a practical aircraft configuration.

This investigation was conducted in two phases in the Langley 16-foot transonic tunnel over a Mach number range from 0.20 to 1.30 and over a range of Reynolds number per meter from 4.90×10^6 to 14.03×10^6. During the first phase, two nozzle designs with different geometry and wing spans were tested with jet deflection angles of 0^o and 30^o. The effects of a small range of wing incidence angle were also studied. The purpose of this report is to present the basic data measured during the first phase of this investigation. Subsequent analysis of these data indicated that additional tests to determine the effects of nozzle deflection angle were desirable and would aid in the design of any follow-on configuration. Accordingly, one of the nozzle designs was chosen and the second phase of the investigation was conducted with this nozzle design at several jet deflection angles up to 30^o. The results of the second phase of the investigation are presented in reference 1.

The jet-flap concept is based on the premise that the spanwise dimension of the propulsive exhaust jet is several times greater than the jet thickness and that the exhaust nozzles are articulated so that the exhaust jet may be deflected in the mode of a trailing-edge flap. The foregoing partial-span jet permits the use of all the engine exhaust to simulate the jet flap, avoids ducting through the wing, and limits mechanical articulation to the exhaust nozzles (and possibly to wing leading-edge flaps).

The use of a sweptback wing may have an advantage of improved lift augmentation when the jet is deflected. If the induced flow field of an isolated lifting flap or jet flap is regarded, in a very elementary sense, as similar to that induced by a horseshoe vortex, the net induced velocities within the horseshoe are negative and those outside are positive, that is, in the lift direction. When the deflected jet flap is located in the trailing-edge notch of a swept wing, the net induced velocities tend only to increase the wing lift. Having the outboard panels of the wing swept back places this portion of the wing in a stronger upwash than if the wing were not swept and tends to compensate for the short span of the jet flap.

Analytical studies of the foregoing concept, using the methods of references 2 and 3, indicated that for a plane wing at zero angle of attack, the lift induced on the wing by the deflected jet flap would be about three times the magnitude of the lift component of the nozzle gross thrust.

SYMBOLS

Model forces and moments are referred to a stability-axis system with the model moment reference center located at the intersection of the body center line and the nozzle exit plane for both models investigated.

A_e exhaust-nozzle exit area

A_{gap} model total cross-sectional area at metric break at station 52.07 cm, 182.41 cm^2

$C_{(F-D)}$ resultant-axial-force coefficient, $\frac{F_{AX}}{qS}$

C_L lift coefficient, $\frac{L}{qS}$

$C_{L,\Gamma}$ jet-circulation lift coefficient

$C_{L,s}$ static lift coefficient, $\frac{N}{p_\infty S}$

C_m pitching-moment coefficient, $\frac{\text{Pitching moment}}{qS\bar{c}}$

C_T nozzle gross thrust coefficient, $\frac{F_g}{qS}$

$C_{T,i}$ ideal isentropic gross thrust coefficient, $\frac{F_i}{qS}$

$C_{T,i,s}$ static ideal isentropic gross thrust coefficient, $\frac{F_i}{p_\infty S}$

$C_{T,s}$ static coefficient of resultant axial force, $\frac{F_{AX}}{p_\infty S}$

$\bar{c}$ wing mean geometric chord

D drag in streamwise direction

F thrust component parallel to body longitudinal axis, positive toward nose, $F_g \cos \delta$

$F_{A,bal}$ axial force measured by balance including gap pressure force, positive toward nose

F_{AX} resultant axial force parallel to body axis, positive toward nose

F_g nozzle gross thrust parallel to nozzle axis, ηF_i

F_i ideal isentropic nozzle gross thrust parallel to nozzle axis

$\frac{F - D}{F_i}$ thrust-minus-drag ratio

G gain factor (see eq. (2))

i_w wing angle of incidence, positive for trailing edge deflected down

L lift normal to relative wind and spanwise axis

M Mach number

$\dot{m}$ measured mass-flow rate

N normal force or static lift normal to body longitudinal axis and spanwise axis, positive toward top of airframe

$\bar{p}_{gap}$ average static pressure acting on body metric break

$p_{t,j}$ jet total pressure

p_∞ free-stream or ambient static pressure

q free-stream dynamic pressure

R gas constant (for $\gamma = 1.4$), 287.3 N-m/kg-K

S wing reference area

$T_{t,j}$ jet total temperature

x_{cp} center of pressure, percent $\bar{c}$

α body angle of attack

γ ratio of specific heats, 1.40 for air

δ effective jet deflection angle (see eq. (3))

δ_d design or nominal nozzle deflection angle, angle between body longitudinal axis and nozzle geometric axis in plane of symmetry

η nozzle thrust ratio, $\frac{F_g}{F_i}$

APPARATUS AND PROCEDURE

Exhaust-Nozzle Simulation System

A sketch of the strut-supported jet-engine exhaust-nozzle simulation system used in the present investigation is presented as figure 1. The body consisted of a conical forebody with a 14^o half-angle and a 15.24-centimeter-diameter cylindrical centerbody to which various exhaust nozzles could be attached at station 104.14. The forebody was supported from the tunnel floor by a fixed strut having a 45^o leading-edge sweep and a 5-percent-thick (streamwise) hexagonal airfoil section. The body center line was 91.40 centimeters below the wind-tunnel center line.

A continuous flow of dry, high-pressure air at approximately 300 K was used to simulate the jet exhaust. The air was introduced perpendicularly to the model axis into the section of the model supported by the force balance through eight sonic nozzles equally spaced around a center core to eliminate transfer of axial momentum. Two flexible metal bellows, arranged so that one was ahead and one was behind the respective points of attachment to the fixed portion of the model, sealed the forward portion of the low-pressure air chamber; this arrangement prevented the pressurizing of the bellows from loading the balance. The flow-straightening screens were made of wire cloth (four 0.0635-centimeter-diameter wires per centimeter) supported by a coarse grid of streamlined vanes.

Only that portion of the configuration aft of the metric break at station 52.07 was supported by the force balance and hereinafter is referred to as the wind-tunnel model.

Models

An overall planform view of models 1 and 2 is presented in figure 2. Reference 1 presents the experimental results for model 1. An existing axisymmetric afterbody, attached at station 104.14 and terminated at station 121.92, was modified so that wings and nozzle inserts of varying deflection angles could be attached. Initially a wing planform was chosen so that the quarter-chord of the wing mean geometric chord would be located at the jet exit in order to minimize large changes in pitching moment with opera-

tion of the jet at deflected conditions. However, from structural considerations necessary for attaching the existing wing panels, the requirement to have the wing geometric center at the nozzle exit was relaxed.

Transforming the flow from axisymmetric to two-dimensional and turning the flow were both accomplished internally for the nozzles used with both models. Because of wing-mounting limitations the nozzle exit was fixed at station 127.00 for model 1 and 121.92 for model 2. The nozzles for both models were convergent. For both models, nozzle inserts with deflection angles of 0° and 30° were built.

Model 1.- Photographs of model 1 are shown as figure 3, and details of the wing and nozzle are presented in figures 4 and 5, respectively. The wing used for model 1 had a leading-edge sweep of 66.88°, a trailing-edge sweep of 58.00°, and an NACA 63A008 airfoil section that was parallel to the actual tip chord. This wing had a reference area of 1554.84 centimeters^2, a mean geometric chord of 27.51 centimeters, a span of 61.98 centimeters, and an aspect ratio of 2.47. The wing pivoted about the trailing edge which was fixed at the nacelle center line when wing incidence angle was varied from -2.26° to 0.62°.

Nozzle geometry is shown in figure 5. The nozzle aspect ratio was approximately 3.40. The nozzle exit was fixed at station 127.00. Because of this and the limitations imposed by the wing attachment, this nozzle had an unusually large boattail angle of 36.29°.

Model 2.- An overall planform of model 2 is presented in figure 2. Photographs of this model are shown in figure 6, and details of the wing and nozzles are presented in figures 7 and 8, respectively. Because of the design of the nozzle for this model, the nozzle exit was assumed to be at model station 121.92. The wing for model 2 had a smaller span than that for model 1, and the leading- and trailing-edge sweeps and the airfoil section were the same. The wing for model 2 had a reference area of 1209.02 centimeters^2, a span of 51.82 centimeters, and an aspect ratio of 2.22. Wing incidence angle could be set at -2.04° and -0.18°.

Nozzle geometry is shown in figure 8. The nozzle aspect ratio was 4.00. Two nozzle inserts that attached at station 121.92 with design deflection angles of 0° and 30° were tested. That portion of the nozzle that extended past station 121.92 was hemispherical with a 5.13-centimeter radius.

Wind Tunnel and Instrumentation

This investigation was conducted in the Langley 16-foot transonic tunnel which is a single-return, atmospheric wind tunnel with slotted octagonal test section and continuous air exchange. The wind tunnel has continuously variable airspeed up to a Mach number of 1.30. Test-section plenum suction is used for speeds above a Mach number of 1.10.

From calibrations of the wind tunnel, the test-section-wall divergence is adjusted as a function of airstream dewpoint in order to eliminate any longitudinal static-pressure gradients in the test section that might occur due to condensation of atmospheric moisture.

Aerodynamic forces were measured with an internal three-component strain-gage balance. Internal static pressure at the metric break at station 52.07 was determined by measurement of the pressure at 12 locations in the vicinity of the break by using individual pressure transducers. These pressure measurements were used to adjust the measured balance forces for the force acting across the break station to a free-stream static pressure. Total pressure of the jet flow was measured with two pressure transducers; the total-pressure probes, indicated in figure 1, were located at model stations 95.00 and 96.52 at meridian angles of 340° and 160°, respectively. Total temperatures of the jet flow were measured with two iron-constantan thermocouples with the temperature probes located at model stations 95.76 and 97.28 at meridian angles of 250° and 70°, respectively. A turbine flowmeter was used to obtain air mass-flow rate to the nozzle.

At each test point, approximately 10 frames of data were recorded on magnetic tape over a period of about 5 seconds as Mach number and jet total-pressure ratio were held constant. The average value of these 10 recordings was used for computational purposes.

Tests

This investigation was conducted at Mach numbers from 0 to 1.30. Nozzle deflection angles for both models were 0° and 30°. Model 1 was tested with wings off and at wing incidence angles of -2.26°, -1.38°, and 0.62°. Model 2 was tested with wings off and at wing incidence angles of -2.04° and -0.18°. Reynolds number per meter varied from 4.90×10^6 to 14.03×10^6. Balance load limit on pitching moment limited the maximum obtainable jet pressure ratio for the nozzles with a deflection angle of 30°.

All tests were conducted with 0.25-centimeter-wide boundary-layer transition strips consisting of No. 100 silicon carbide grit sparsely distributed in a thin film of lacquer. These strips were located 2.54 centimeters from the tip of the forebody nose and on both the upper and lower surface of the wings at 10 percent of the local streamwise chord.

DATA ANALYSIS

In the present investigation the body and balance longitudinal axes were at all times coincident and parallel to the free airstream. Body angle of attack was always zero, but wing incidence was varied through a small angle range as has been noted.

The lift measured by the force balance is composed of three parts expressed in coefficient form as follows:

$$C_L = (C_L)_{C_{T=0}} + C_{L,\Gamma} + C_T \sin(\delta + \alpha) \tag{1}$$

and, since $\alpha = 0^o$,

$$C_L = (C_L)_{C_{T=0}} + C_{L,\Gamma} + C_T \sin \delta$$

where $(C_L)_{C_{T=0}}$ is the jet-off lift coefficient of the model, $C_T \sin \delta$ is the component of nozzle gross thrust in the lift direction, and $C_{L,\Gamma}$ is the coefficient of lift on the wing and body induced by the deflected jet, which, following the nomenclature of reference 4, is defined as the jet-circulation lift coefficient.

The gain factor is defined as

$$G = \frac{C_{L,\Gamma} + C_T \sin \delta}{C_T \sin \delta} \tag{2}$$

The numerator of equation (2) is determined by subtracting the jet-off lift coefficient from the total lift coefficient measured with the jet operating. In applying equation (2) in the present investigation, for simplicity C_T in the denominator was replaced by $C_{T,i}$ which makes the values of gain factor presented in the figures conservative by as much as 4 percent at high jet total-pressure ratio (since $C_T = \eta C_{T,i}$).

Because forces were measured with a single balance, the balance reading indicates net force – that is, the sum of forces exerted by the external airstream and jet reaction forces. Therefore, only at static conditions (M = 0), when the external aerodynamic forces are assumed to be zero, can the effective jet deflection angle δ be measured. This angle is defined as

$$\delta = \arctan \frac{N}{F} \tag{3}$$

where N and F are normal and axial forces at static conditions. Figure 9 presents the static data for both models 1 and 2 at jet deflection angles of 0^o and 30^o. In determining the gain factor, it is assumed that the measured effective jet deflection angle δ is a characteristic of the nozzle internal geometry and does not vary with Mach number.

The ideal isentropic gross thrust or exhaust jet momentum is defined as

$$F_i = \dot{m}\sqrt{RT_{t,j}}\sqrt{\left(\frac{2\gamma}{\gamma - 1}\right)\left[1 - \left(\frac{p_\infty}{p_{t,j}}\right)^{\frac{\gamma-1}{\gamma}}\right]} \tag{4}$$

where $\dot{m}$ is the measured mass-flow rate and $p_{t,j}$ is the corrected average jet total pressure. A total-pressure rake was used to survey the jet total-pressure distribution at the exit of the nozzles for both models 1 and 2, and the average jet total-pressure probe readings were corrected to the integrated value of jet total pressure at the exit. This correction to account for flow nonuniformity was approximately 1.2 percent for the nozzles having design deflection angles of 0^o and 30^o. The variation of nozzle ideal isentropic gross thrust coefficient with jet total-pressure ratio for models 1 and 2 is shown in figure 10. The maximum mass-flow rate was about 4.5 kg/sec. Reference 1 presents mass-flow rates and discharge coefficients for model 1.

The coefficient of resultant axial force $C_{(F-D)}$ is obtained by adjusting the measured balance axial force for the gap pressure force as follows:

$$F_{AX} = \left[F_{A,bal} + \left(\bar{p}_{gap} - p_\infty\right)A_{gap}\right]$$

$$F_{AX} = F_g \cos \delta + L \sin \alpha - D \cos \alpha$$

In the present investigation $\alpha = 0^o$ and

$$F_{AX} = \left(F_g \cos \delta - D\right) = (F - D) \tag{5}$$

$$C_{(F-D)} = \frac{F_{AX}}{qS} \tag{6}$$

For static operation, $M = 0$, drag is assumed to be zero, and

$$F_{AX} = F = F_g \cos \delta$$

$$C_{T,s} = \frac{F_{AX}}{p_\infty S}$$

The center of pressure is defined as

$$x_{cp} = \left(x_{cp}\right)' - \frac{C_m}{C_L}$$

where $\left(x_{cp}\right)'$ is the location of the moment reference center.

PRESENTATION OF RESULTS

The results of this investigation are presented in the following figures:

	Figure
Basic aerodynamic characteristics:	
Model 1, wings off	11
Model 1, $i_w = -2.26^o$	12
Model 1, $i_w = -1.38^o$	13
Model 1, $i_w = 0.62^o$	14
Model 2, wings off	15
Model 2, $i_w = -2.04^o$	16
Model 2, $i_w = -0.18^o$	17
Gain factors:	
Model 1	18
Model 2	19
Comparison of thrust-minus-drag ratios for models 1 and 2, wings off	20

The basic data for $M = 0.20$ to 0.98 for model 1, $i_w = -1.38^o$ (fig. 13) and all the gain factors for model 1 (fig. 18) were presented in reference 1.

SUMMARY OF RESULTS

A discussion of the basic aerodynamic characteristics for model 1 at jet deflection angles of 0^o to 30^o (in 5^o increments) at $i_w = -1.38^o$ is given in reference 1. These results are, in general, similar to those for model 2 at $\delta_d = 30^o$ and are briefly summarized herein. There is an increase in total lift as ideal gross thrust coefficient increases for both models at $\delta_d = 30^o$. (See figs. 11 to 17.) Maximum gain factors for both models were approximately 3 to 4 depending upon Mach number and wing incidence angle (figs. 18 and 19). It should be noted that the gain factors are comparable even though the wing for model 2 is smaller. This gain factor indicates that deflecting the jet created an induced flow field which resulted in an increase in lift by an amount up to three times the magnitude of the lift component of the exhaust-nozzle gross thrust. At subsonic speeds, the body-alone configuration for both models developed about one-half as much induced lift as developed on the wing and body combined. (See figs. 18 and 19.)

It is possible that some spanwise spreading of the jet exists, particularly on the lower surface of the wing for model 2, because of the design of the nozzle. It was because of this factor that the additional tests at jet deflection angles reported in reference 1 were conducted with the nozzle of model 1.

There is a positive increase in pitching moment with increasing ideal gross thrust coefficient except at supersonic speeds. (See basic data of figs. 11 to 17.) The negative increase in pitching moment with increasing ideal gross thrust coefficient for $\delta_d = 0^o$ at low Mach numbers (for example, fig. 12(a)) is probably due to the jet deflection angle being negative. (See figs. 9(a) and 9(c) for measured angles.) The nose-up pitching moment is due principally to the induced lift acting forward of the moment reference center since the nozzle thrust vector was designed to act through this moment reference center. There is a rearward shift in center of pressure with increasing ideal gross thrust coefficient at subsonic speeds and a forward shift in center of pressure at supersonic speeds.

Thrust-minus-drag ratios for both models with the wings off are presented in figure 20. Model 1 showed better performance at the higher jet total-pressure ratios.

Langley Research Center,
National Aeronautics and Space Administration,
Hampton, Va., March 7, 1972.

REFERENCES

1. Corson, Blake W., Jr.; Capone, Francis J.; and Putnam, Lawrence E.: Lift Induced on a Swept Wing by a Two-Dimensional Partial-Span Deflected Jet at Mach Numbers From 0.20 to 1.30. NASA TM X-2309, 1971.

2. Korbacher, G. K.; and Sridhar, K.: A Review of the Jet Flap. UTIA Rev. No. 14, Inst. Aerophys., Univ. of Toronto, May 1960.

3. Lamar, John E.: A Modified Multhopp Approach for Predicting Lifting Pressures and Camber Shape for Composite Planforms in Subsonic Flow. NASA TN D-4427, 1968.

4. Lowry, John G.; Riebe, John M.; and Campbell, John P.: The Jet-Augmented Flap. Preprint No. 715, S.M.F. Fund Paper, Inst. Aeronaut. Sci., Jan. 1957.

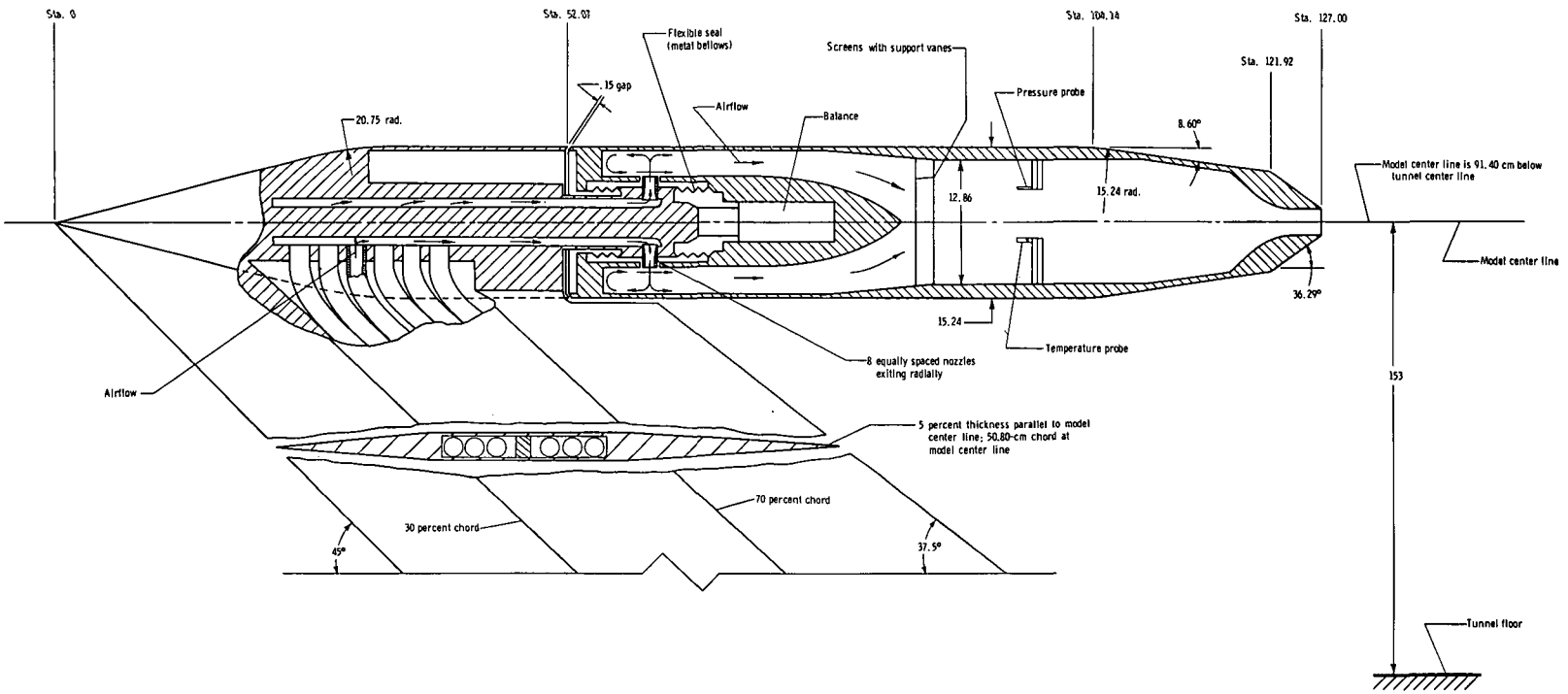

Figure 1.- Simplified sketch of jet-engine exhaust-nozzle simulator with model 1 nozzle, $\delta_d = 0^o$. All dimensions are in centimeters unless otherwise noted.

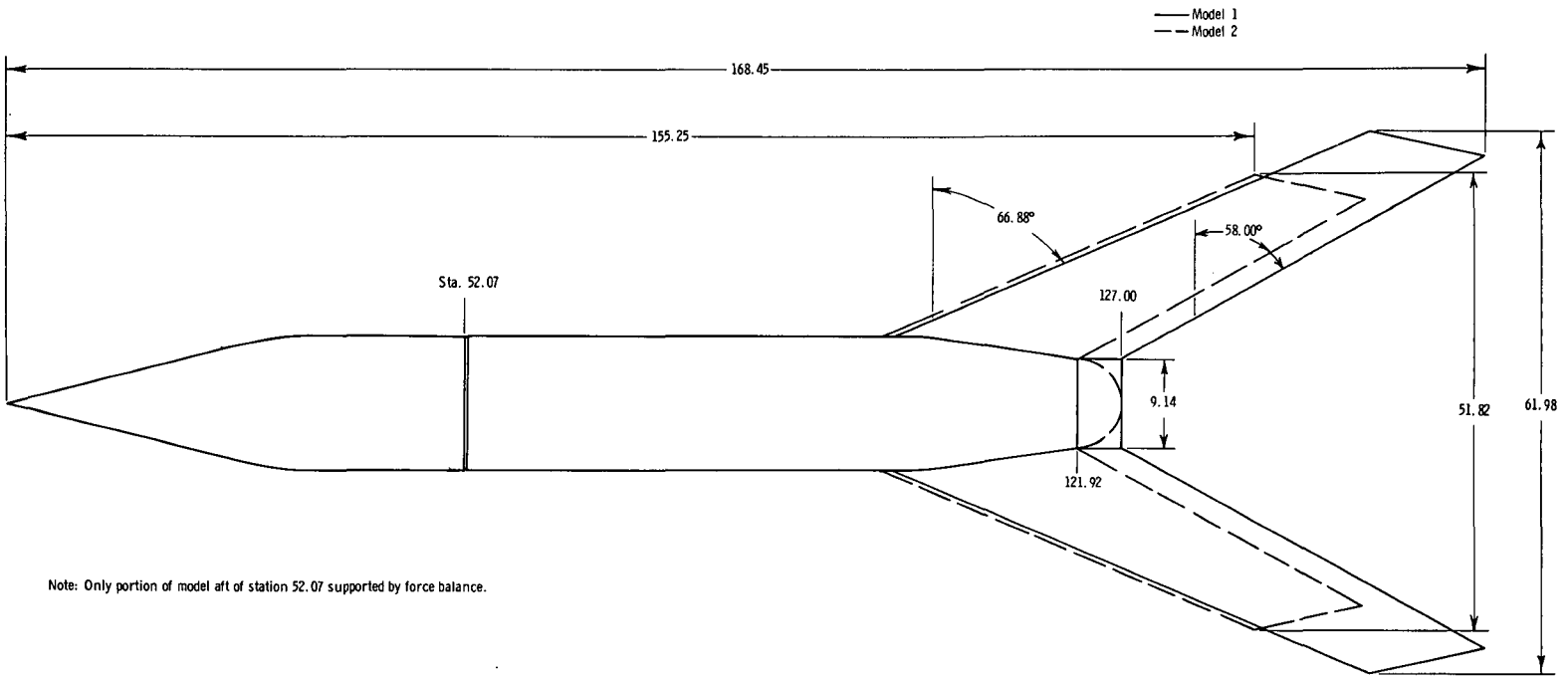

Figure 2.- Overall planform view of models 1 and 2. All dimensions are in centimeters unless otherwise noted.

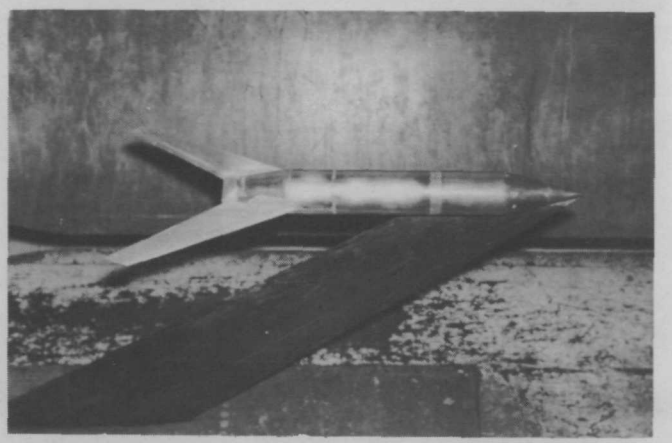

(a) Overall view with $\delta_d = 0^o$.

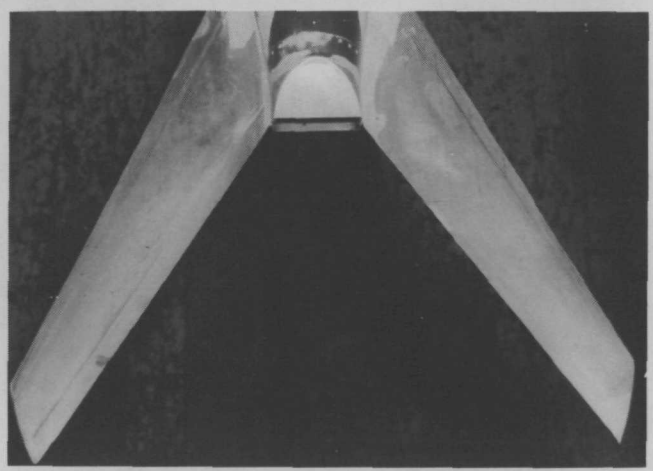

(b) Top view with $\delta_d = 0^o$.

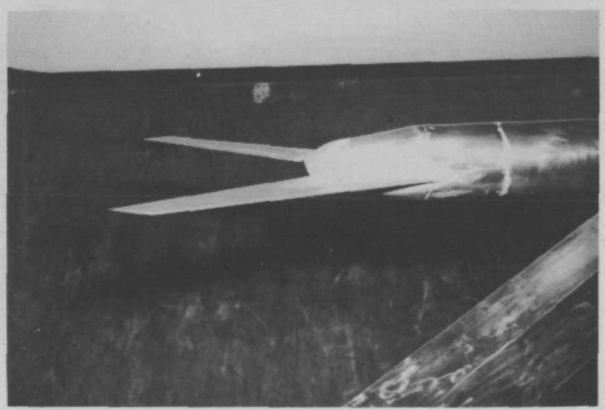

L-71-642

(c) Side view with $\delta_d = 30^o$.

Figure 3.- Photographs of model 1.

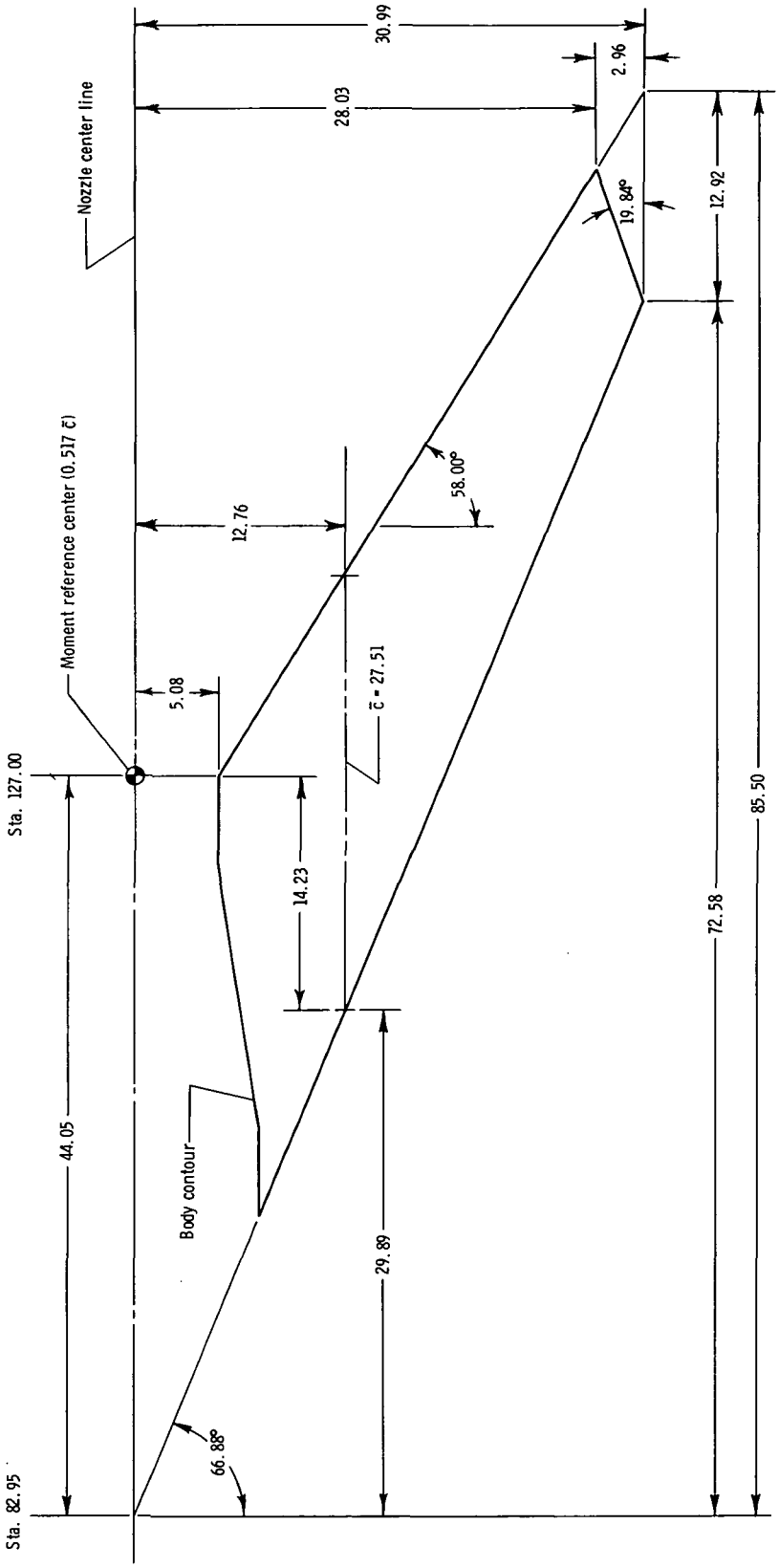

Figure 4.- Wing planform geometry for model 1. All dimensions are in centimeters unless otherwise noted.

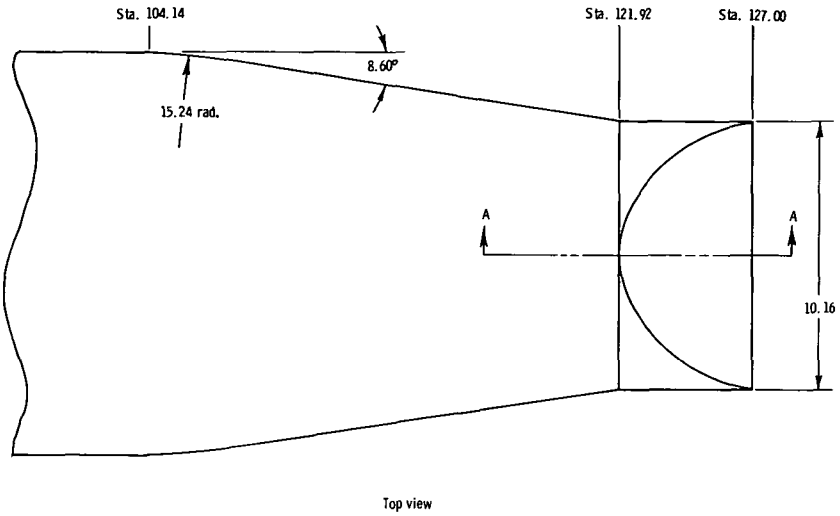

Top view

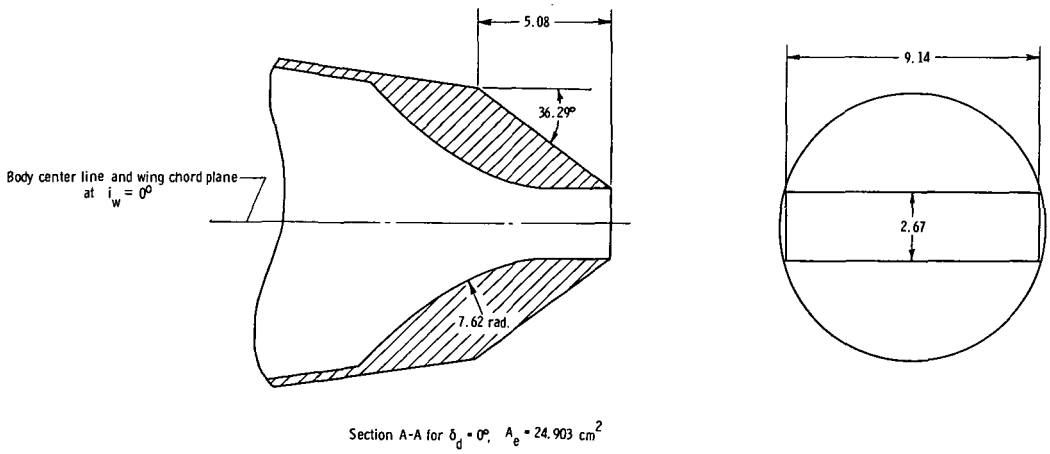

Section A-A for $\delta_d = 0°$, $A_e = 24.903\ cm^2$

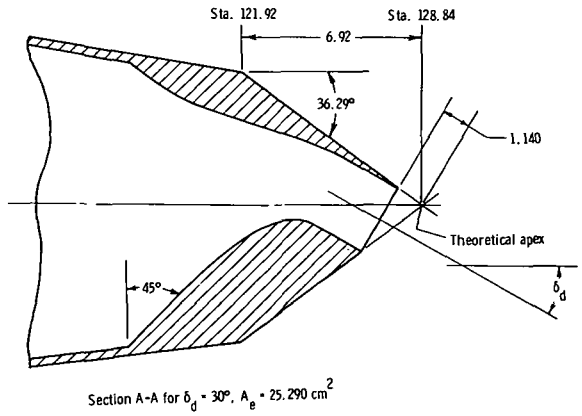

Section A-A for $\delta_d = 30°$, $A_e = 25.290\ cm^2$

Figure 5.- Nozzle geometry for model 1. All dimensions are in centimeters unless otherwise noted.

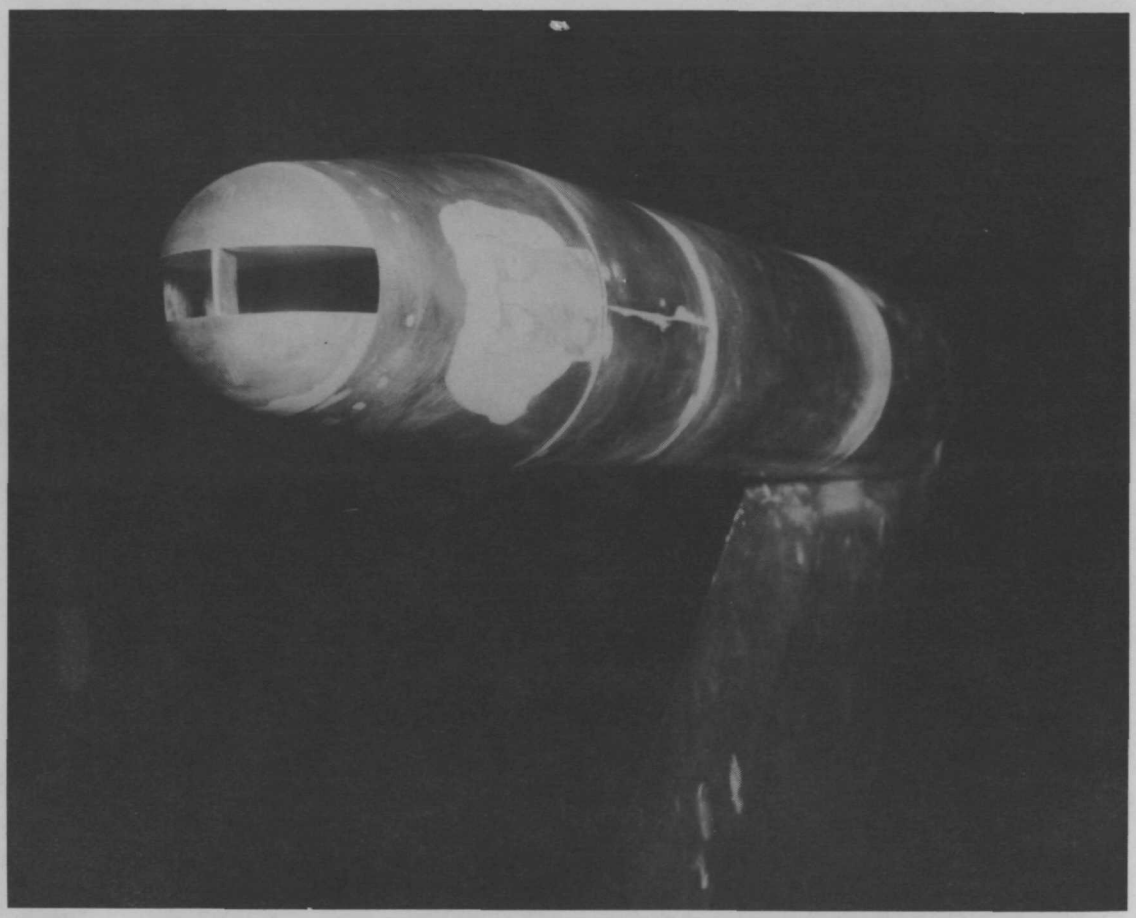

L-69-1932

(a) Rear view, wings off with $\delta_d = 0^o$.

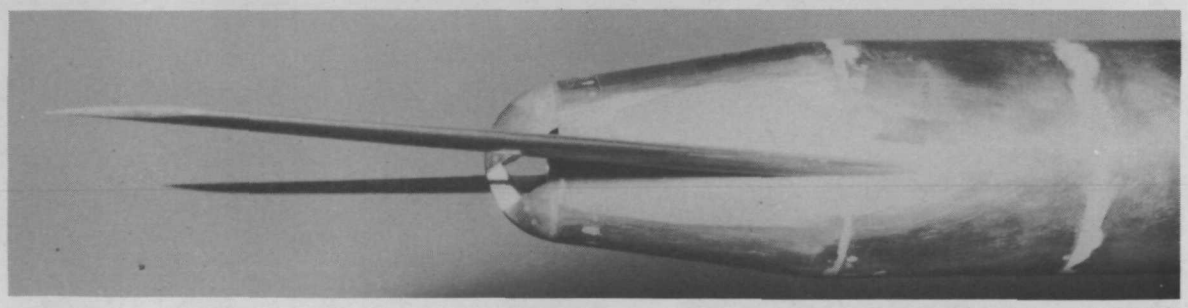

L-69-1953

(b) Side view, wings on with $\delta_d = 30^o$.

Figure 6.- Photographs of model 2.

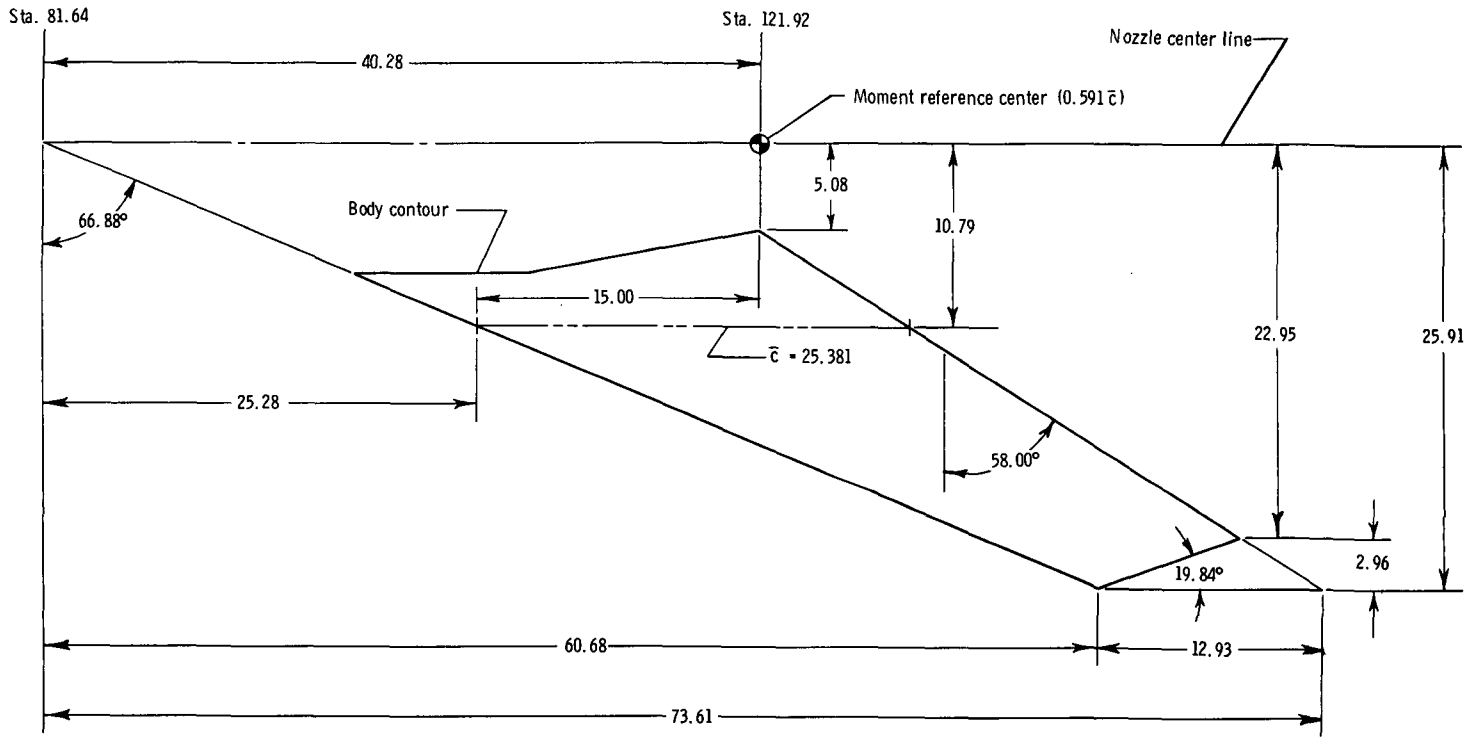

Figure 7.- Wing planform geometry for wing used with model 2. All dimensions are in centimeters unless otherwise noted.

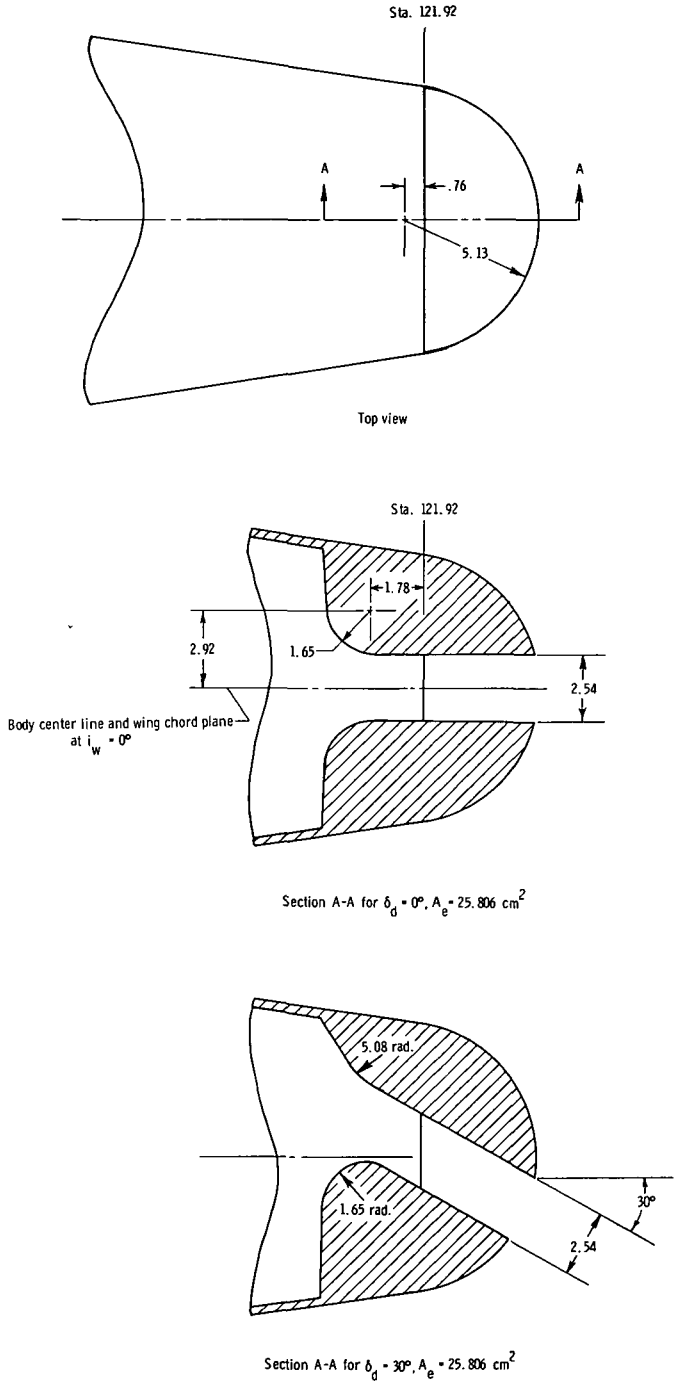

Figure 8.- Model 2 nozzle geometry. Each nozzle had a 1.78- by 0.25-cm strut installed to insure structural rigidity between nozzle halves (struts not shown). All dimensions are in centimeters unless otherwise noted.

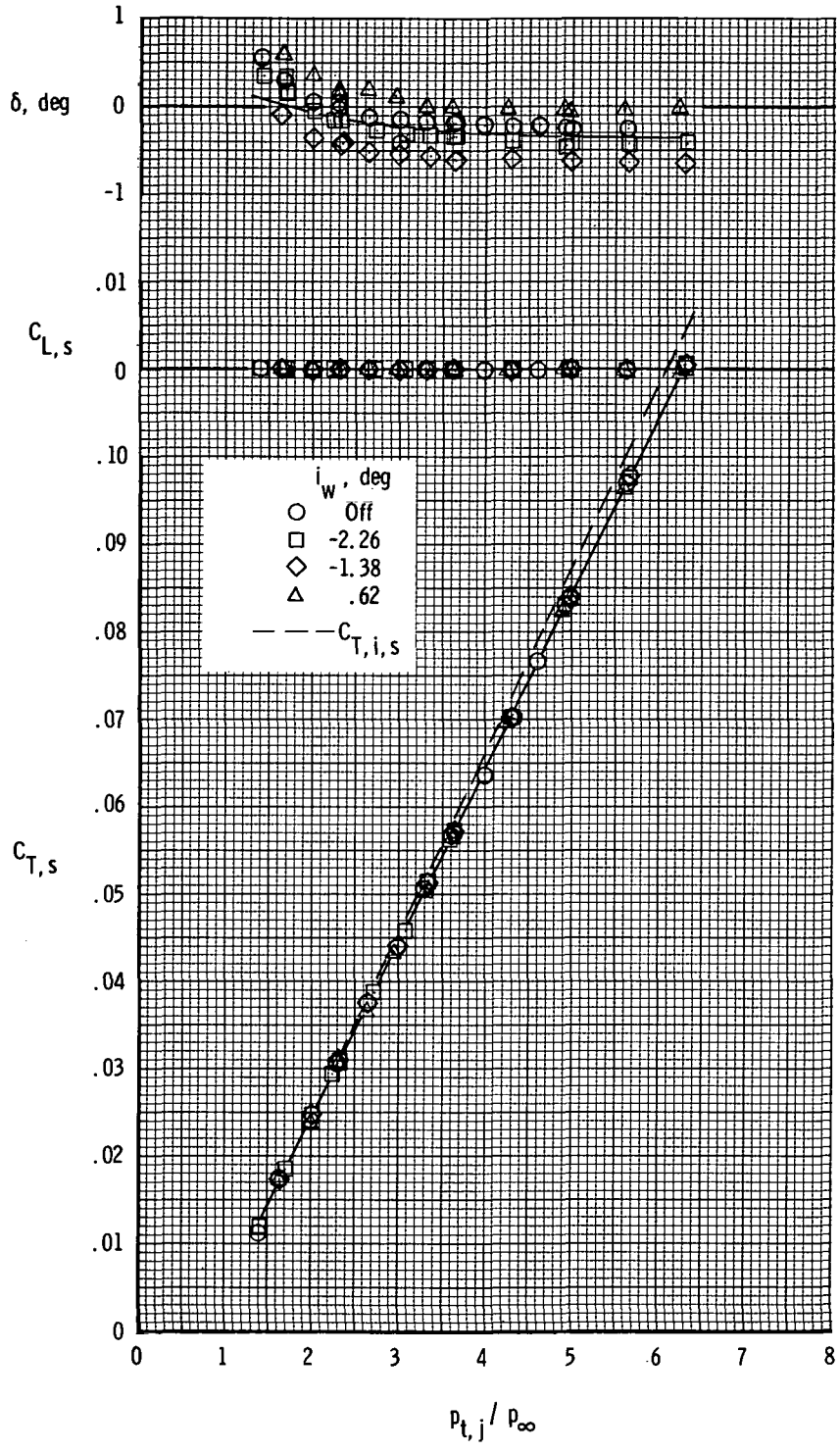

(a) Model 1, $\delta_d = 0^o$.

Figure 9.- Variation of measured static thrust and lift coefficients with jet total-pressure ratio.

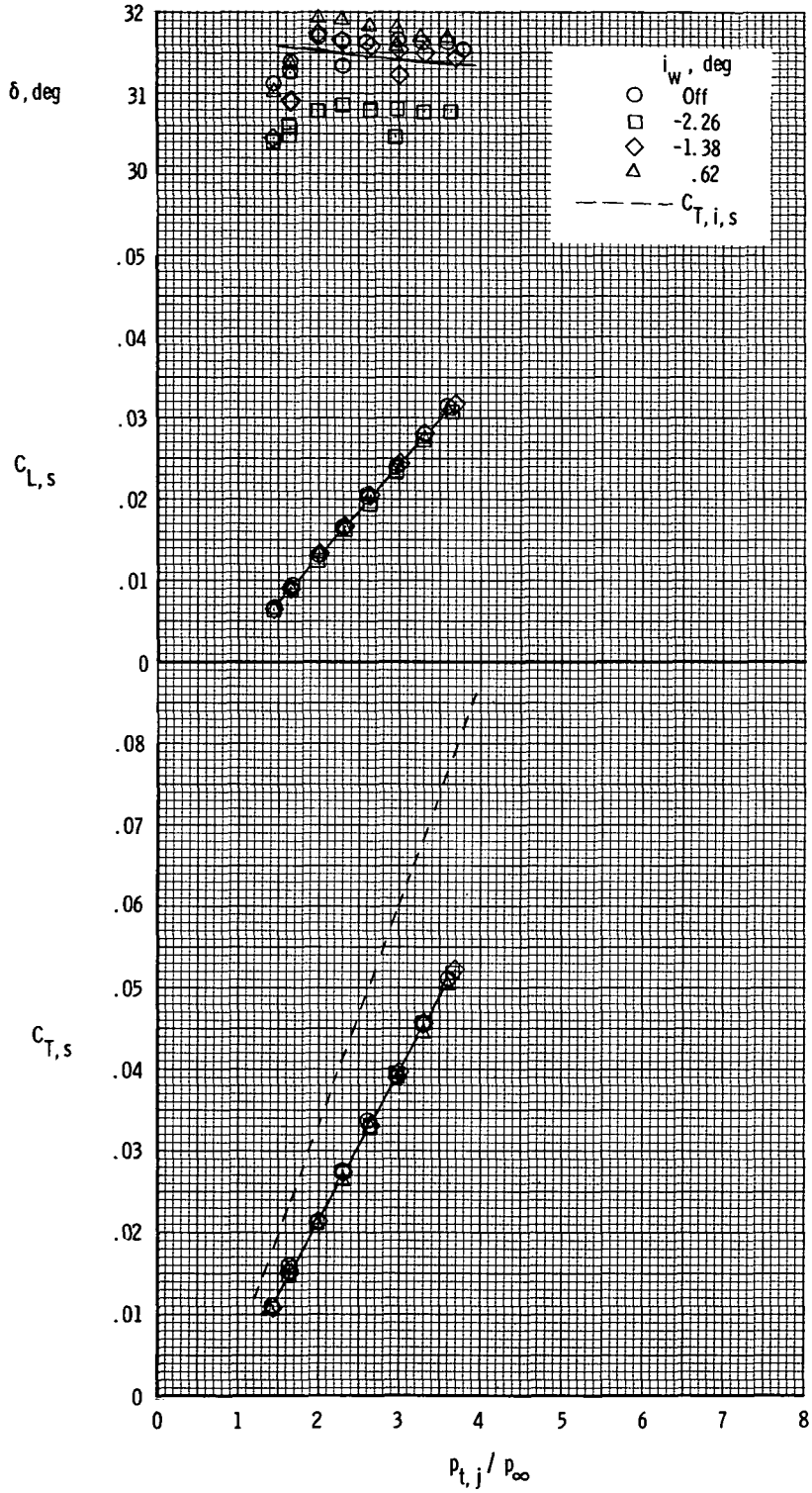

(b) Model 1, $\delta_d = 30^o$.

Figure 9.- Continued.

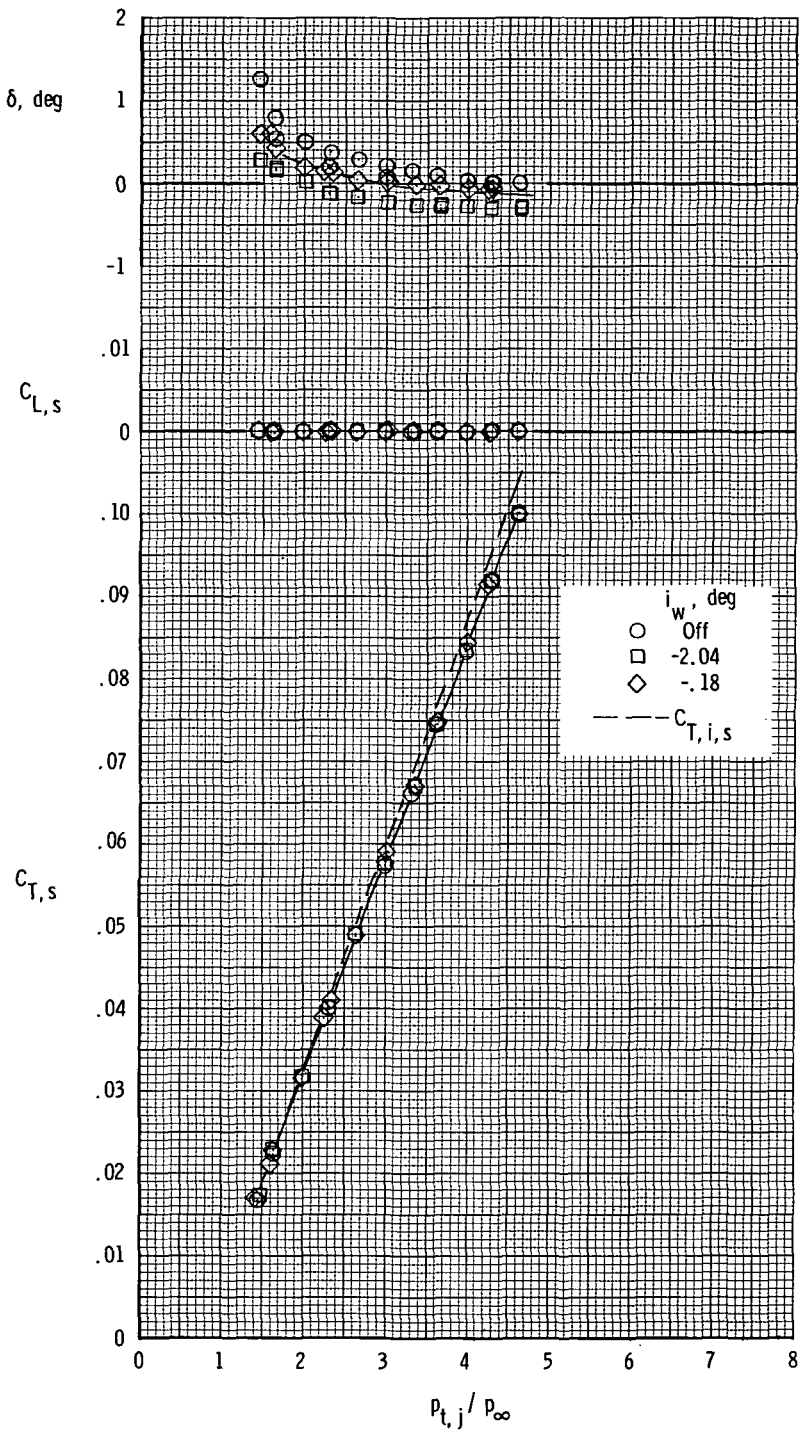

(c) Model 2, $\delta_d = 0^o$.

Figure 9.- Continued.

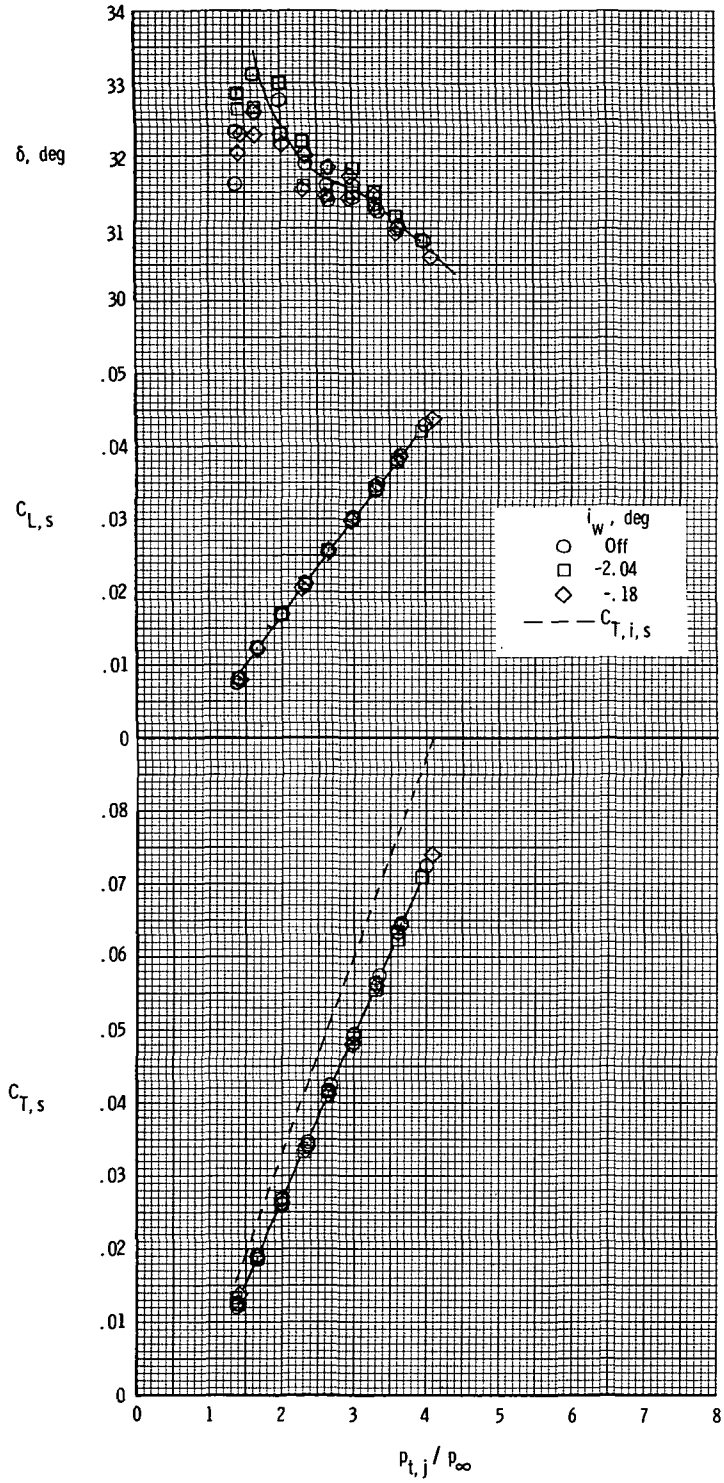

(d) Model 2, $\delta_d = 30^o$.

Figure 9.- Concluded.

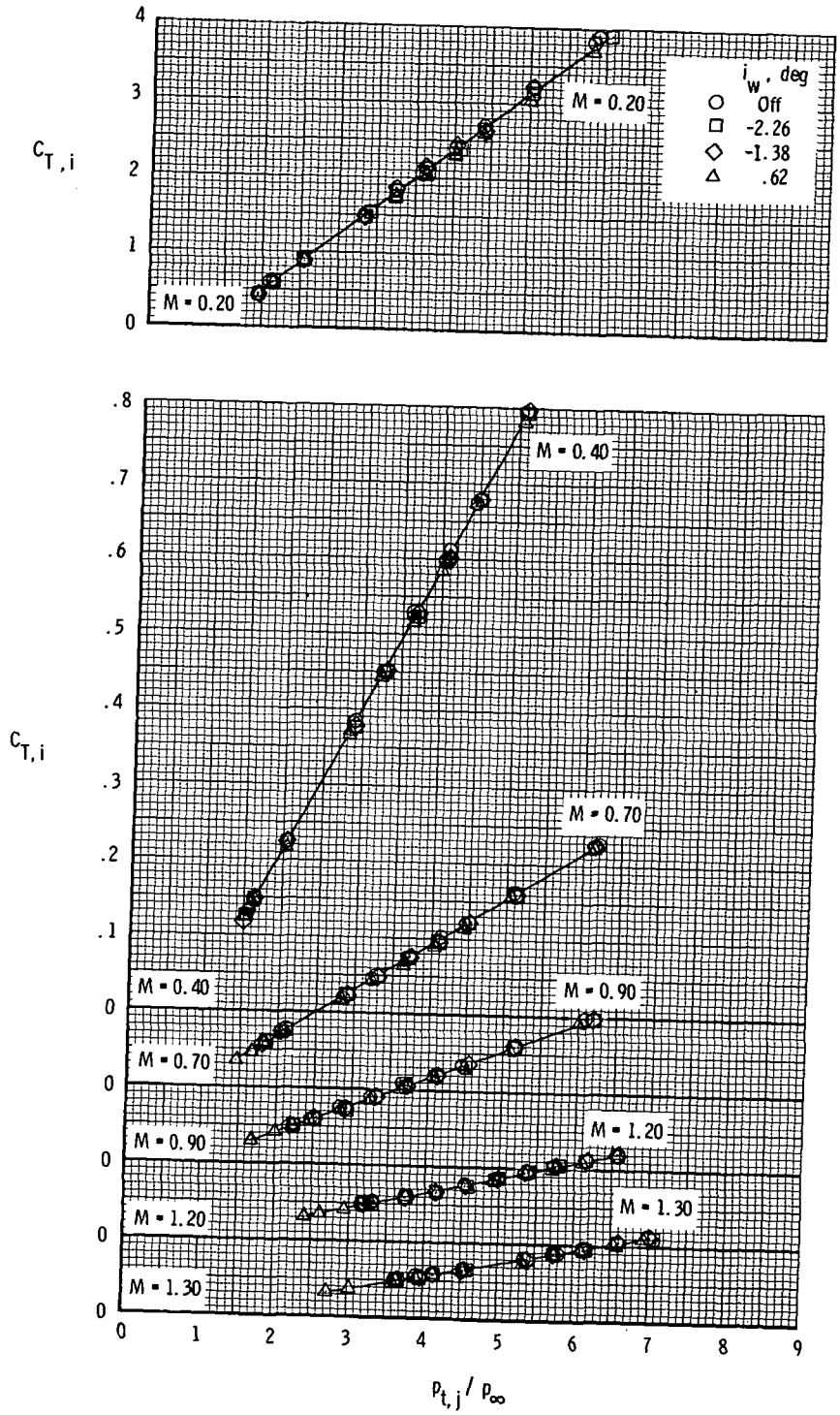

(a) Model 1, $\delta_d = 0^o$.

Figure 10.- Variation of ideal gross thrust coefficient with jet total-pressure ratio.

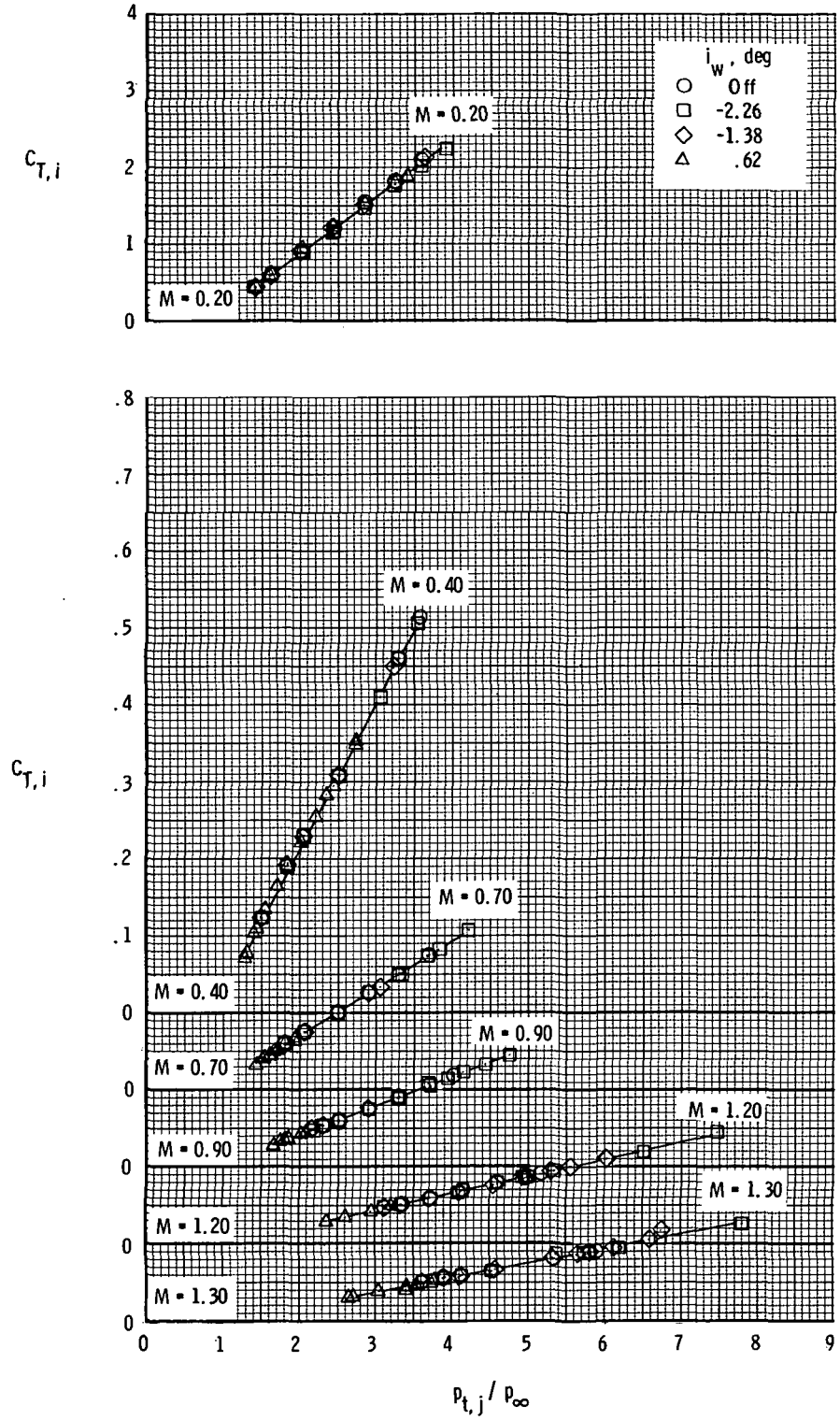

(b) Model 1, $\delta_d = 30^o$.

Figure 10.- Continued.

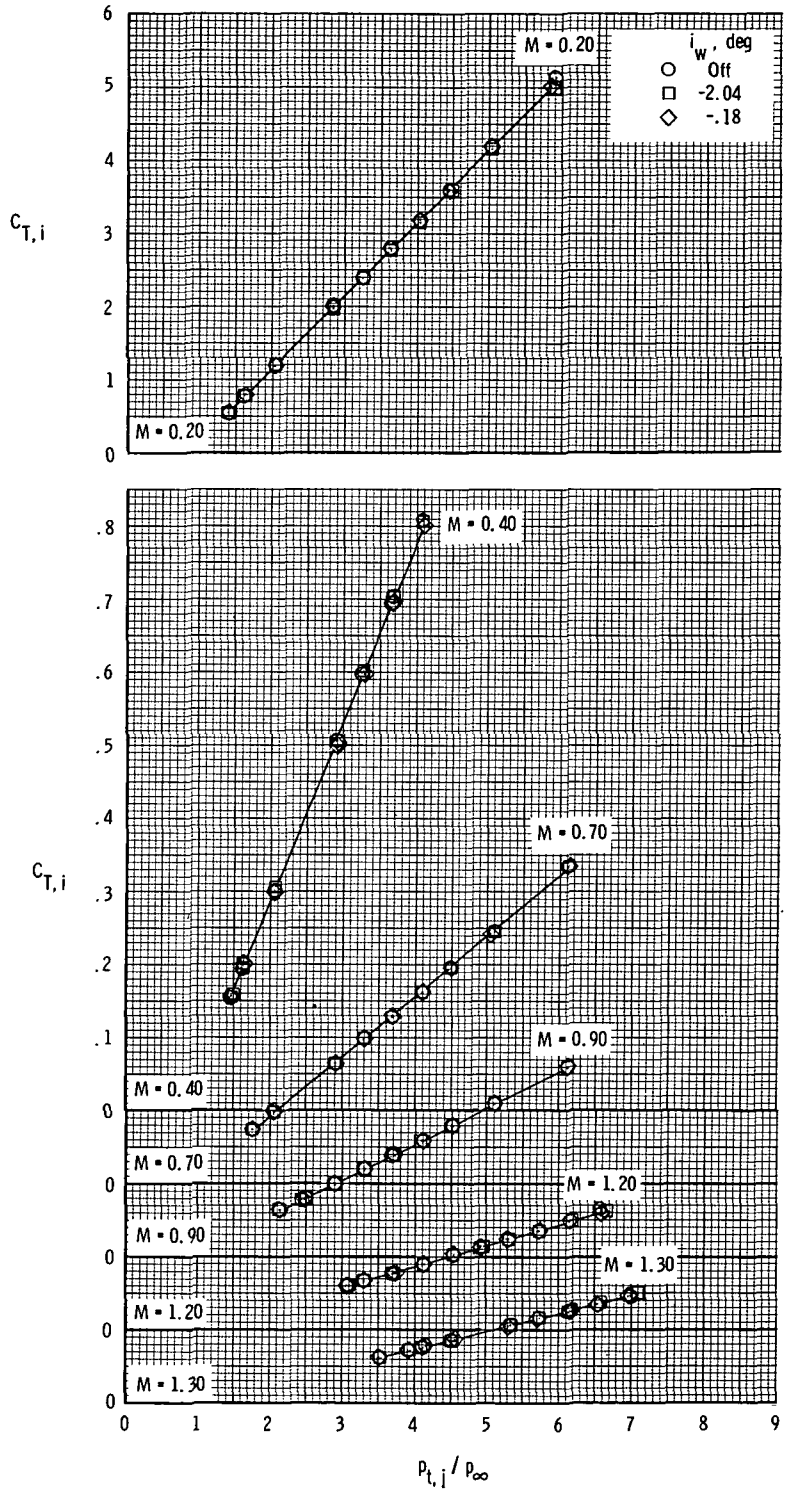

(c) Model 2, $\delta_d = 0^o$.

Figure 10.- Continued.

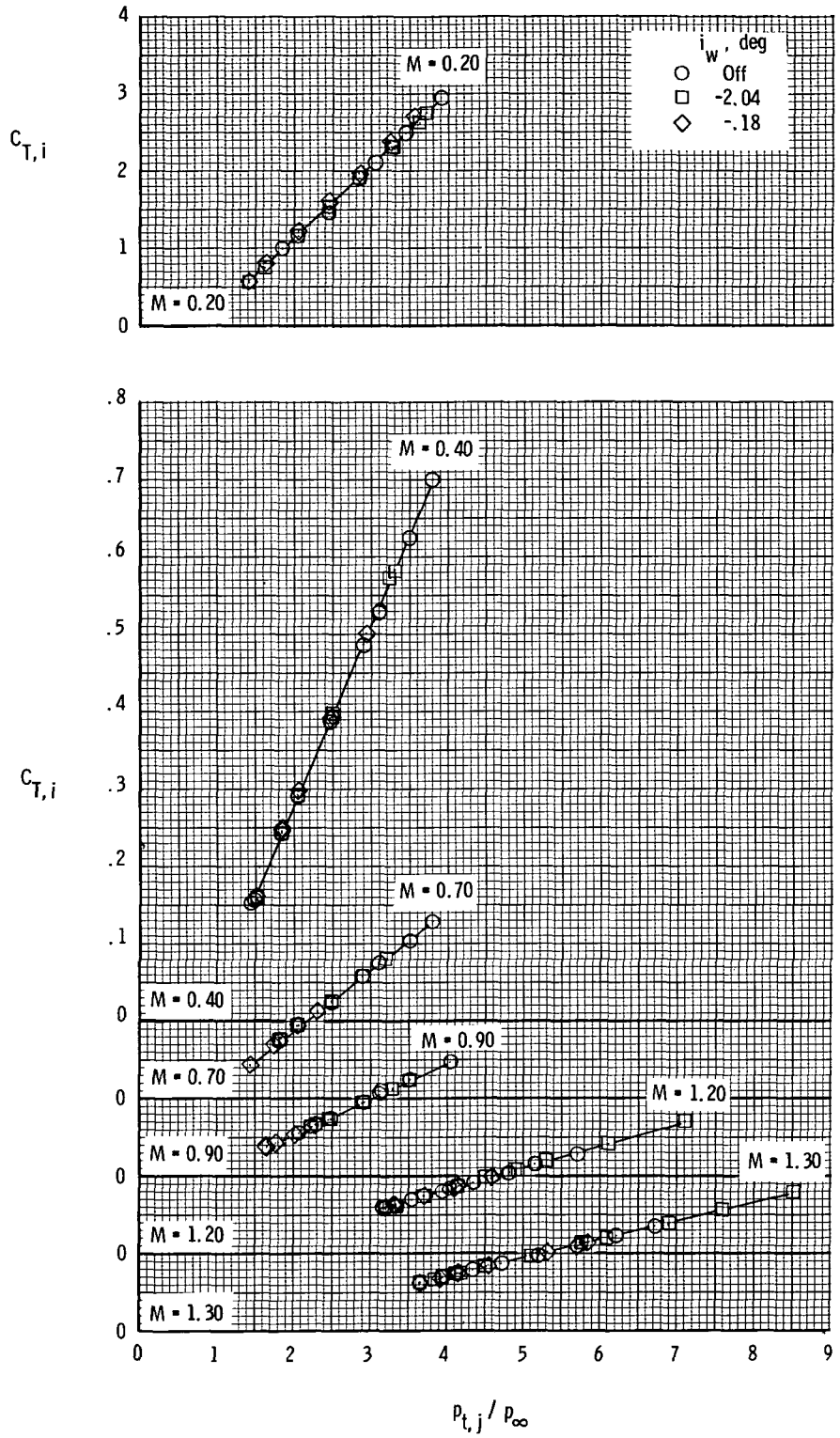

(d) Model 2, $\delta_d = 30^o$.

Figure 10.- Concluded.

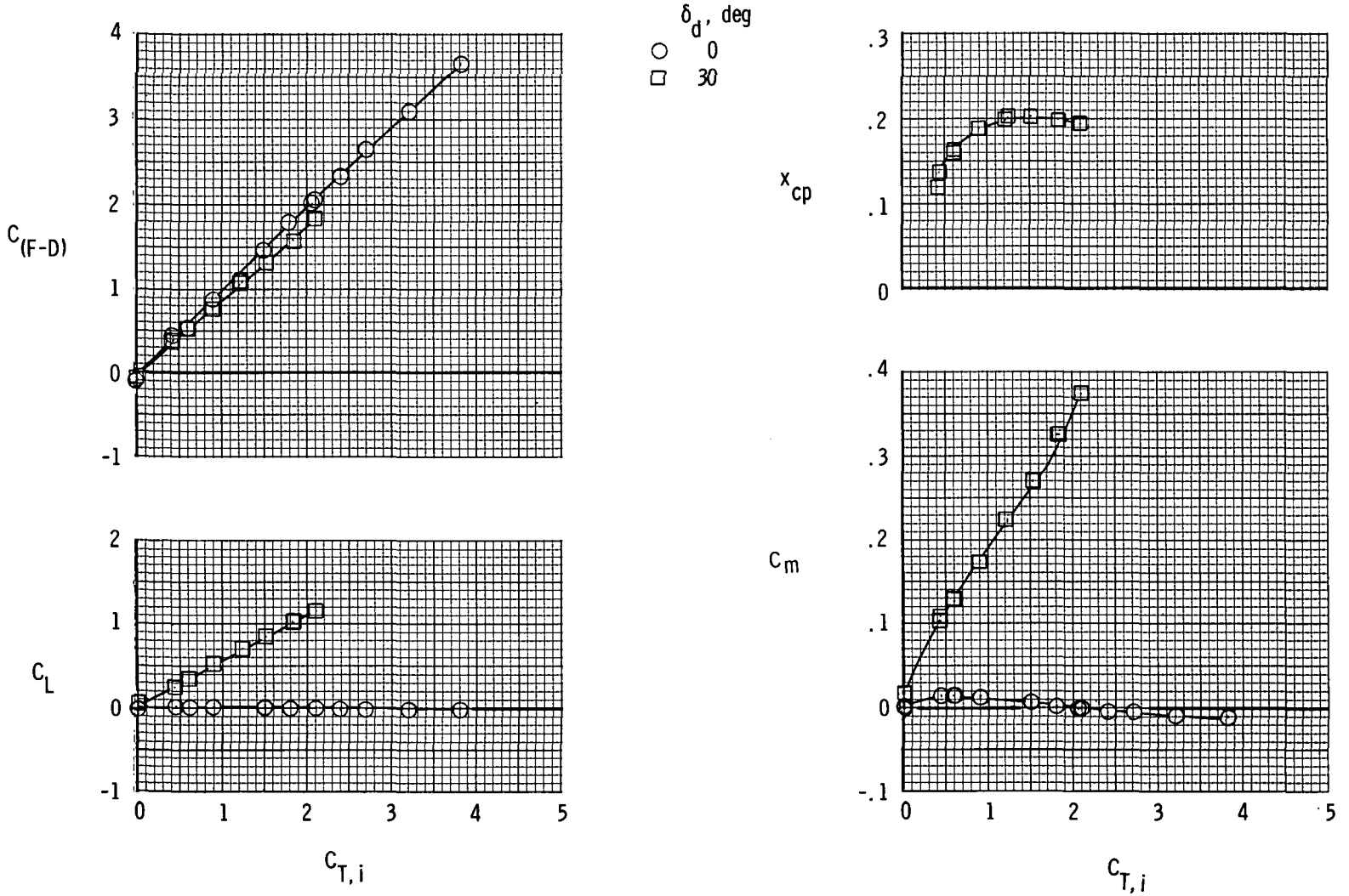

(a) M = 0.20.

Figure 11.- Variation of measured aerodynamic parameters with ideal gross thrust coefficient for model 1 with wings off.

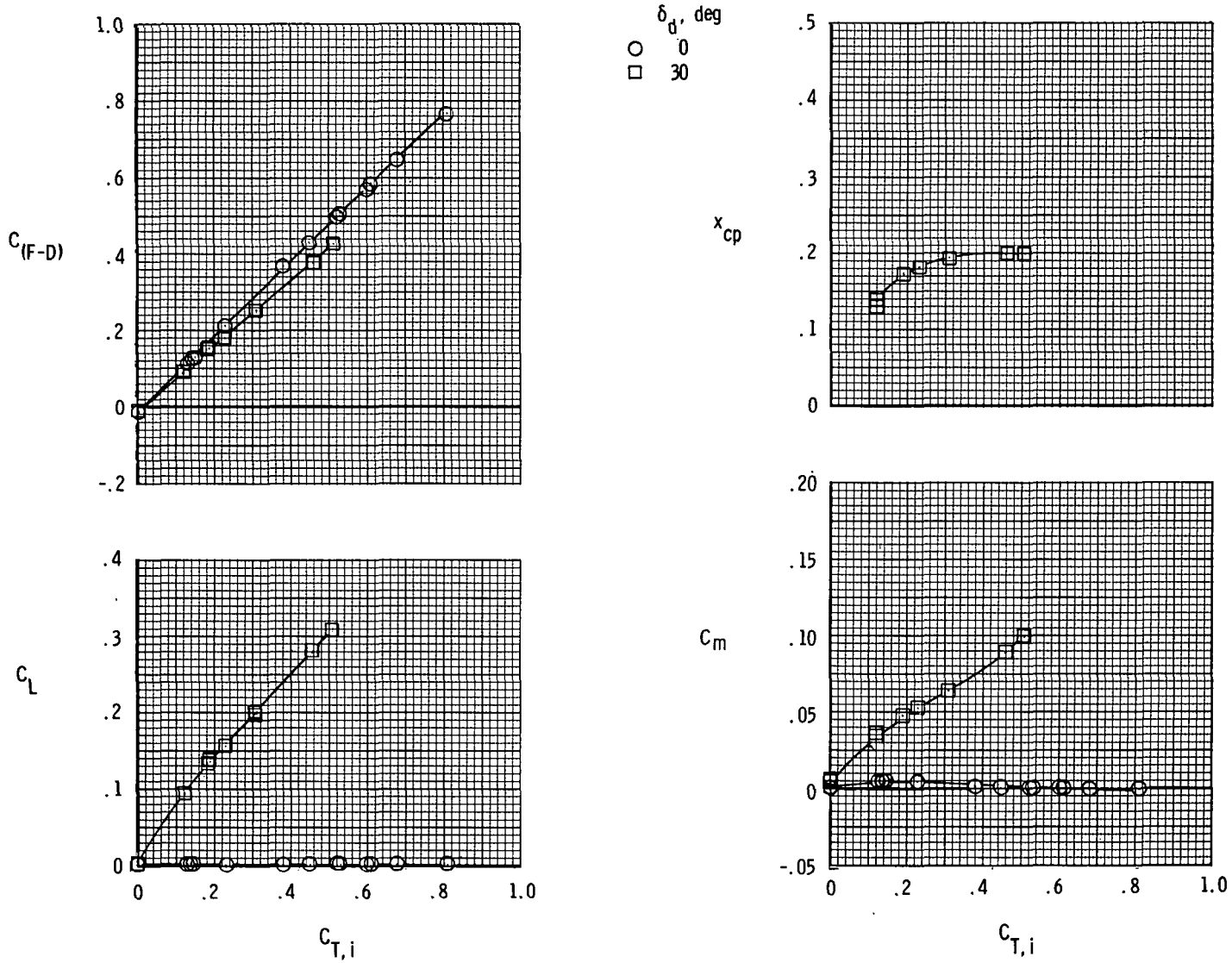

(b) M = 0.40.

Figure 11.- Continued.

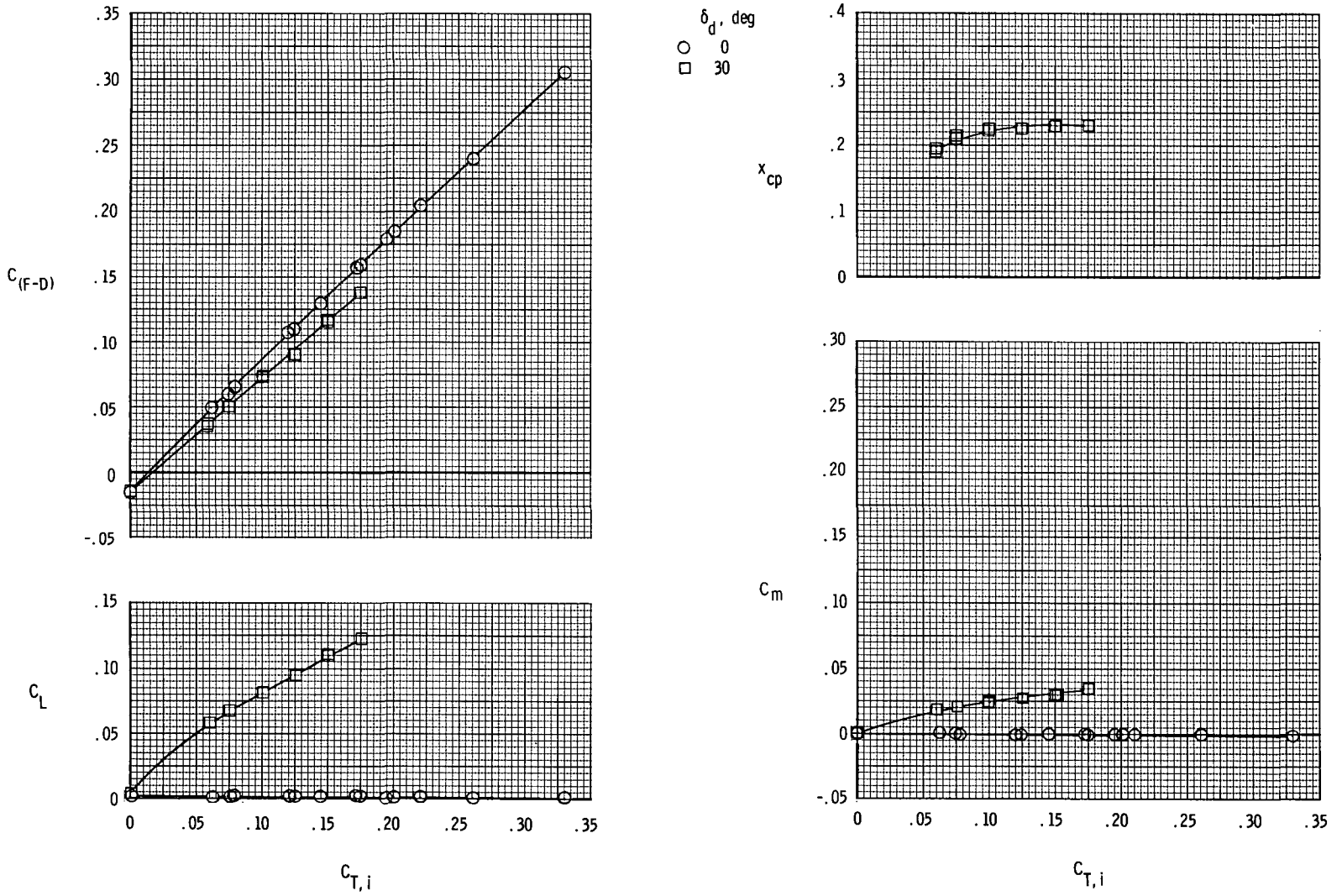

(c) M = 0.70.

Figure 11.- Continued.

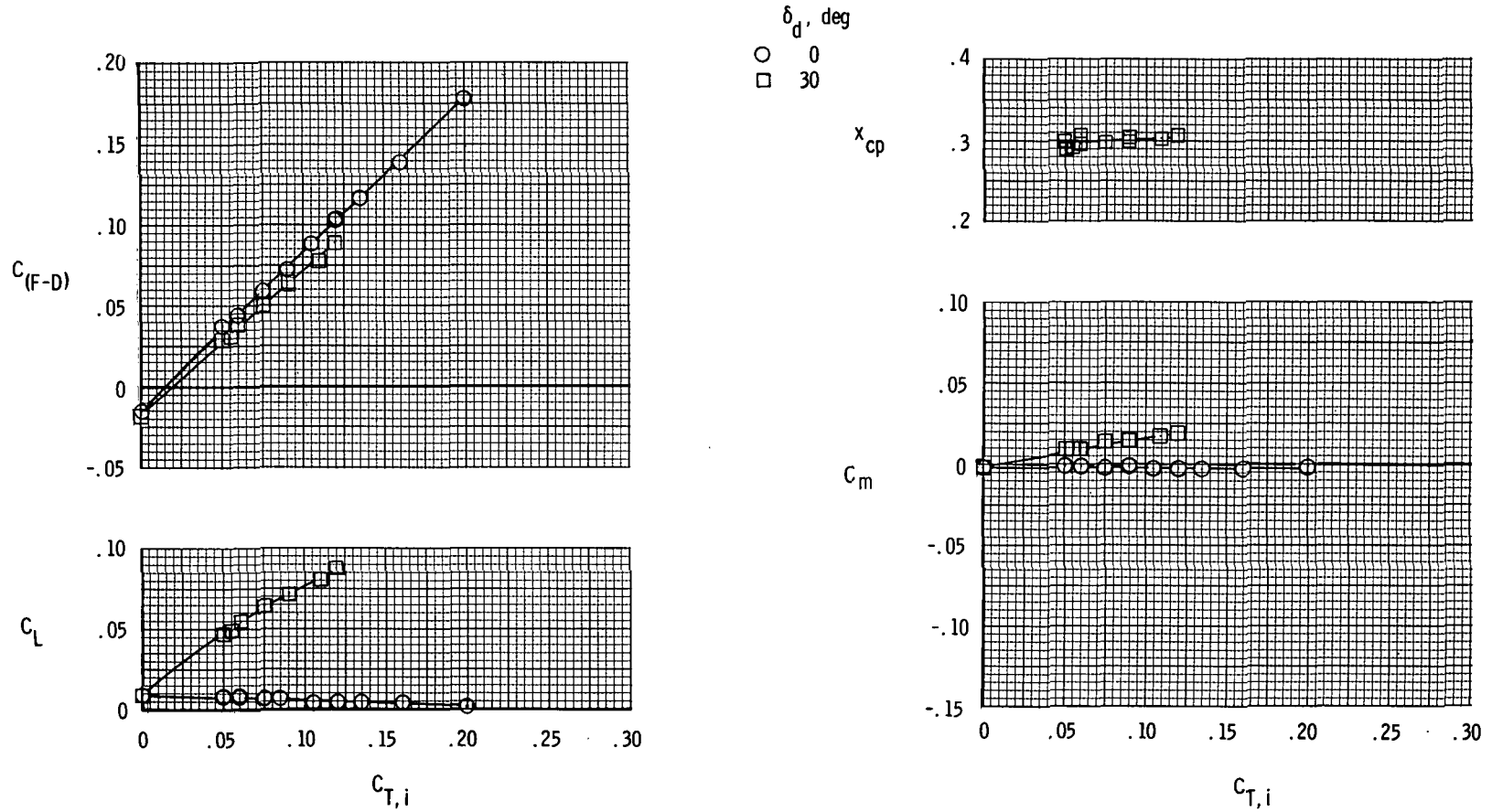

(d) M = 0.90.

Figure 11.- Continued.

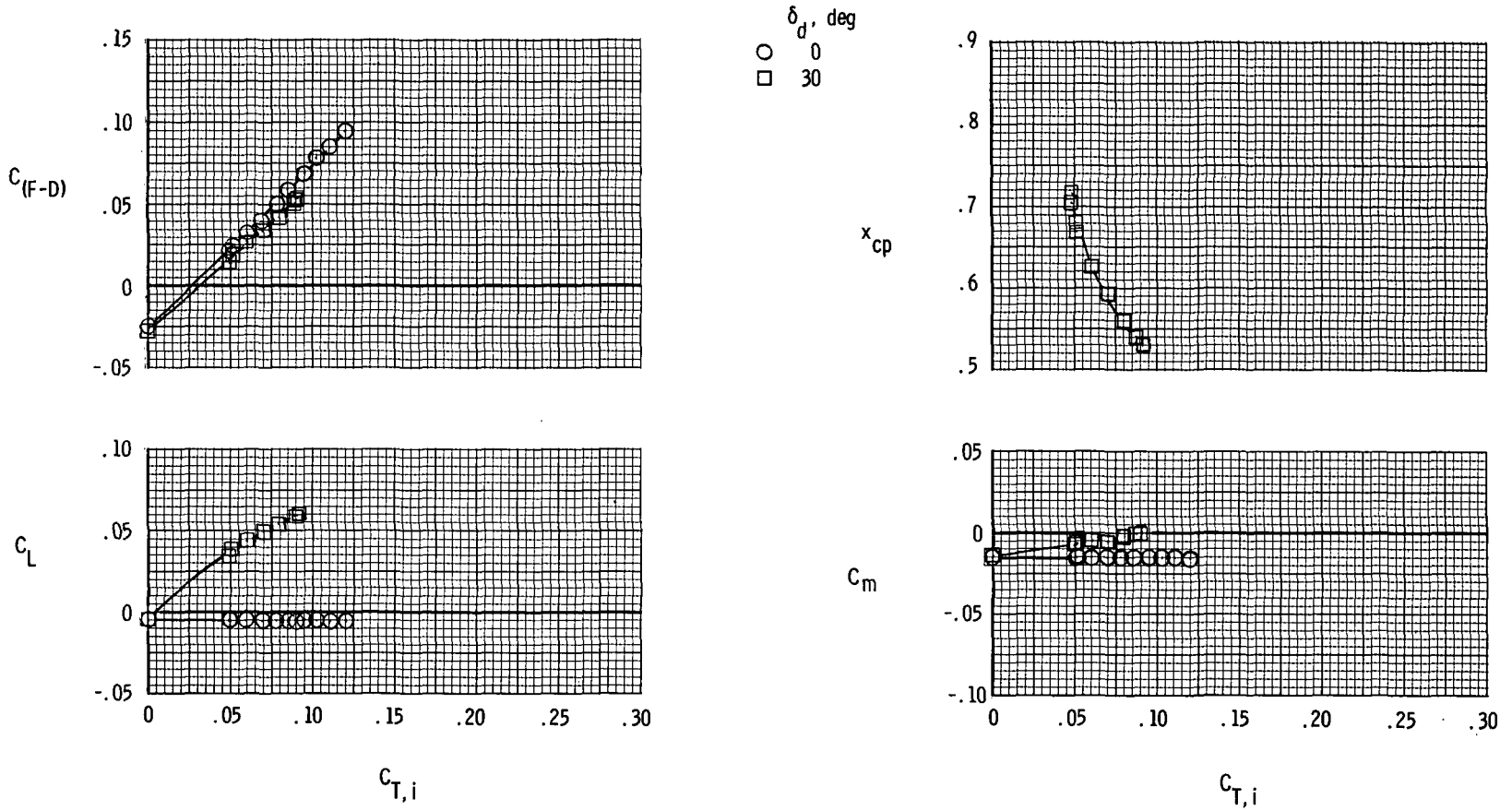

(e) M = 1.20.

Figure 11.- Continued.

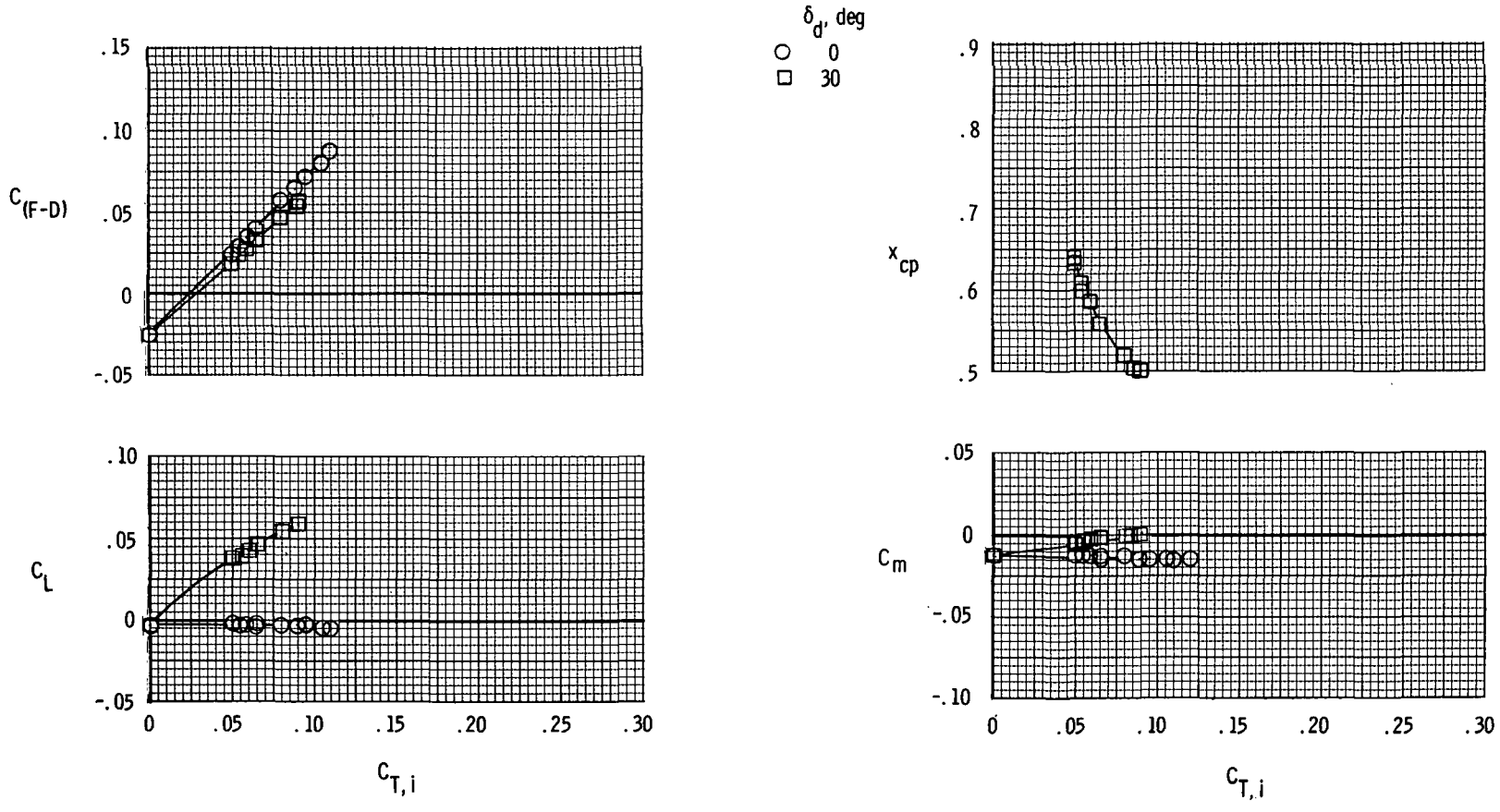

(f) M = 1.30.

Figure 11.- Concluded.

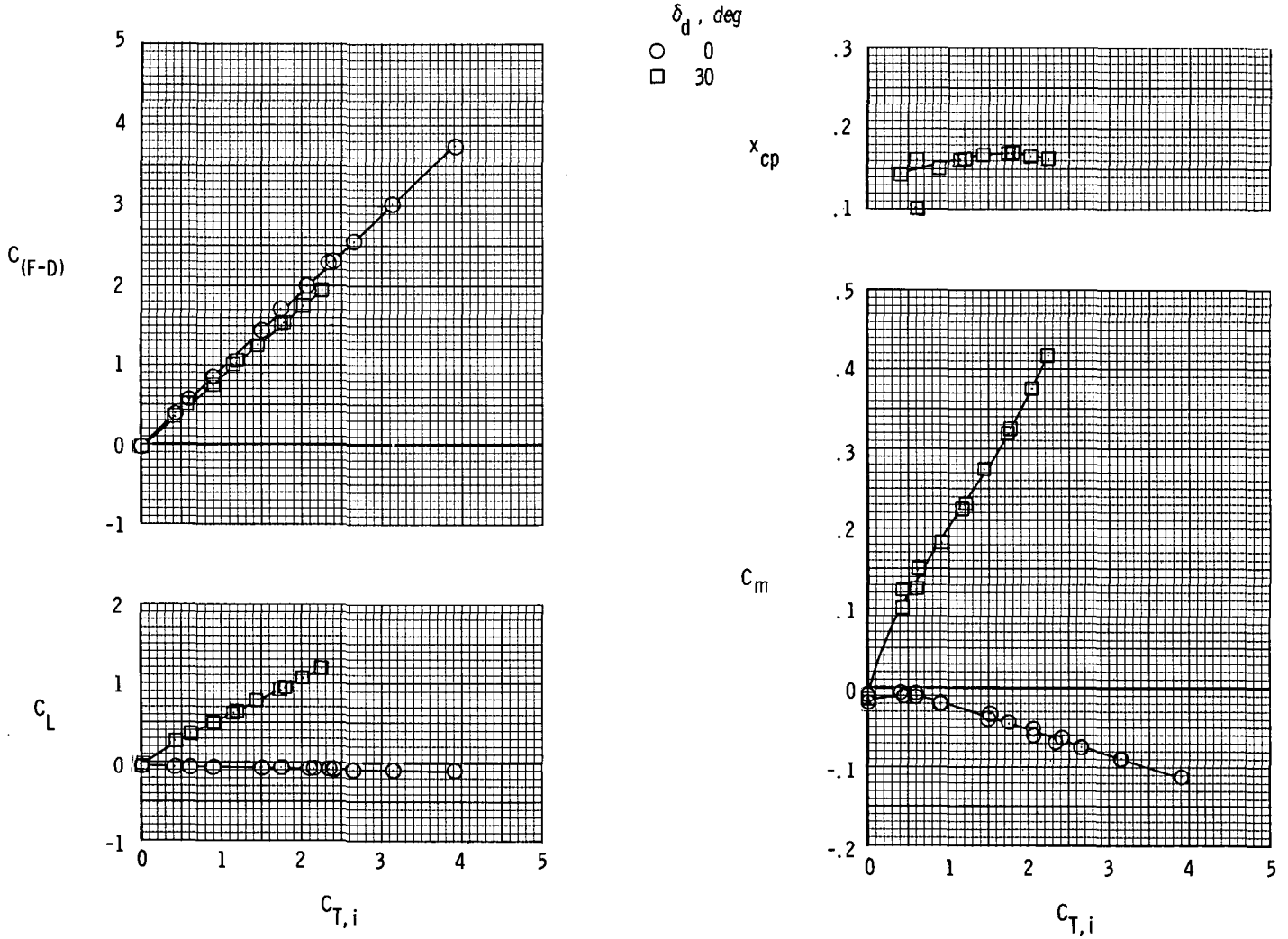

(a) M = 0.20.

Figure 12.- Variation of measured aerodynamic parameters with ideal gross thrust coefficient *for model 1 with* $i_w = -2.26^o$.

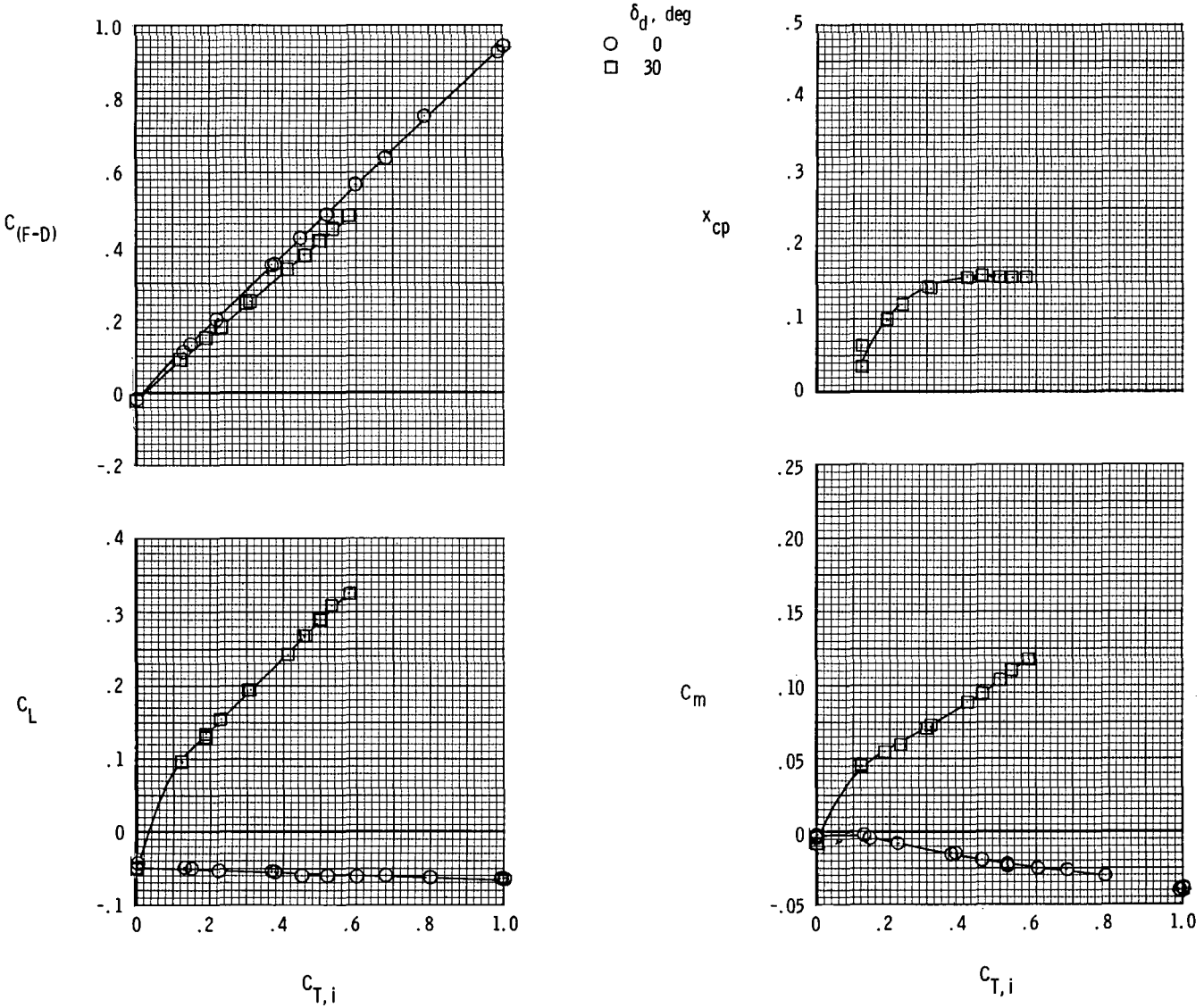

(b) M = 0.40.

Figure 12.- Continued.

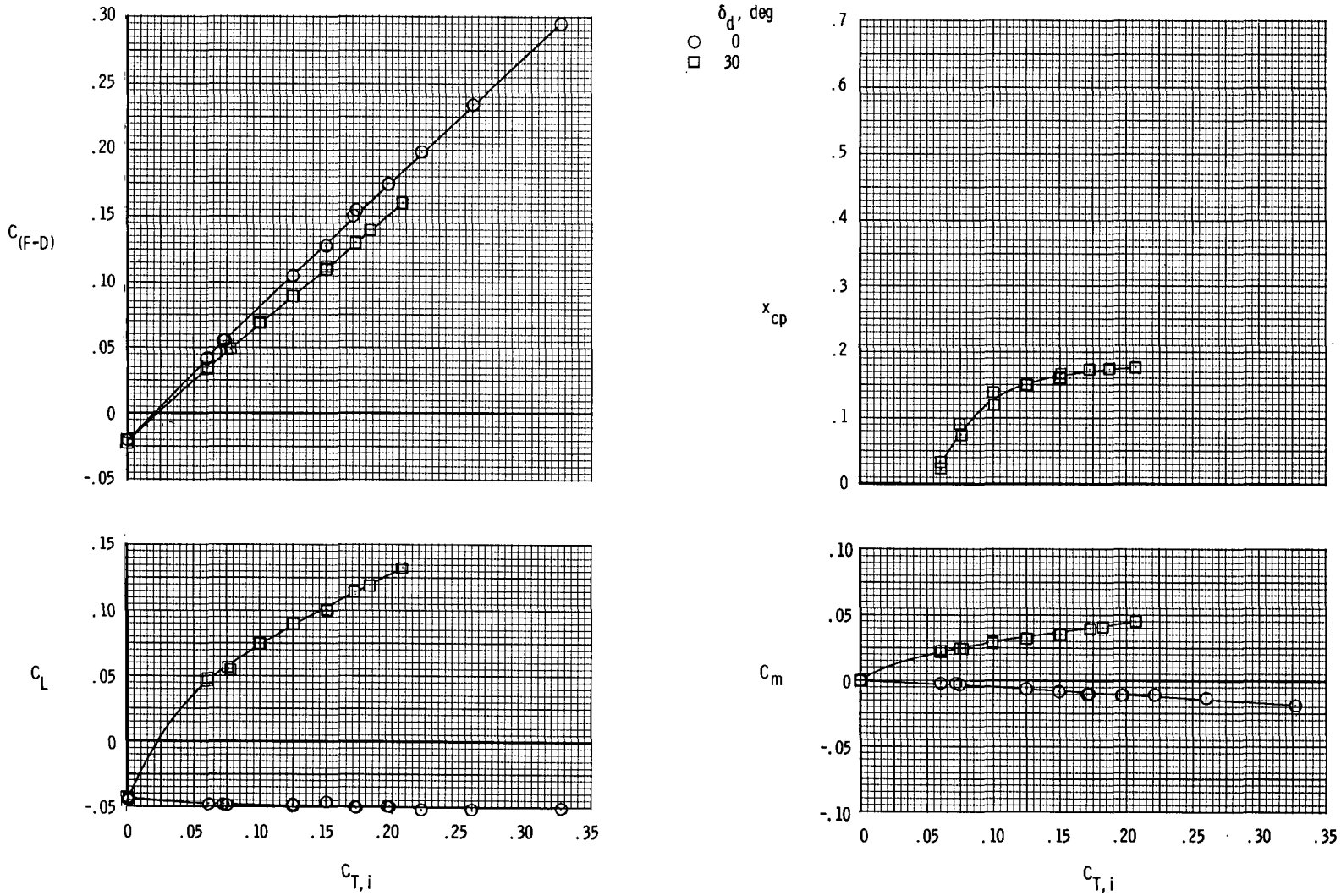

(c) M = 0.70.

Figure 12.- Continued.

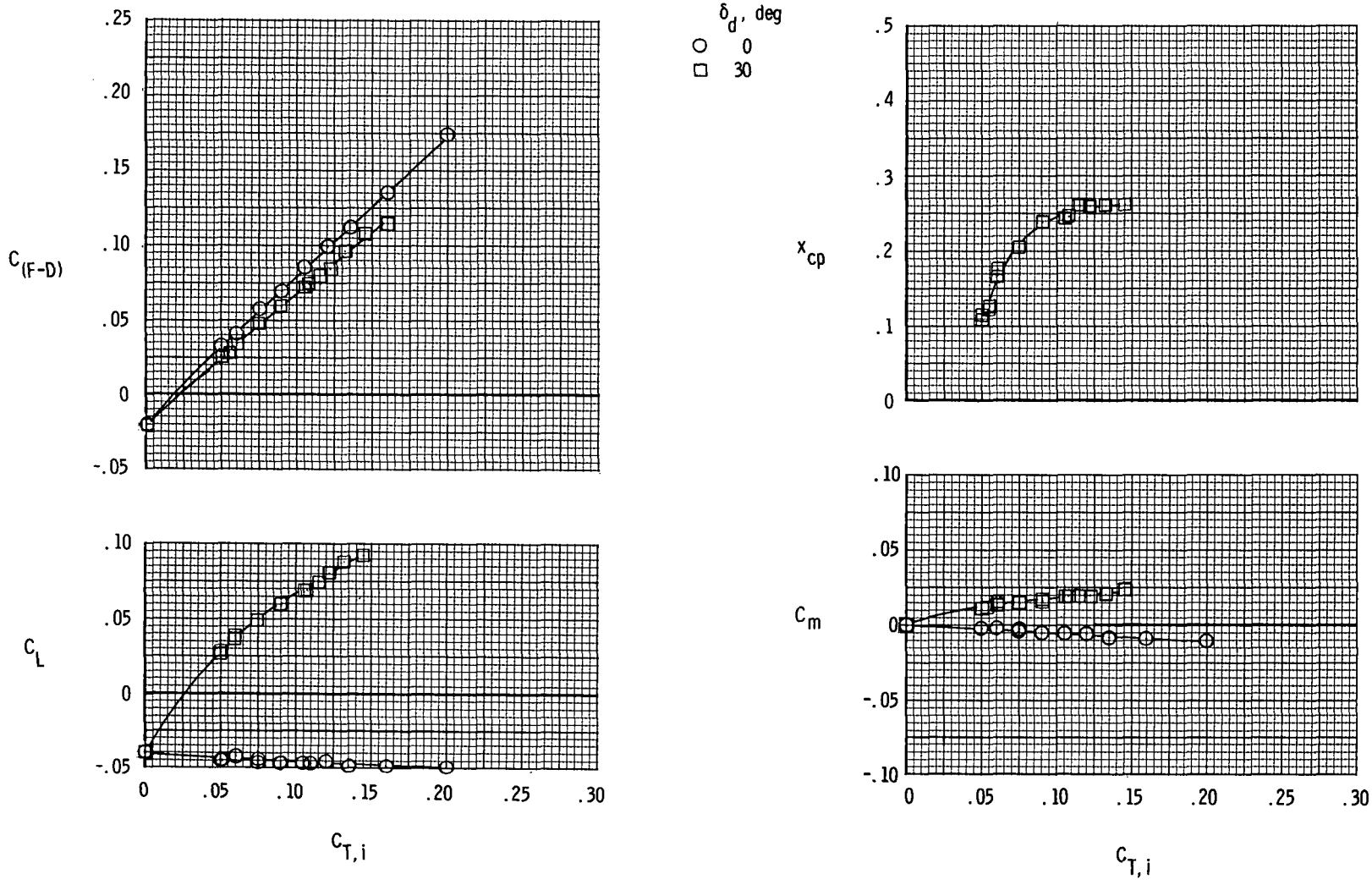

(d) M = 0.90.

Figure 12.- Continued.

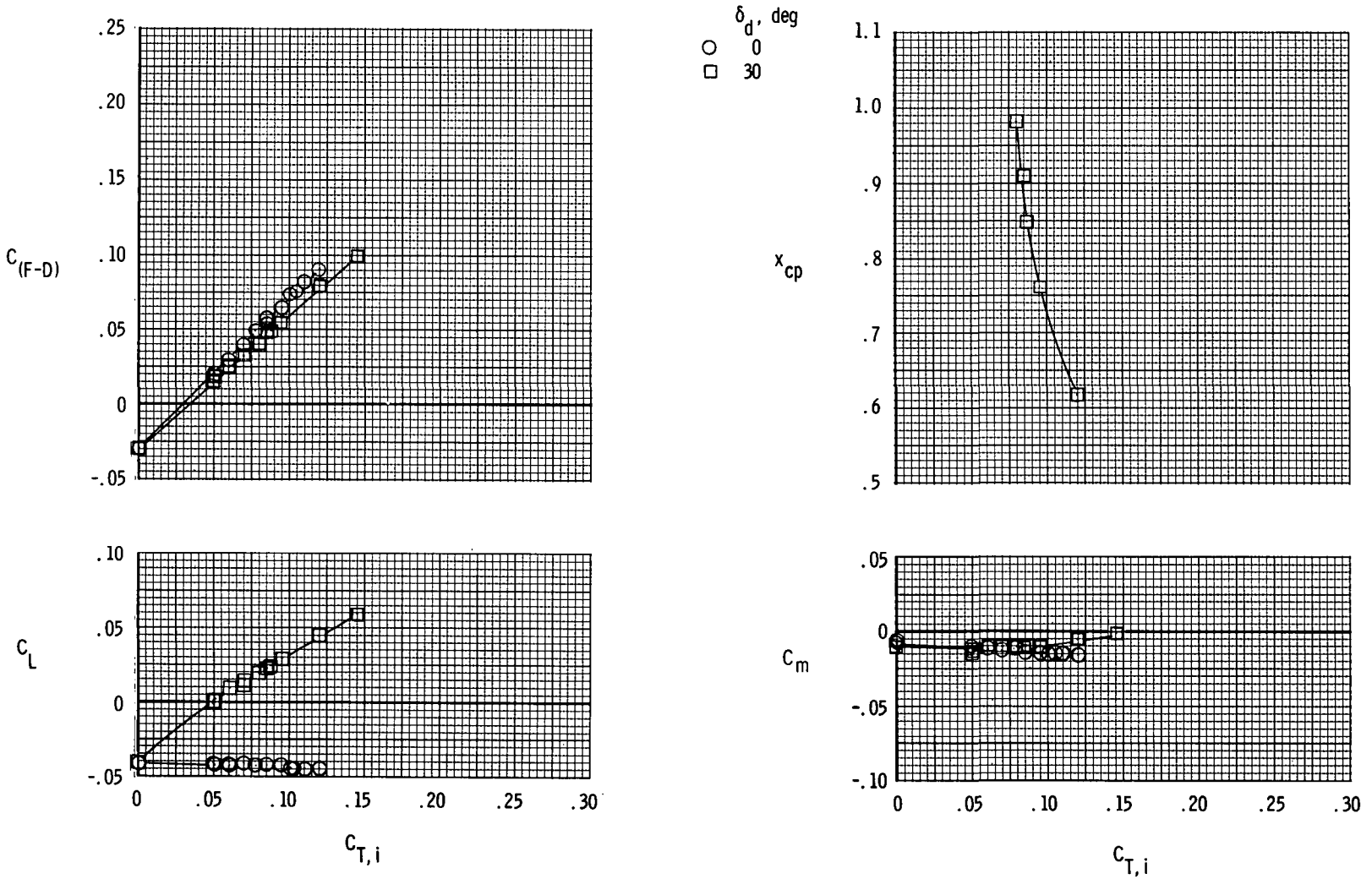

(e) M = 1.20.

Figure 12.- Continued.

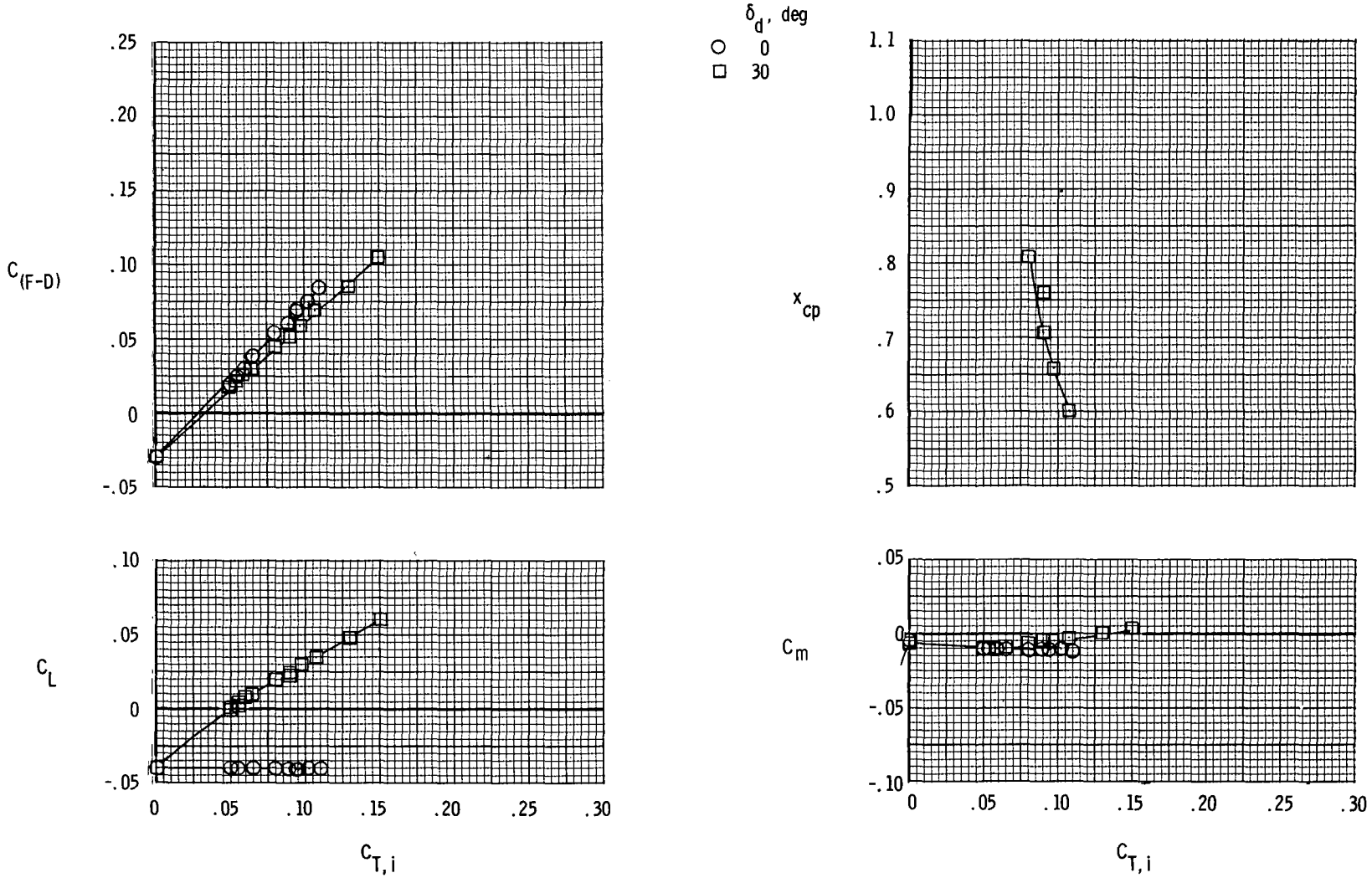

(f) M = 1.30.

Figure 12.- Concluded.

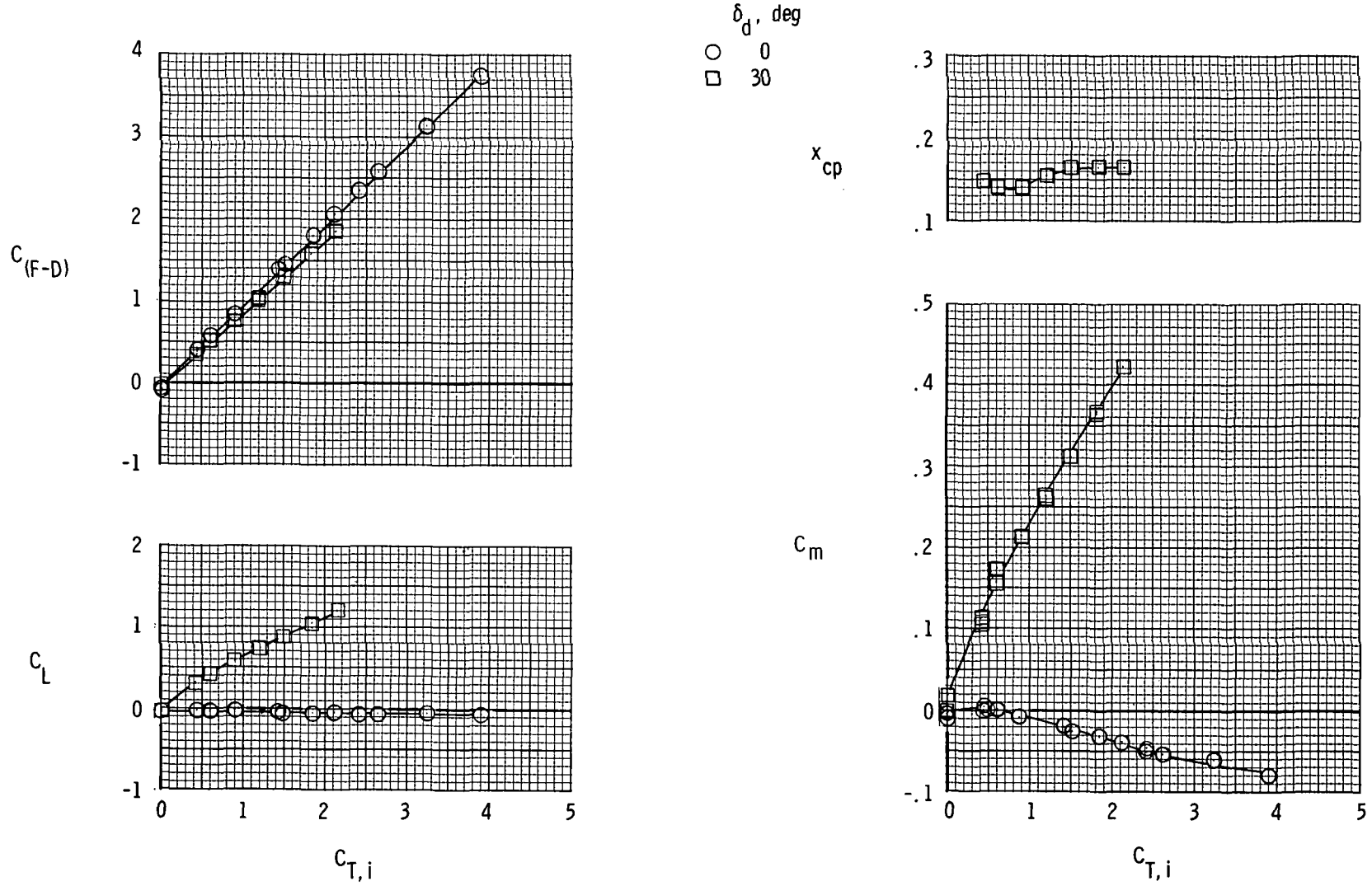

(a) M = 0.20.

Figure 13.- Variation of measured aerodynamic parameters with ideal gross thrust coefficient for model 1 with $i_w = -1.38^o$.

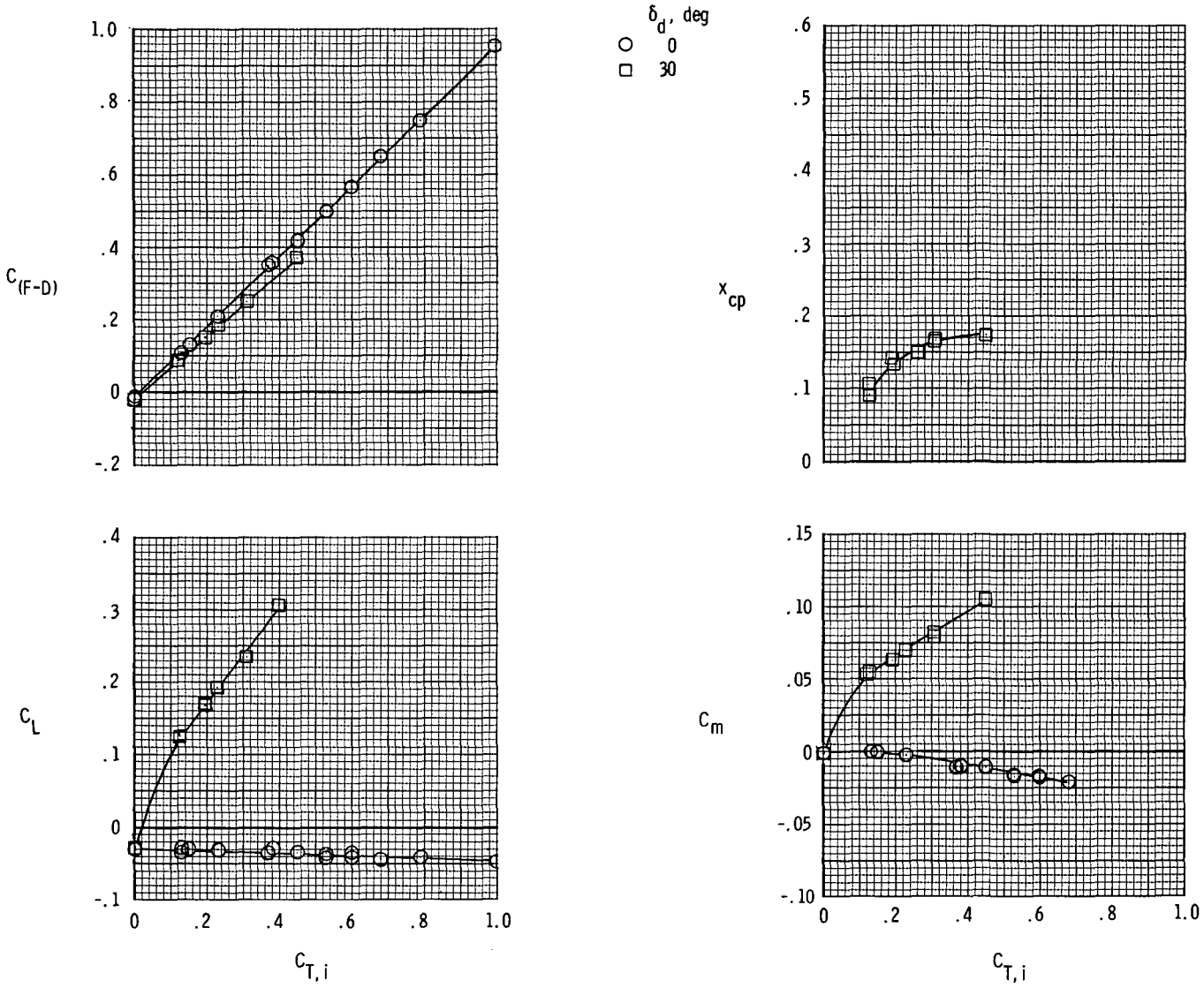

(b) M = 0.40.

Figure 13.- Continued.

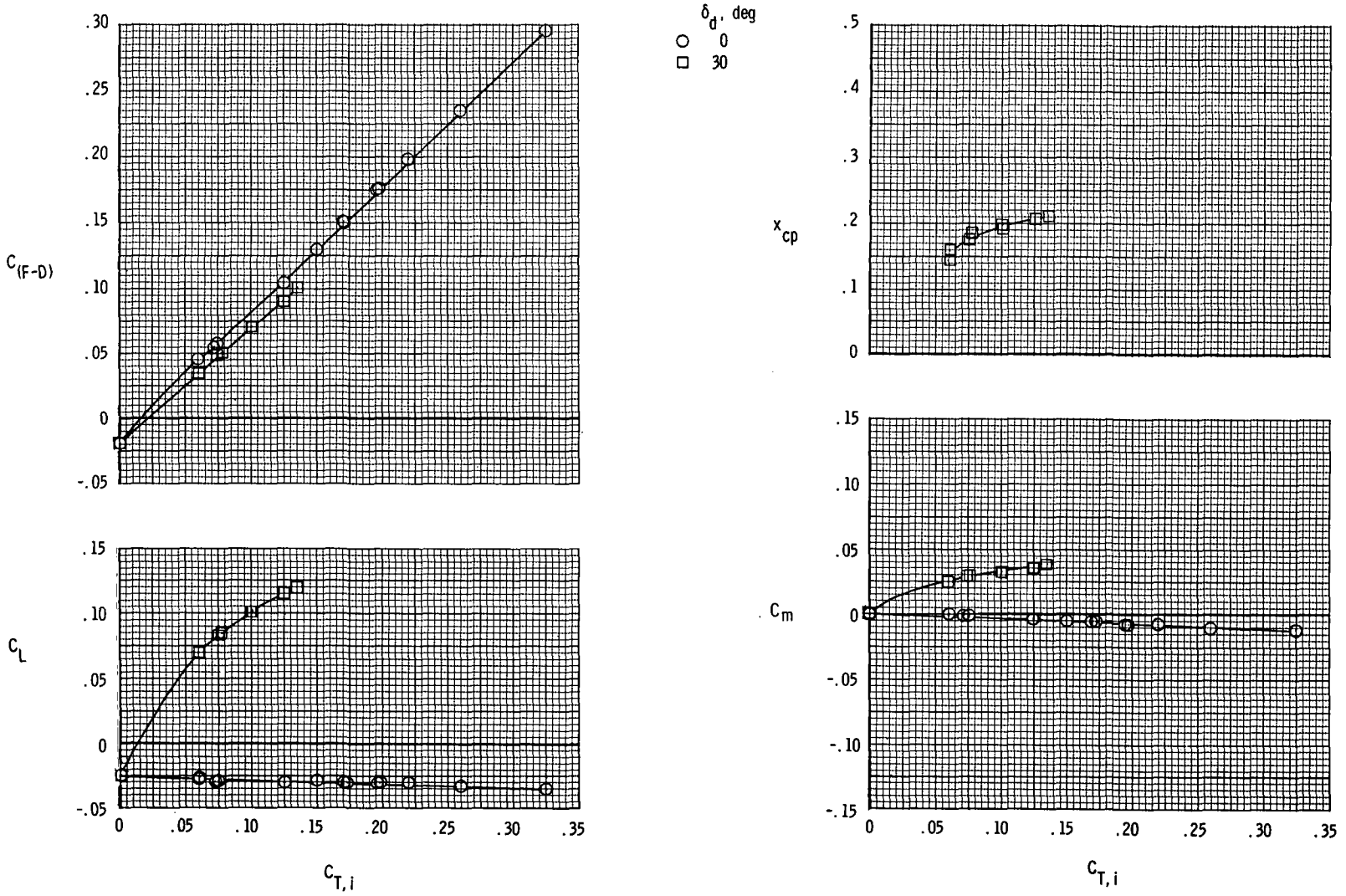

(c) M = 0.70.

Figure 13.- Continued.

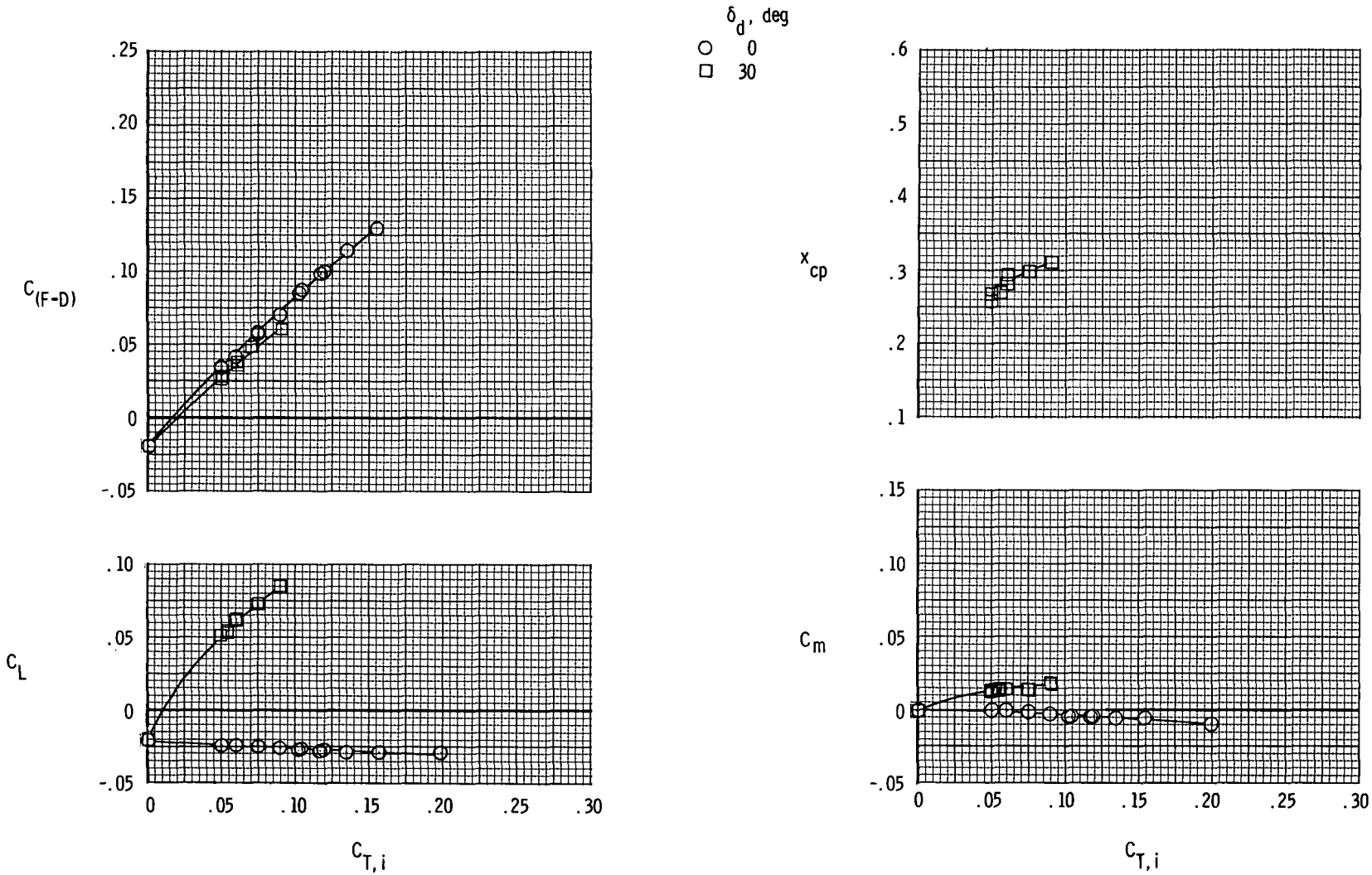

(d) M = 0.90.

Figure 13.- Continued.

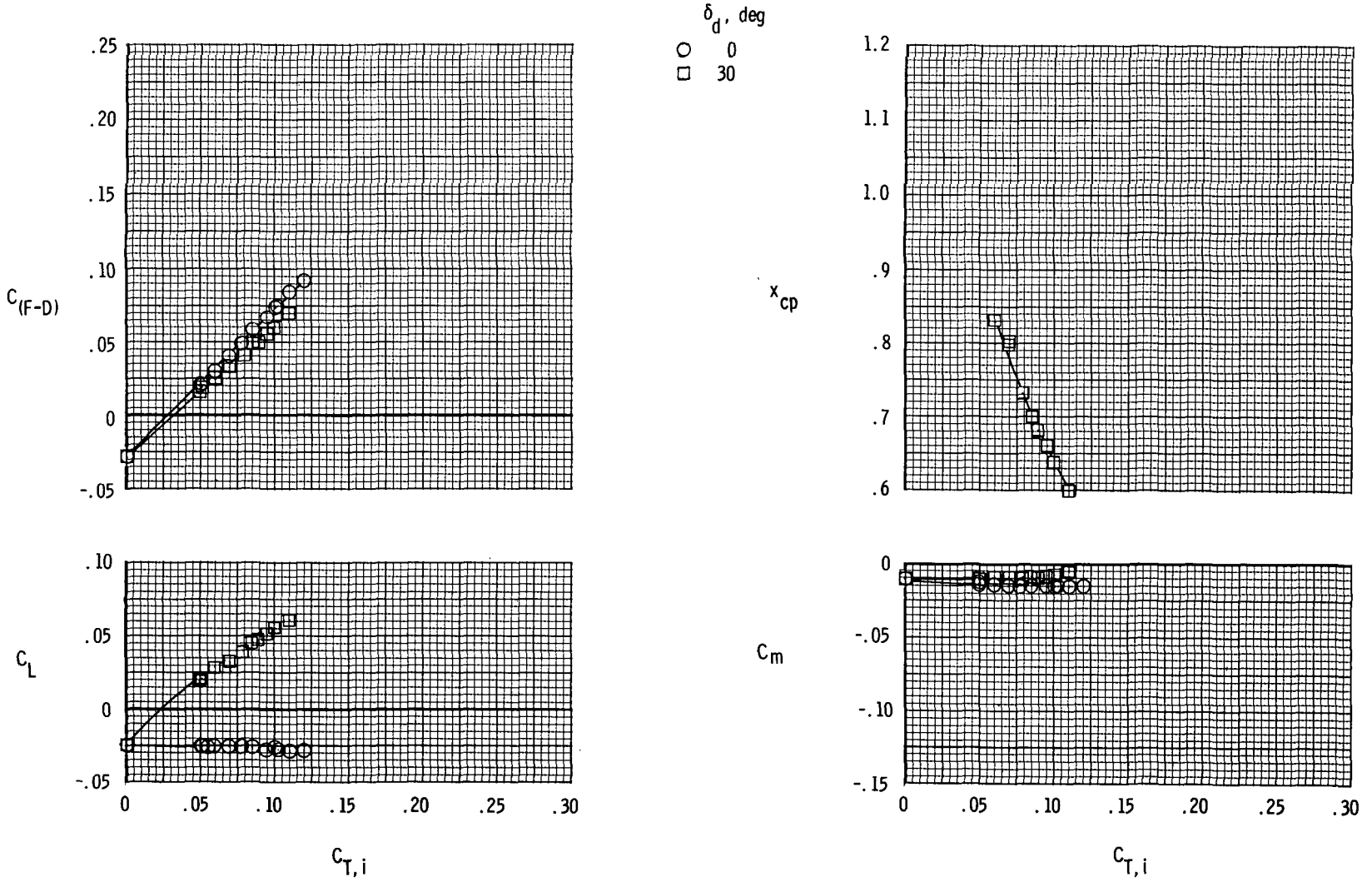

(e) M = 1.20.

Figure 13.- Continued.

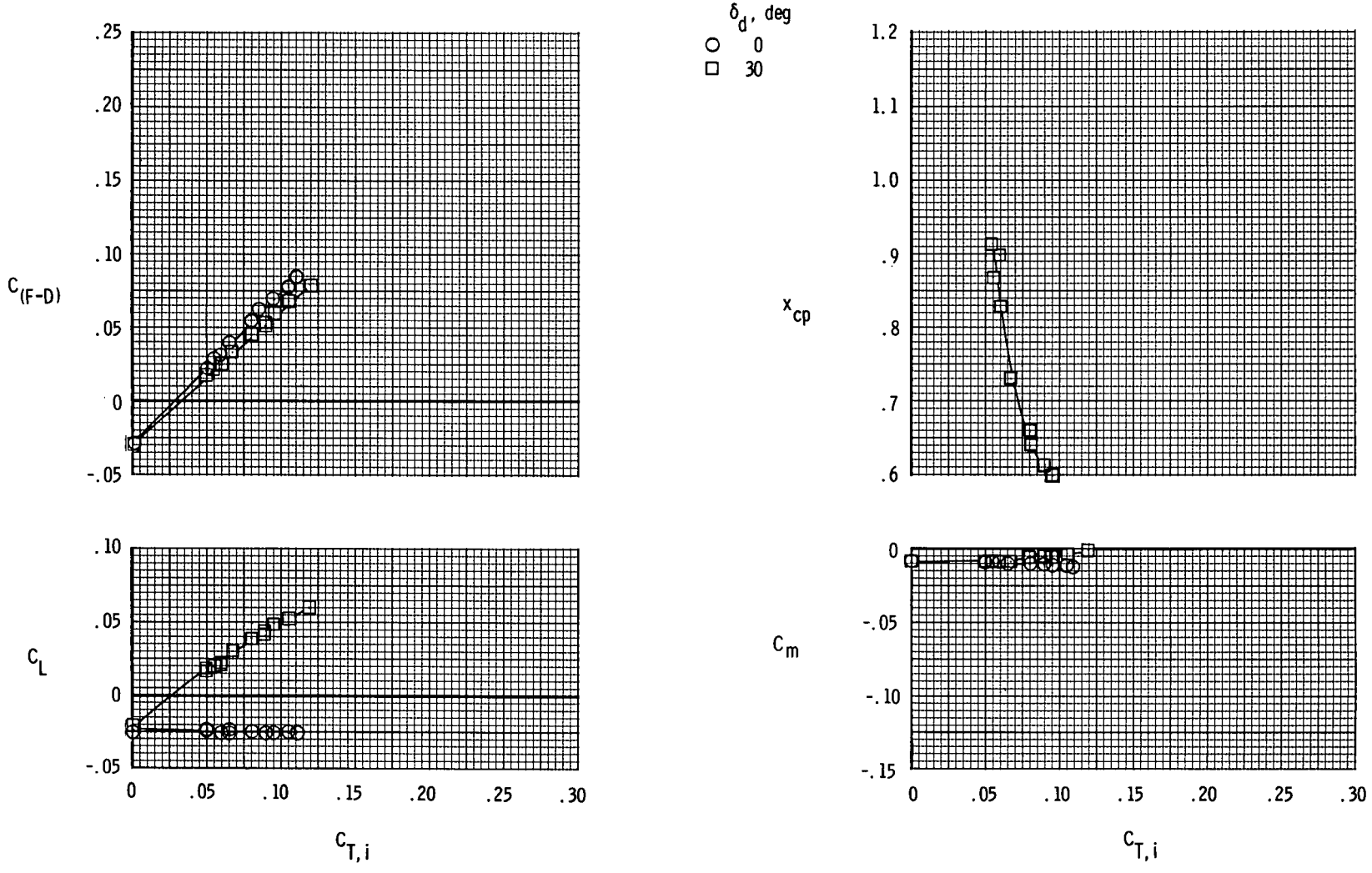

(f) M = 1.30.

Figure 13.- Concluded.

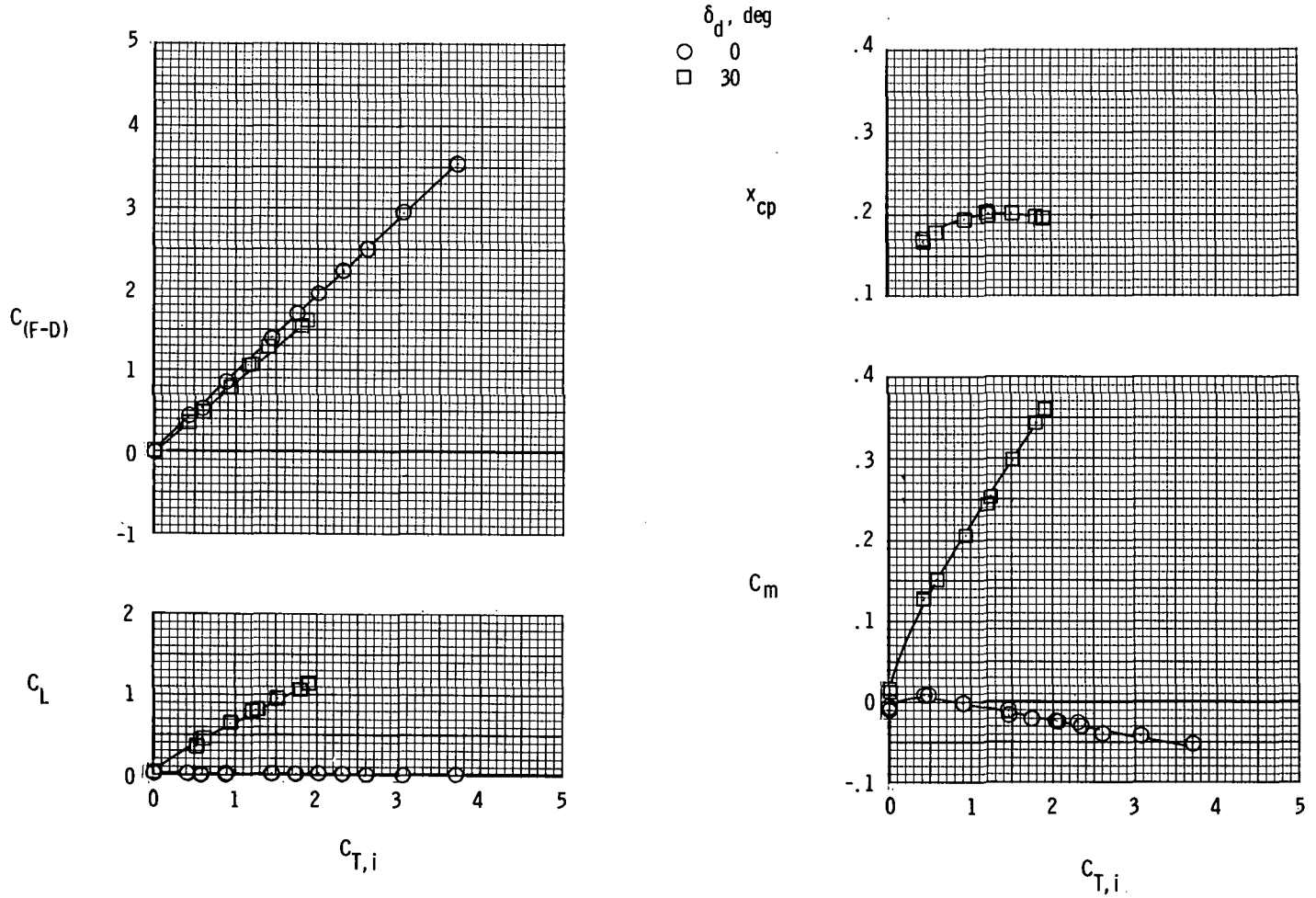

(a) M = 0.20.

Figure 14.- Variation of measured aerodynamic parameters with ideal gross thrust coefficient for model 1 with $i_w = 0.62^o$.

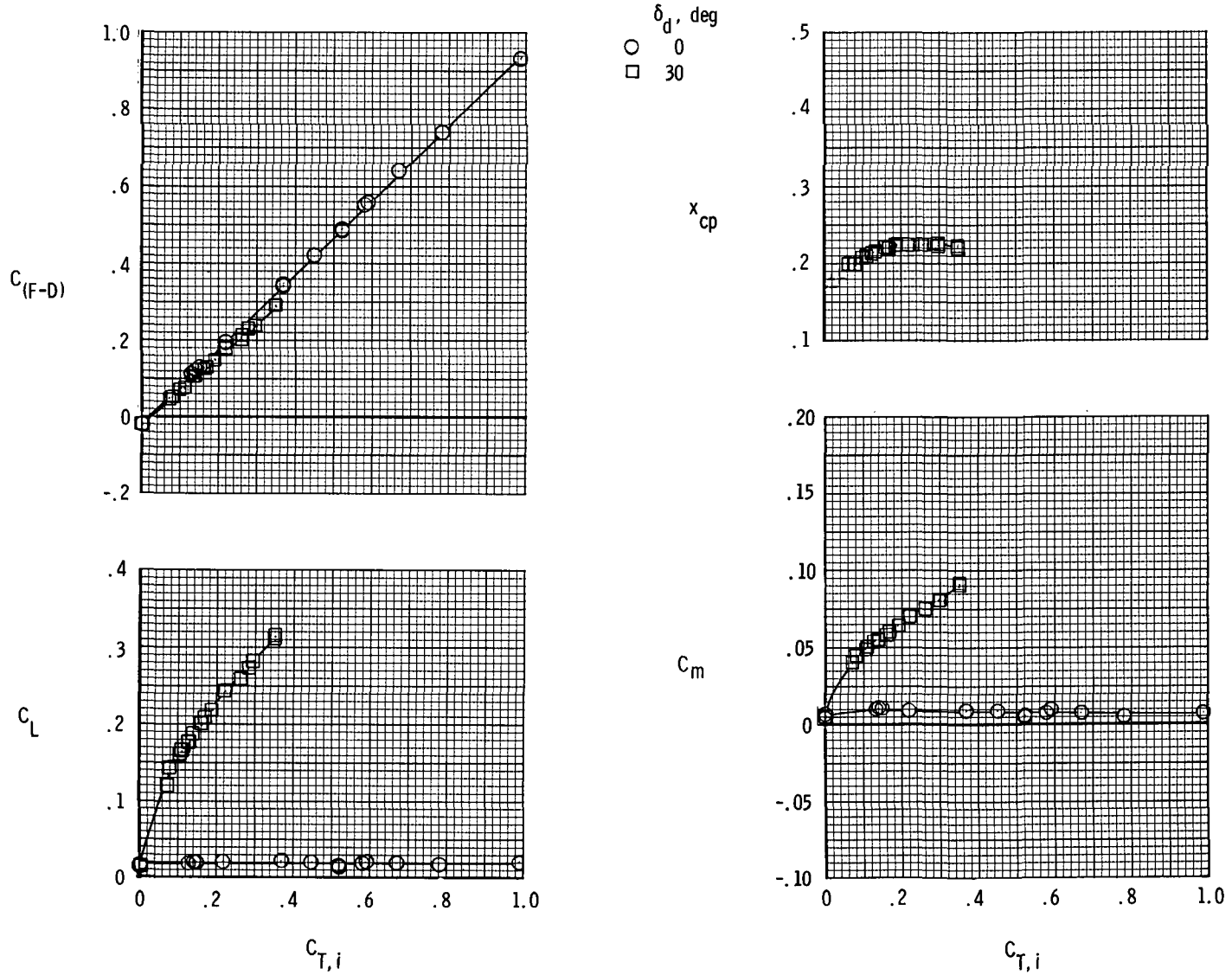

(b) M = 0.40.

Figure 14.- Continued.

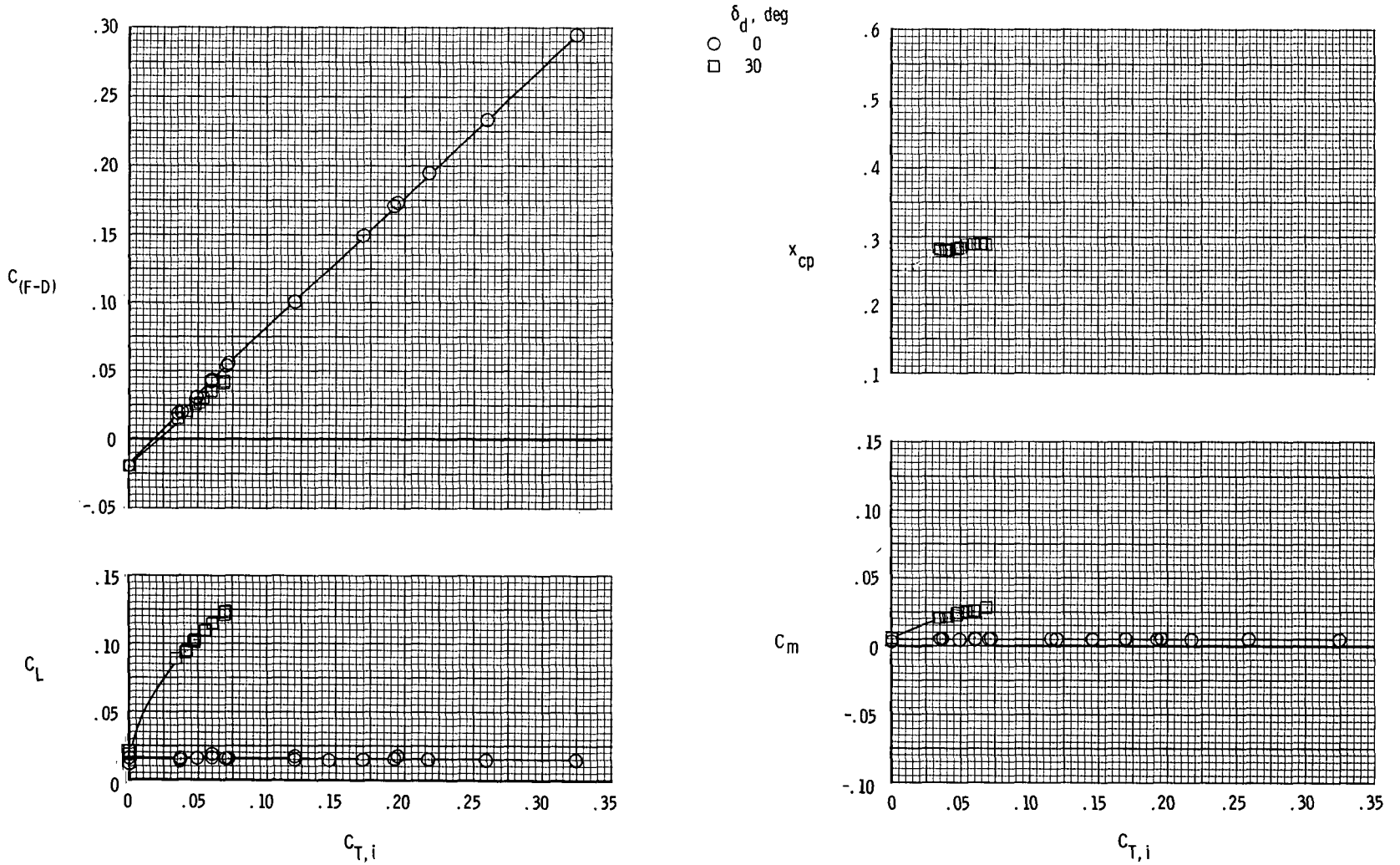

(c) M = 0.70.

Figure 14.- Continued.

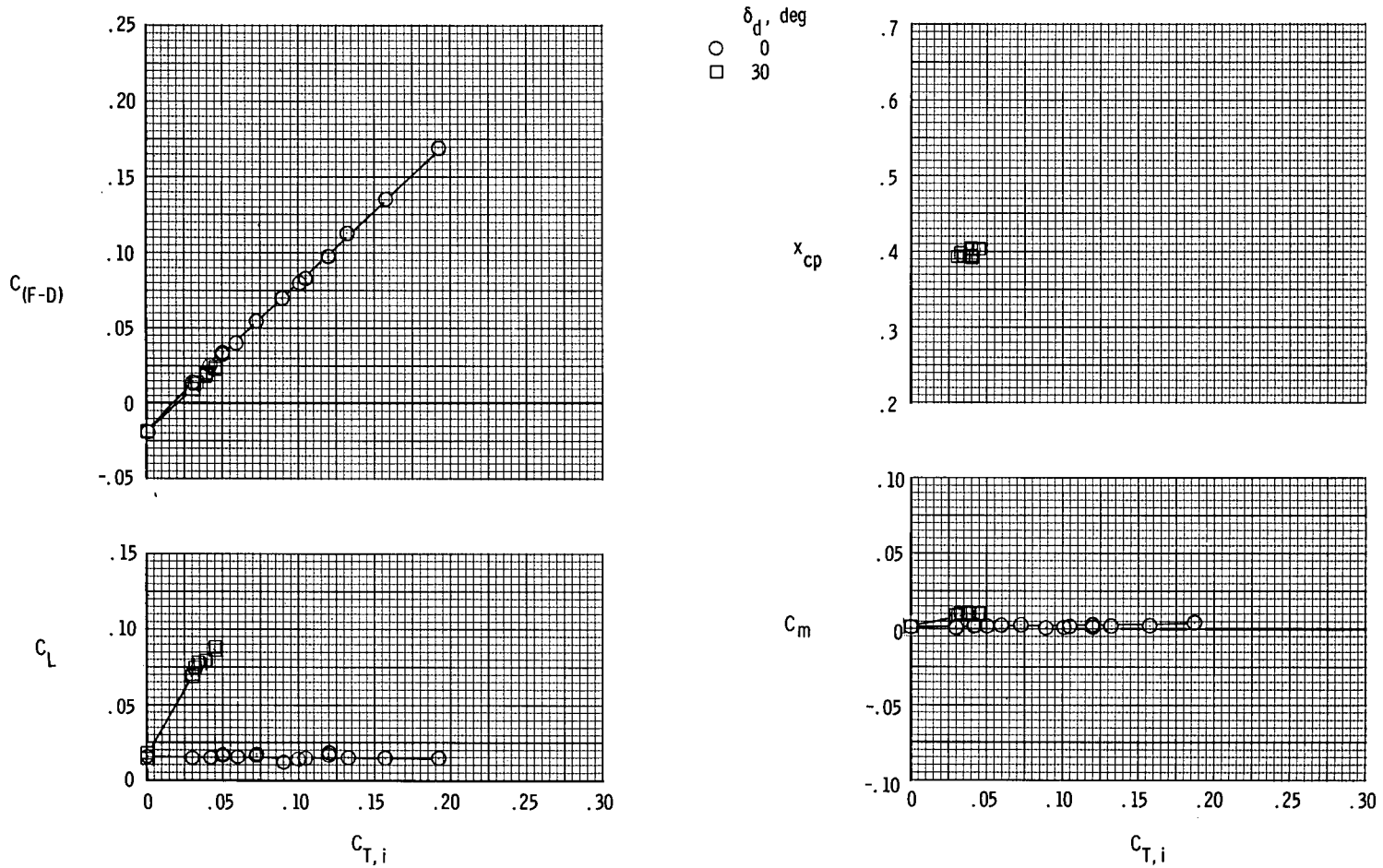

(d) M = 0.90.

Figure 14.- Continued.

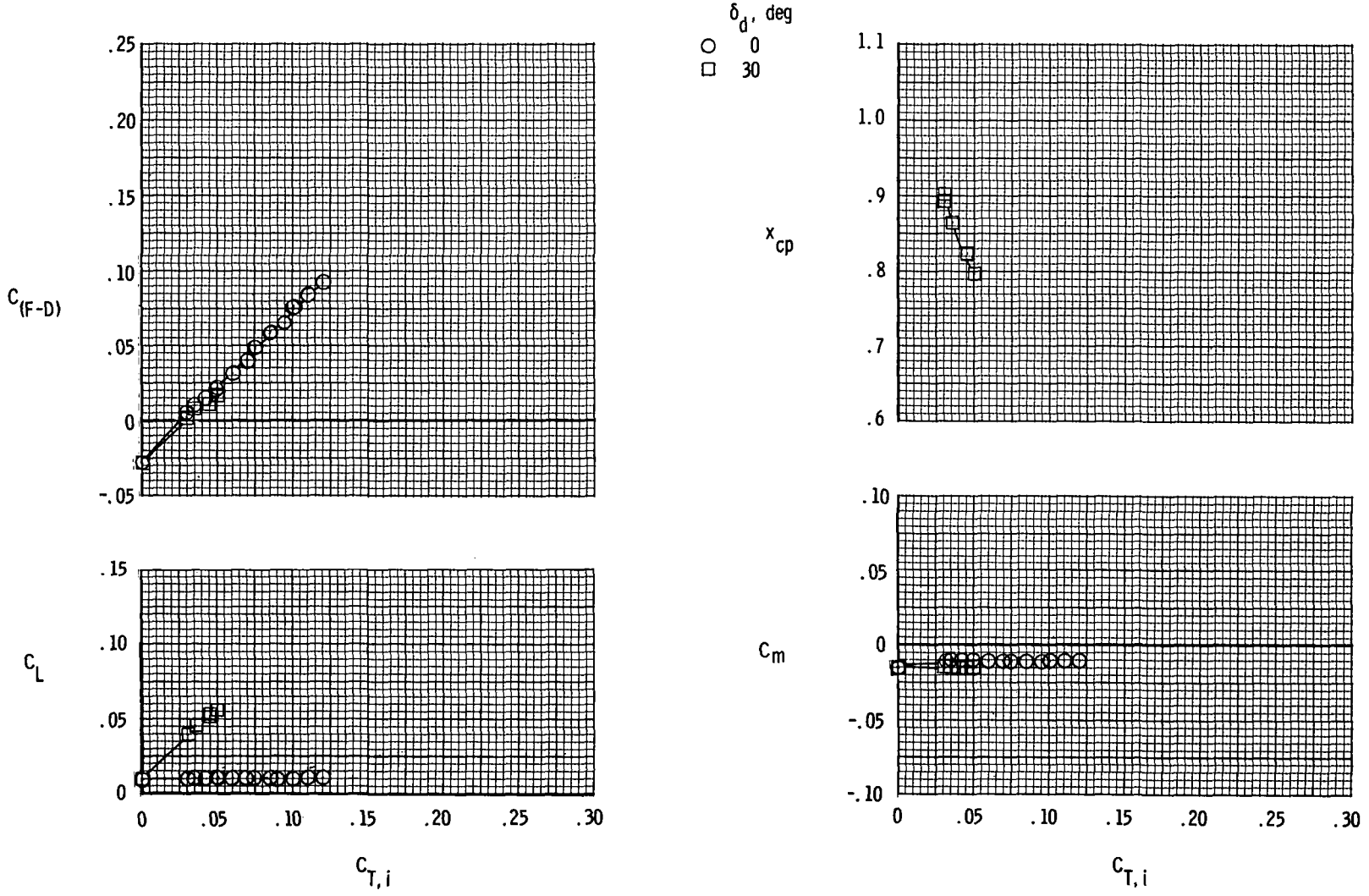

(e) M = 1.20.

Figure 14.- Continued.

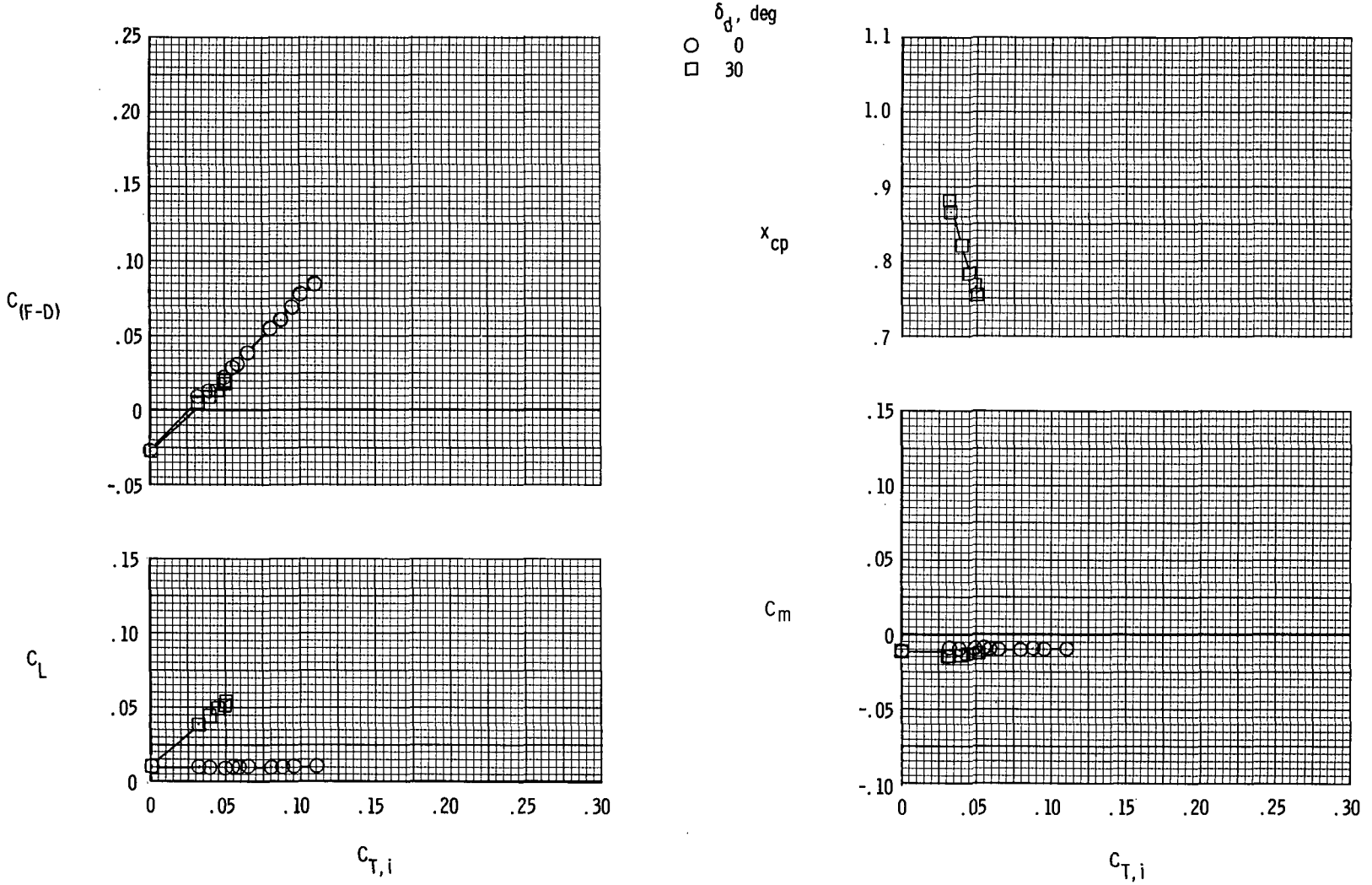

(f) M = 1.30.

Figure 14.- Concluded.

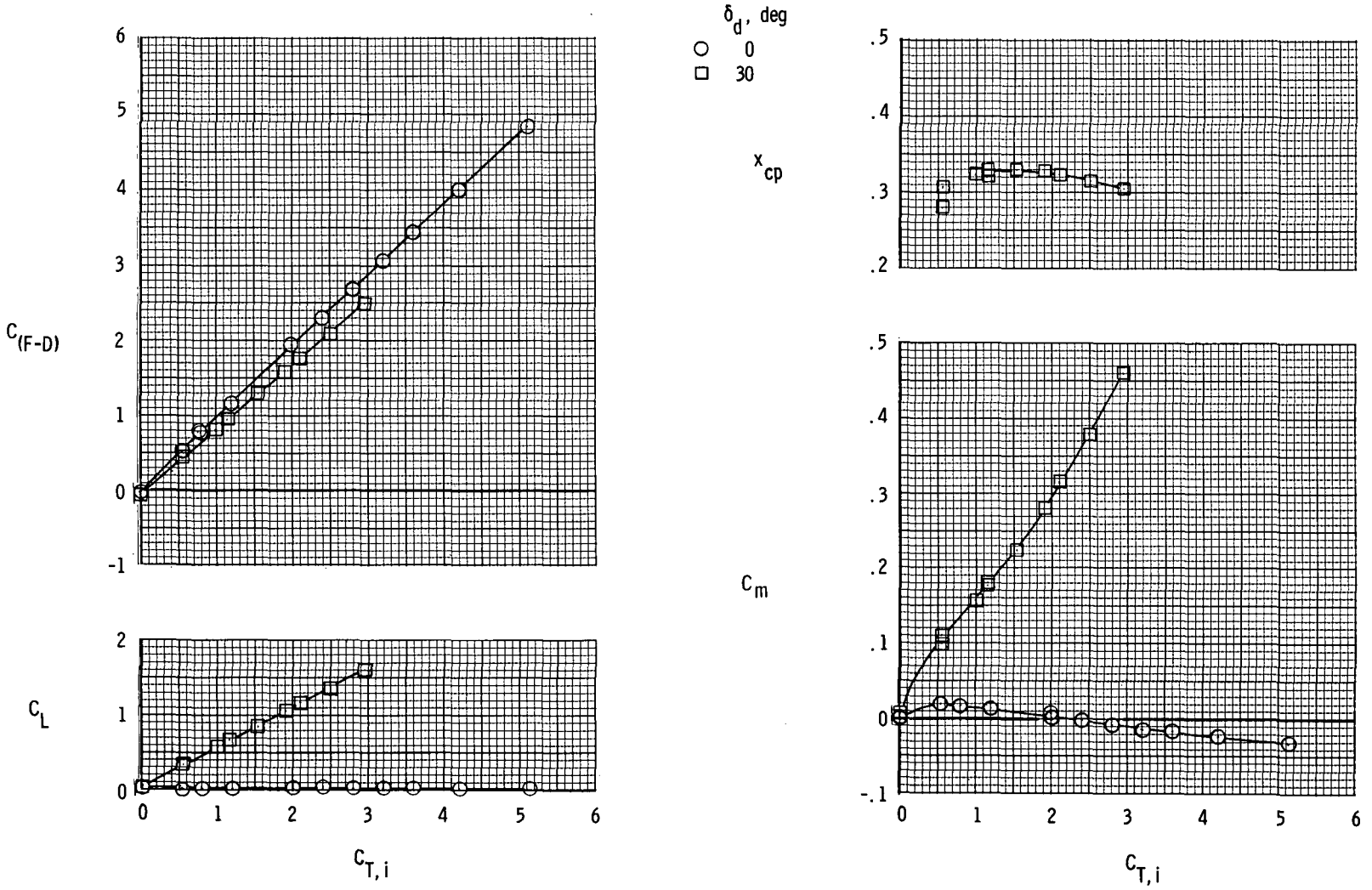

(a) M = 0.20.

Figure 15.- Variation of measured aerodynamic parameters with ideal gross thrust coefficient for model 2 with wings off.

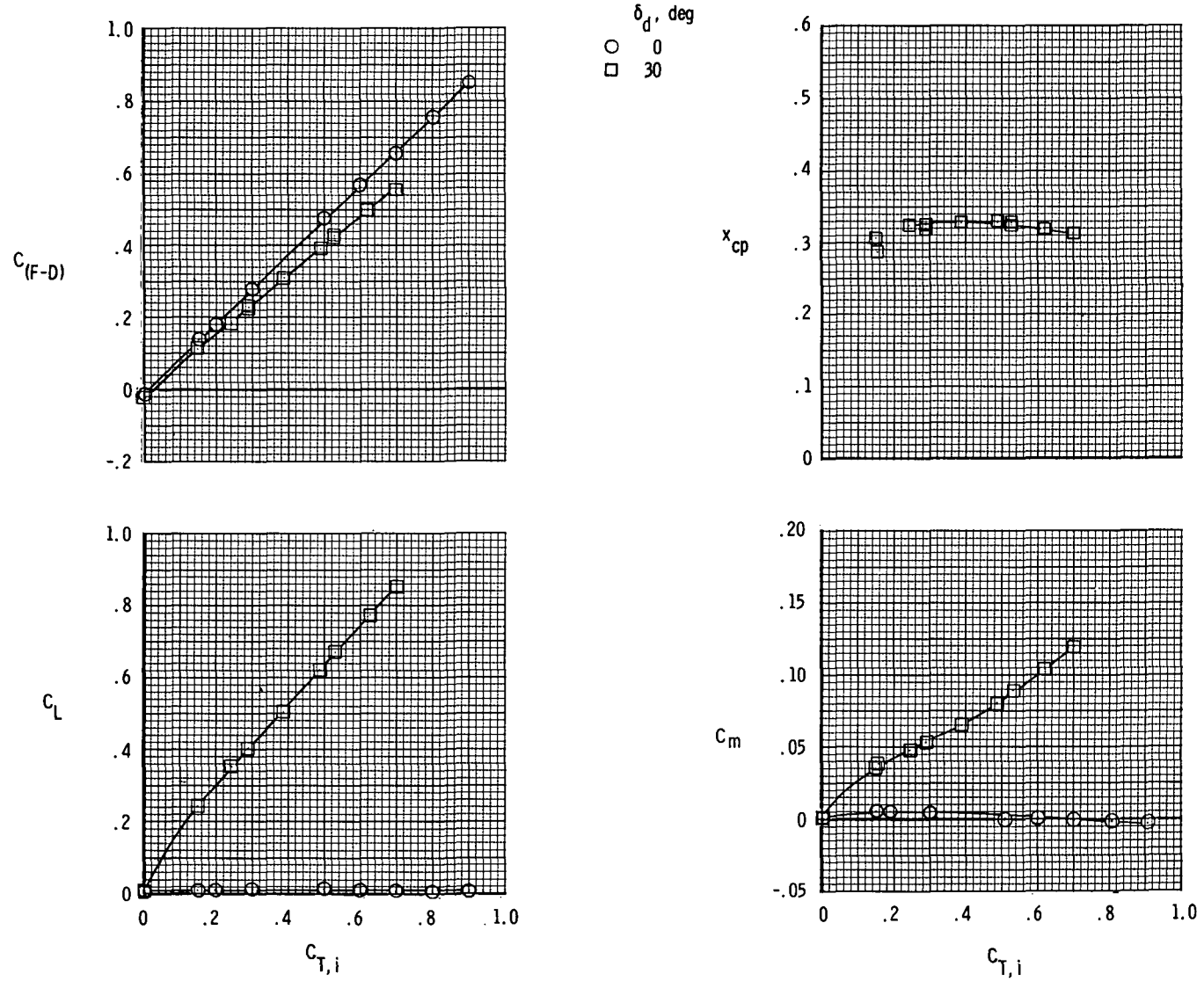

(b) M = 0.40.

Figure 15.- Continued.

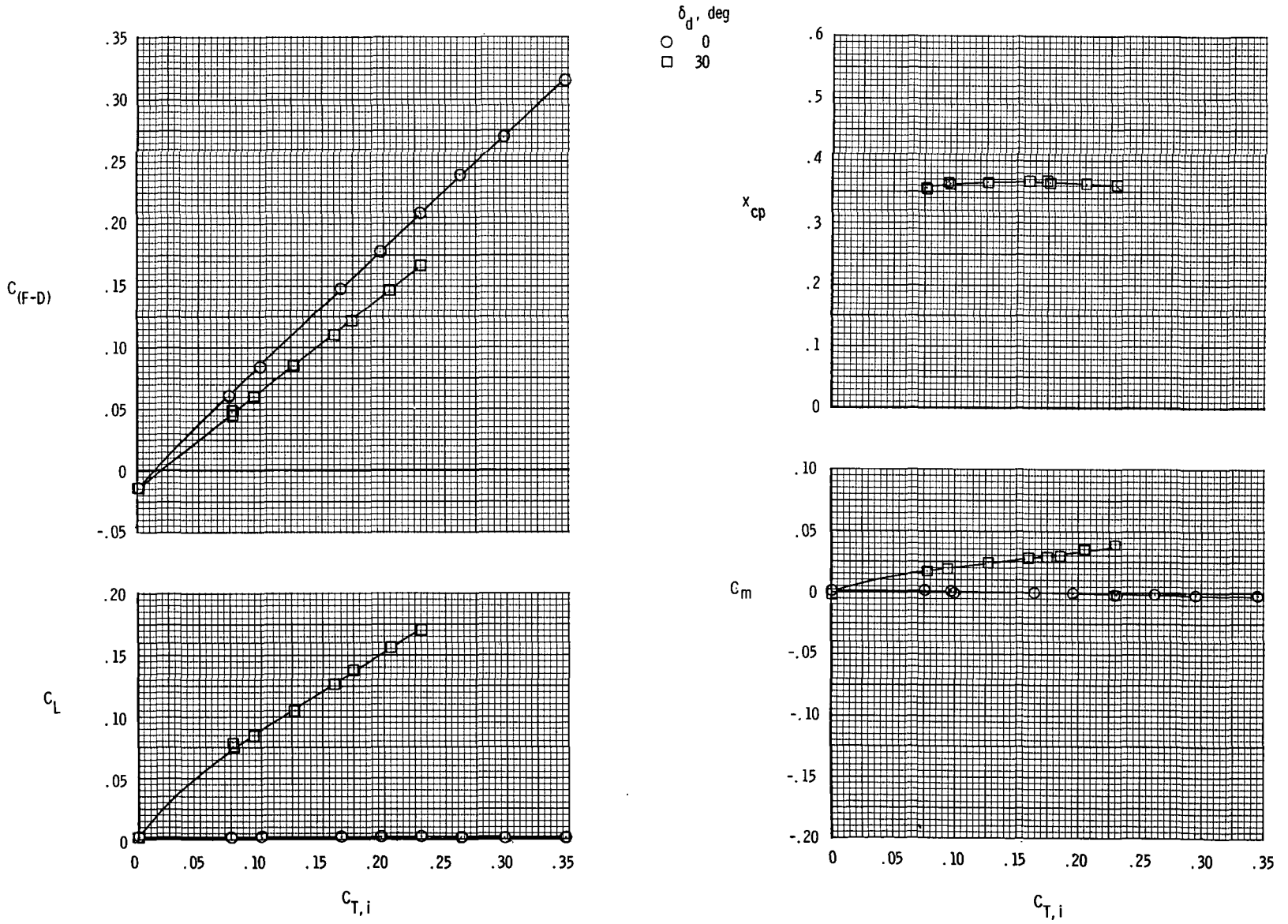

(c) M = 0.70.

Figure 15.- Continued.

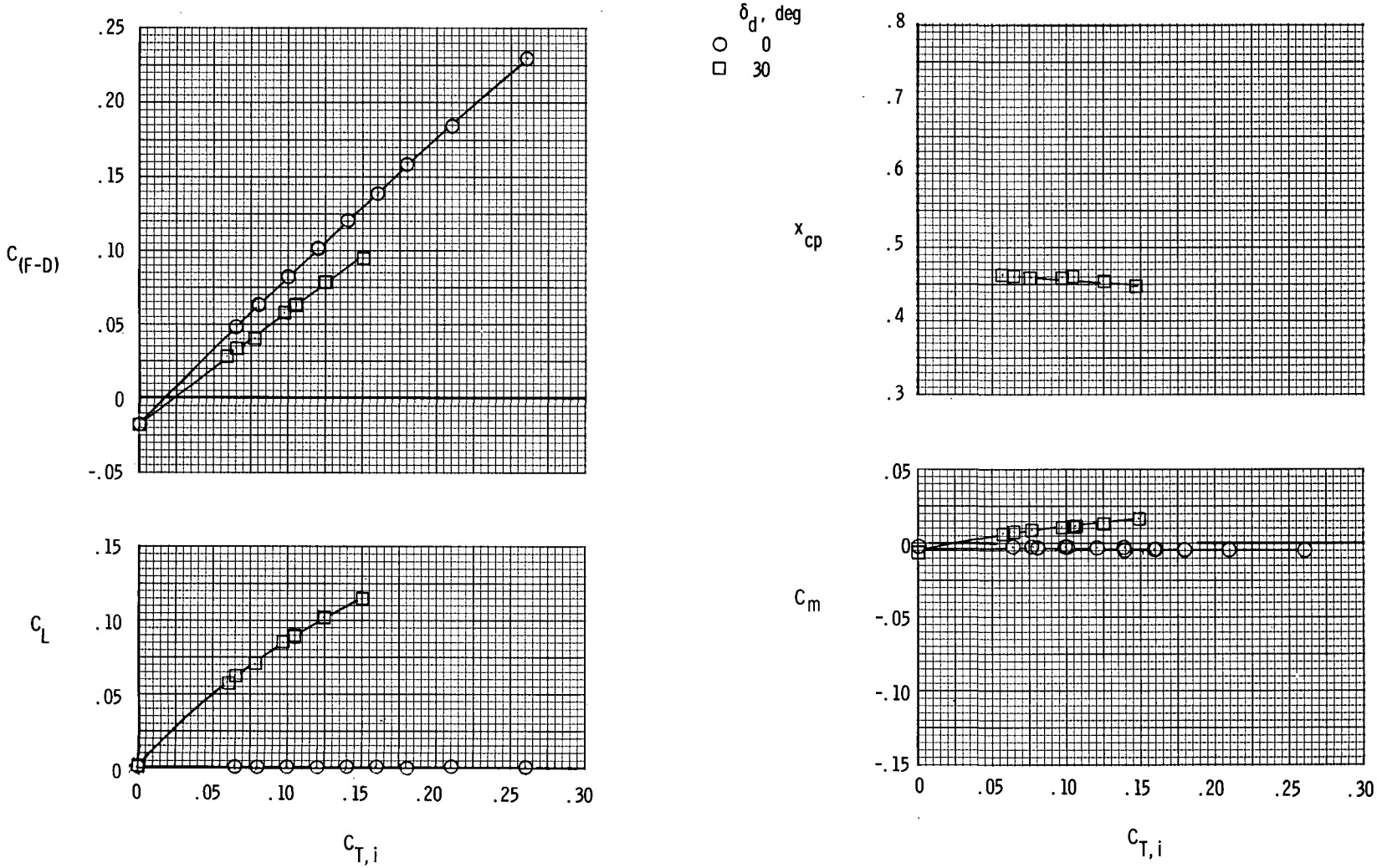

(d) M = 0.90.

Figure 15.- Continued.

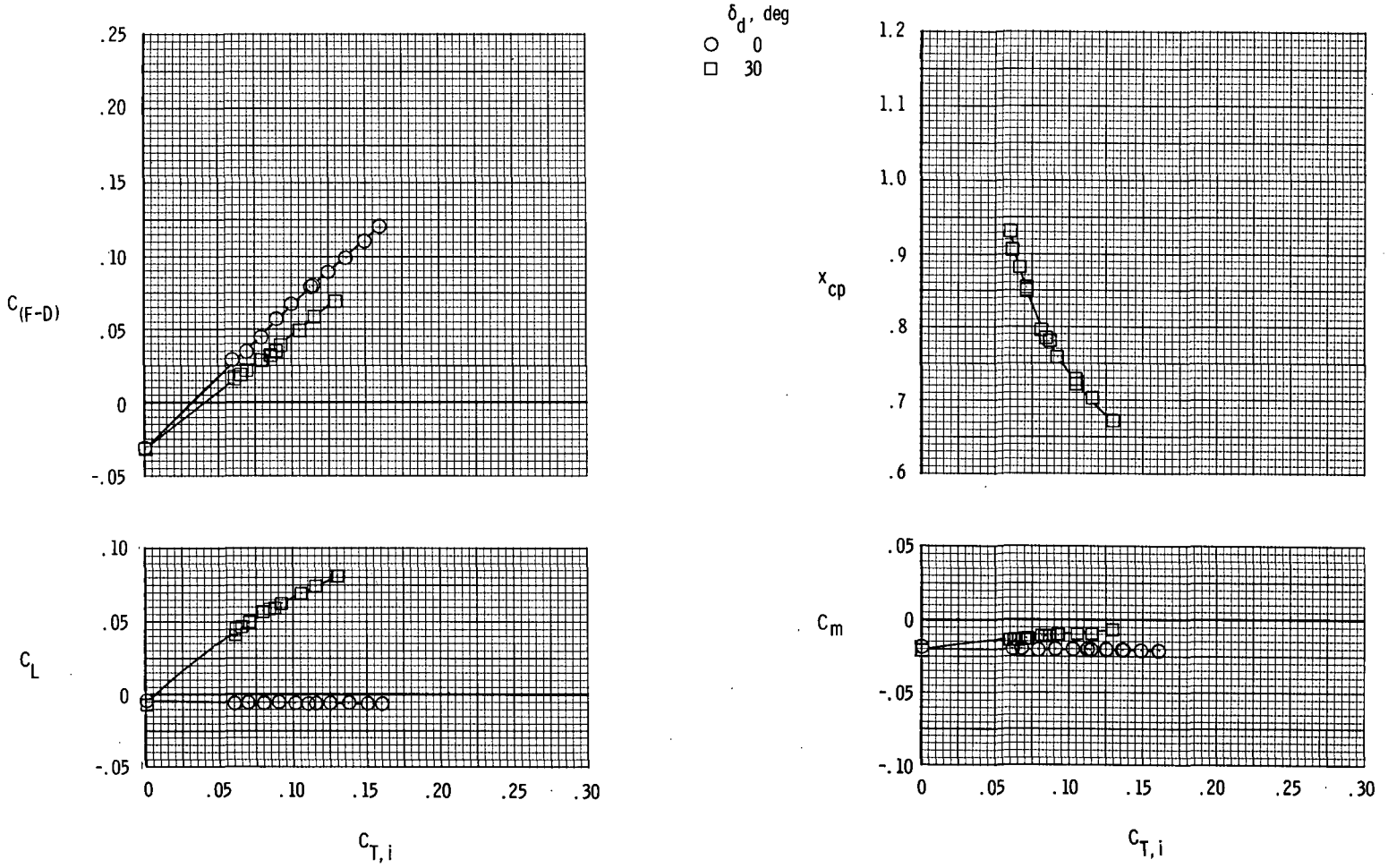

(e) M = 1.20.

Figure 15.- Continued.

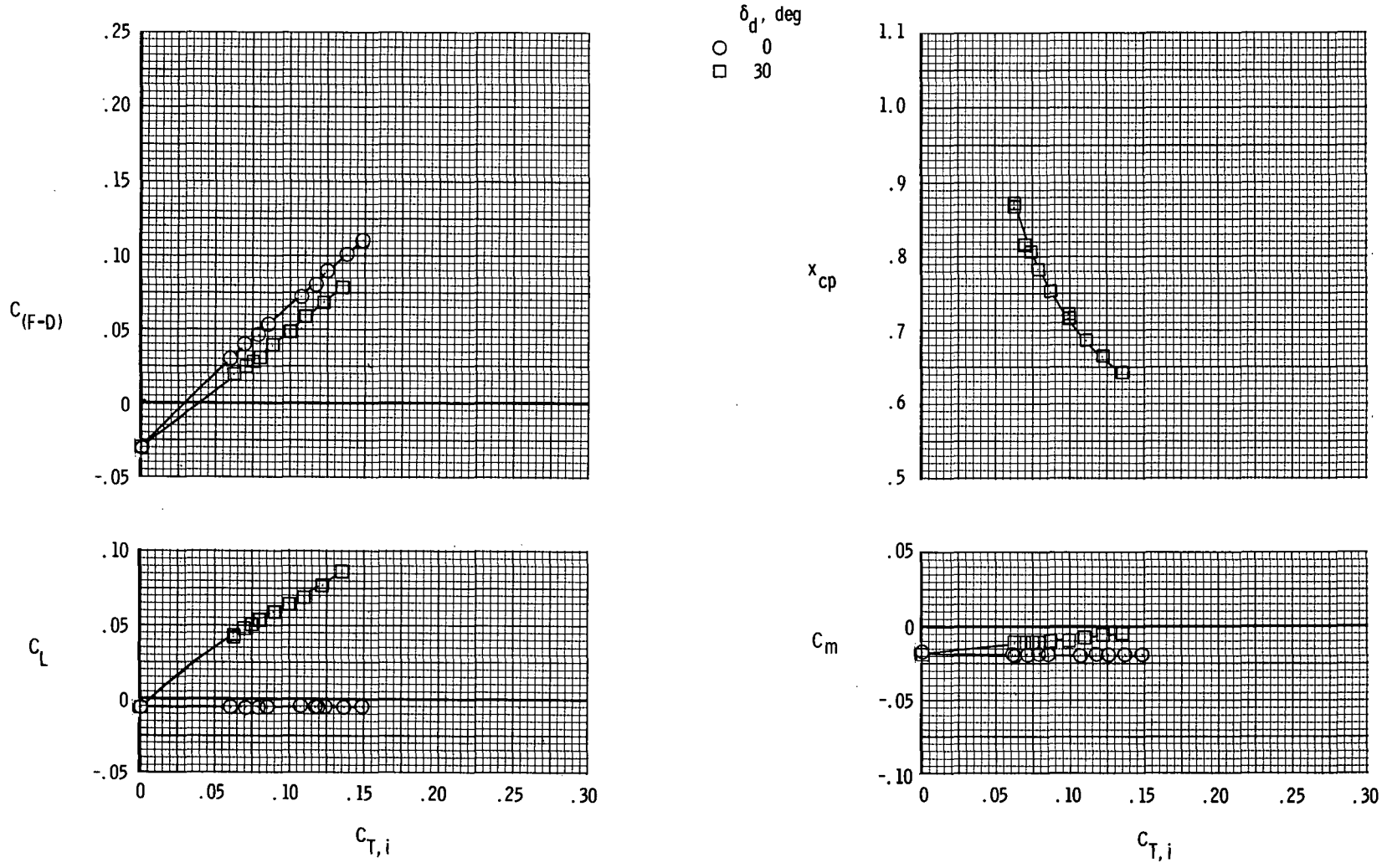

(f) M = 1.30.

Figure 15.- Concluded.

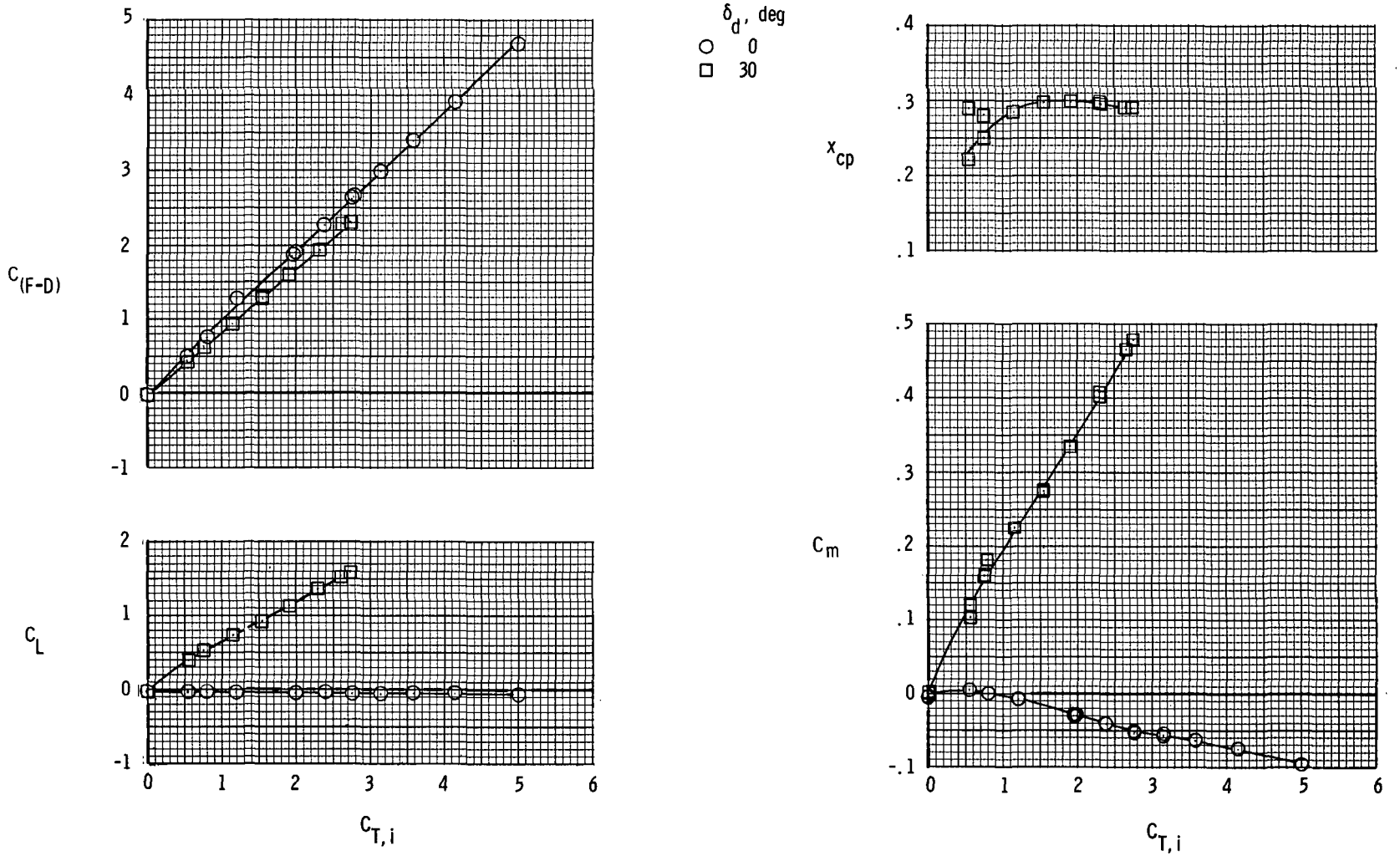

(a) M = 0.20.

Figure 16.- Variation of measured aerodynamic parameters with ideal gross thrust coefficient for model 2 with $i_w = -2.04^o$.

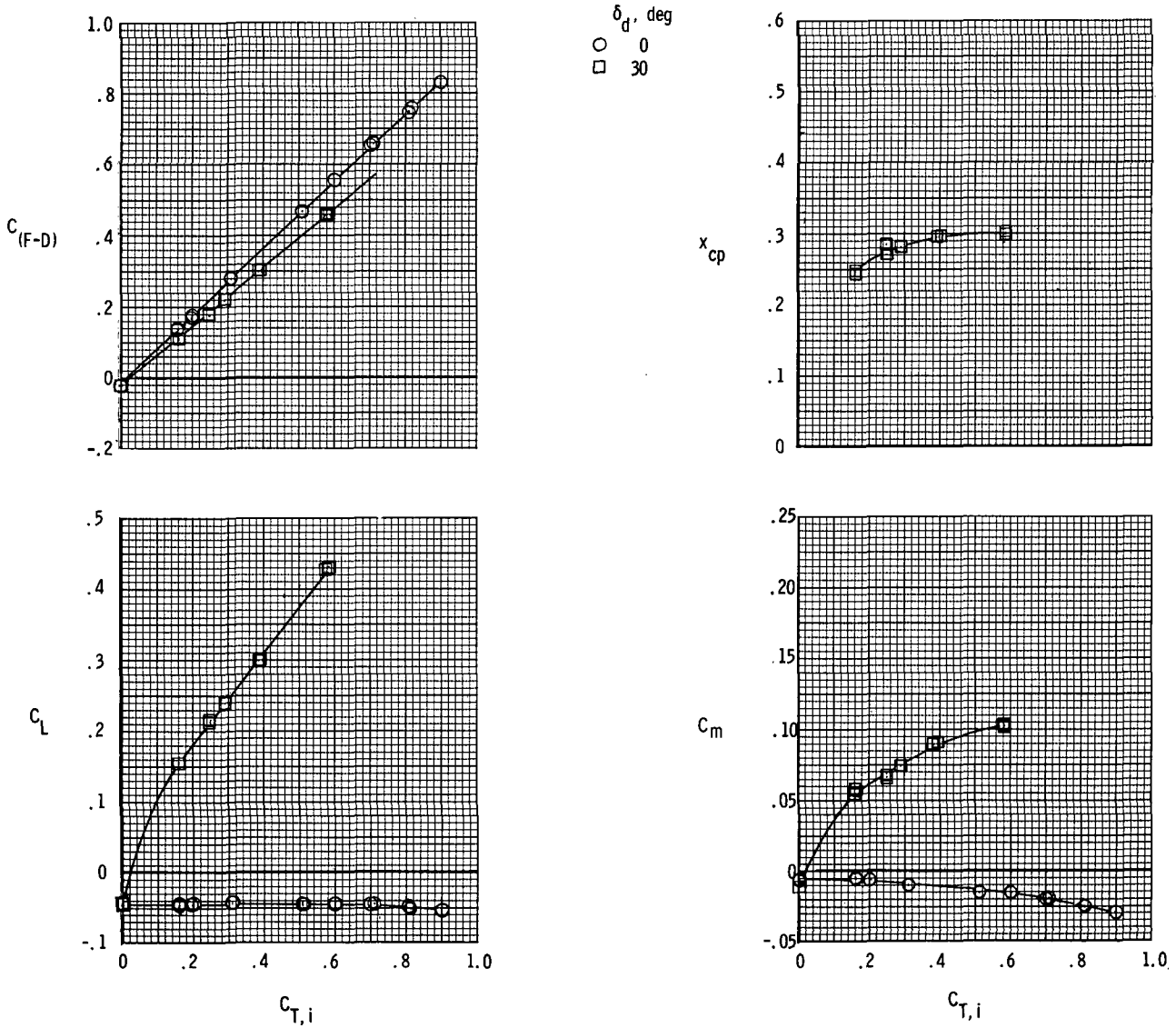

(b) M = 0.40.

Figure 16.- Continued.

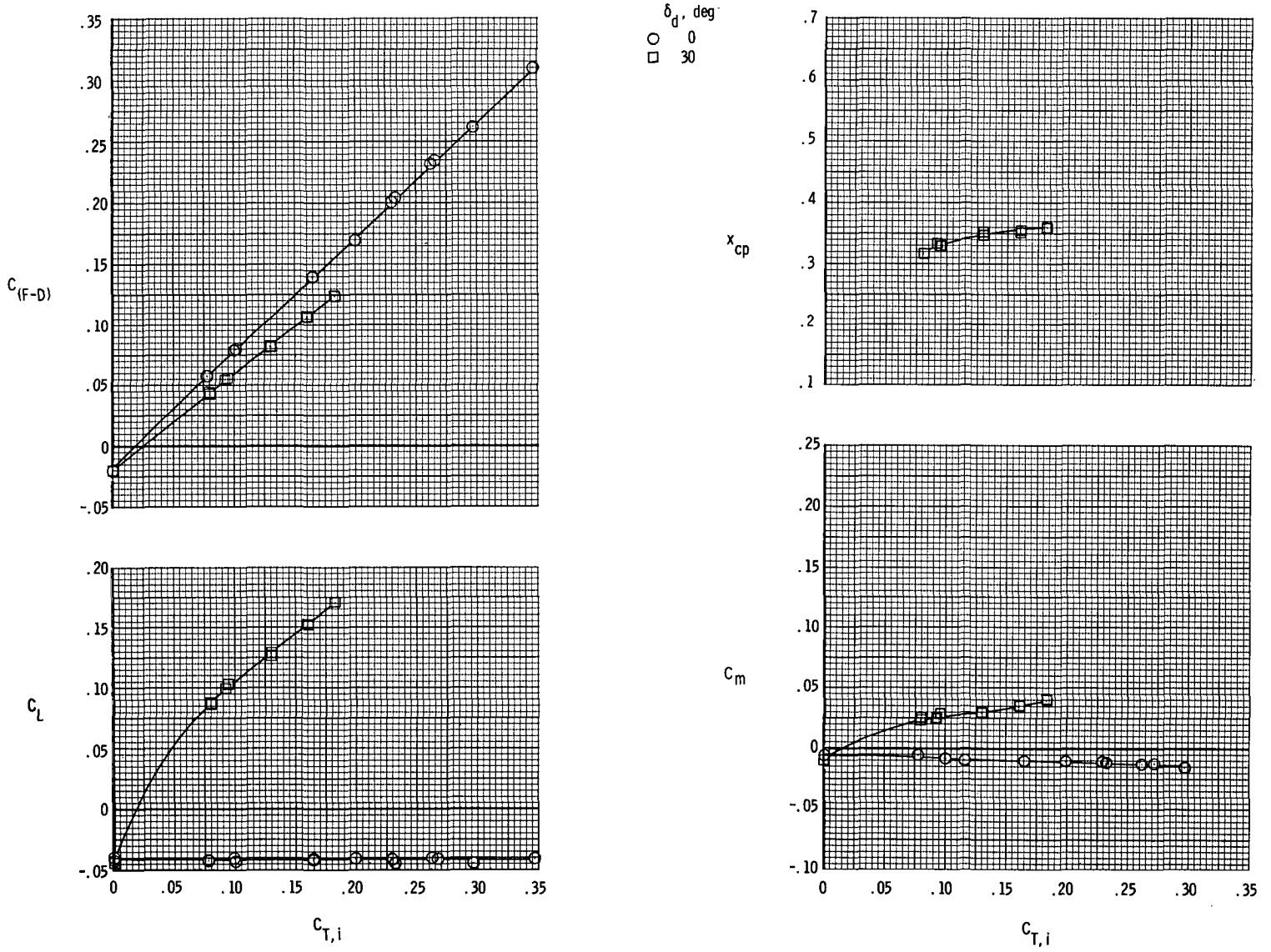

(c) M = 0.70.

Figure 16.- Continued.

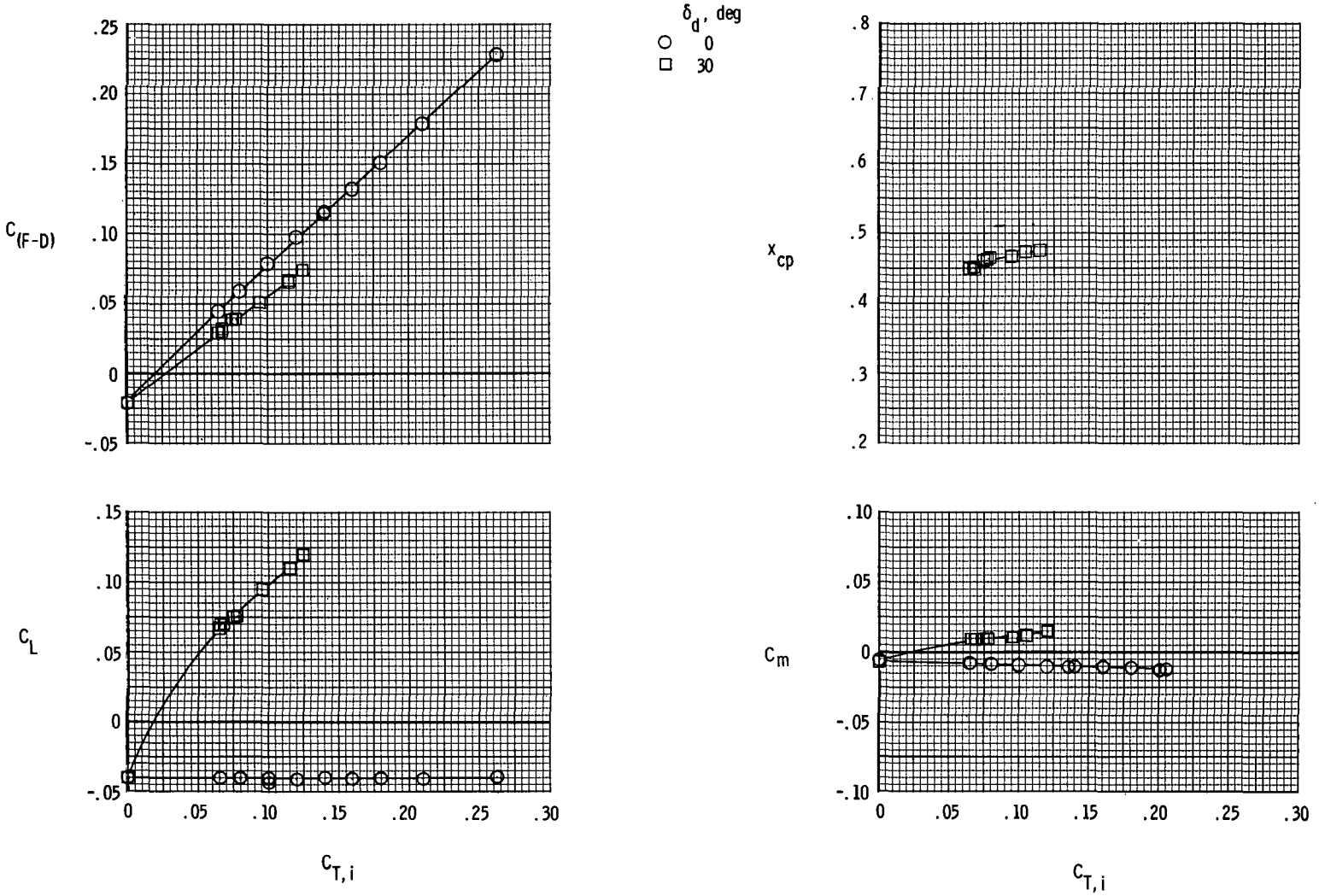

(d) M = 0.90.

Figure 16.- Continued.

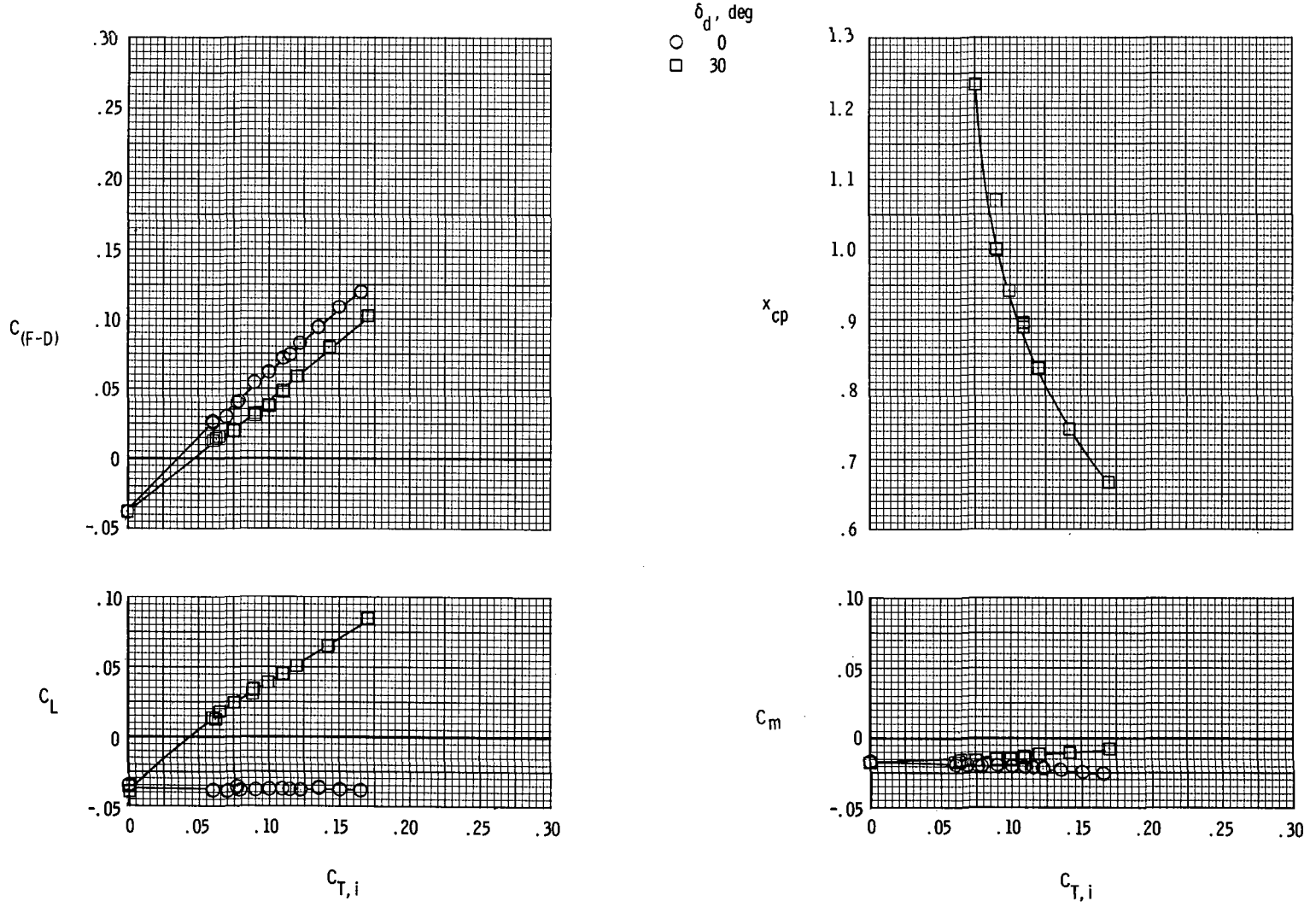

(e) M = 1.20.

Figure 16.- Continued.

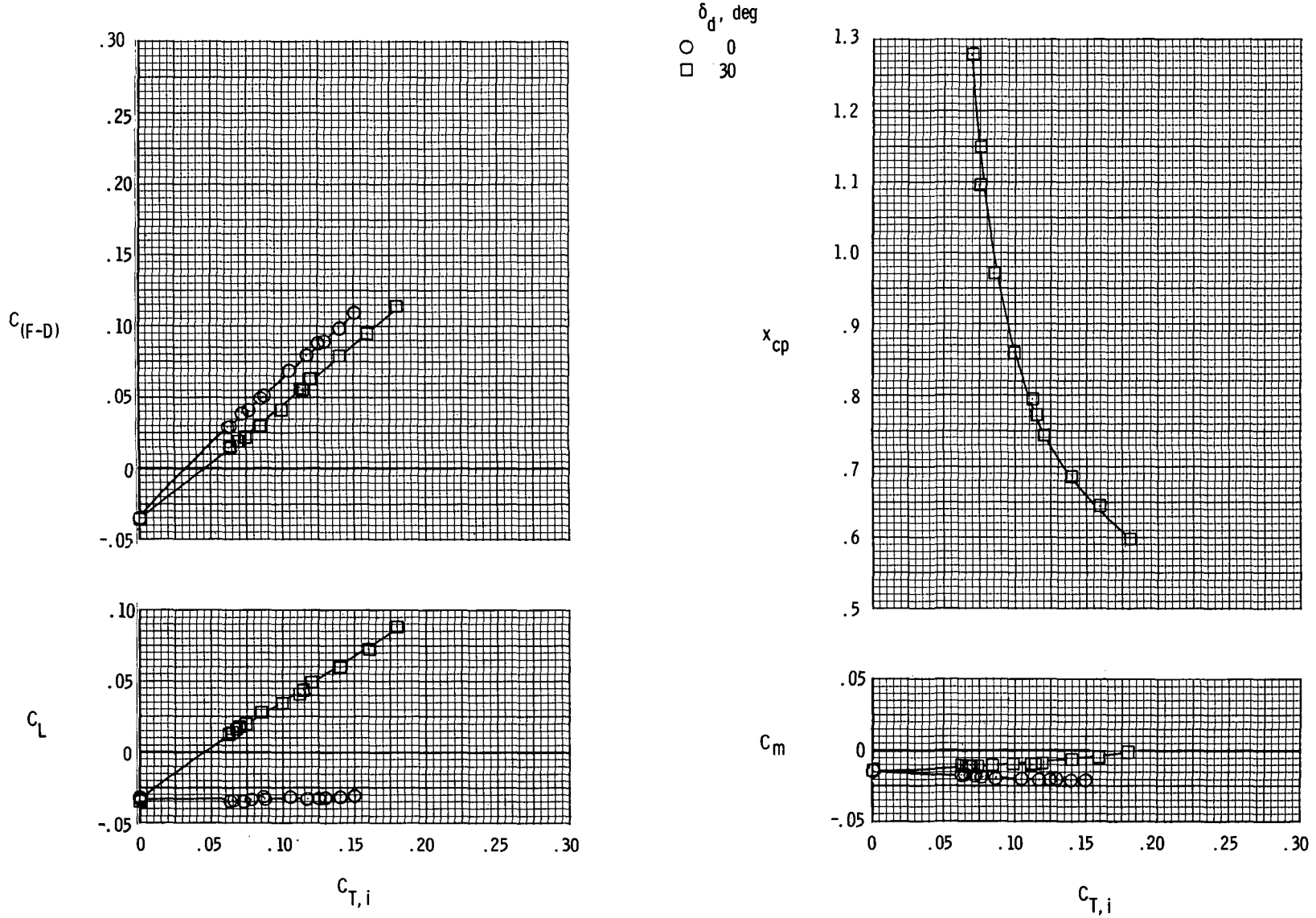

(f) M = 1.30.

Figure 16.- Concluded.

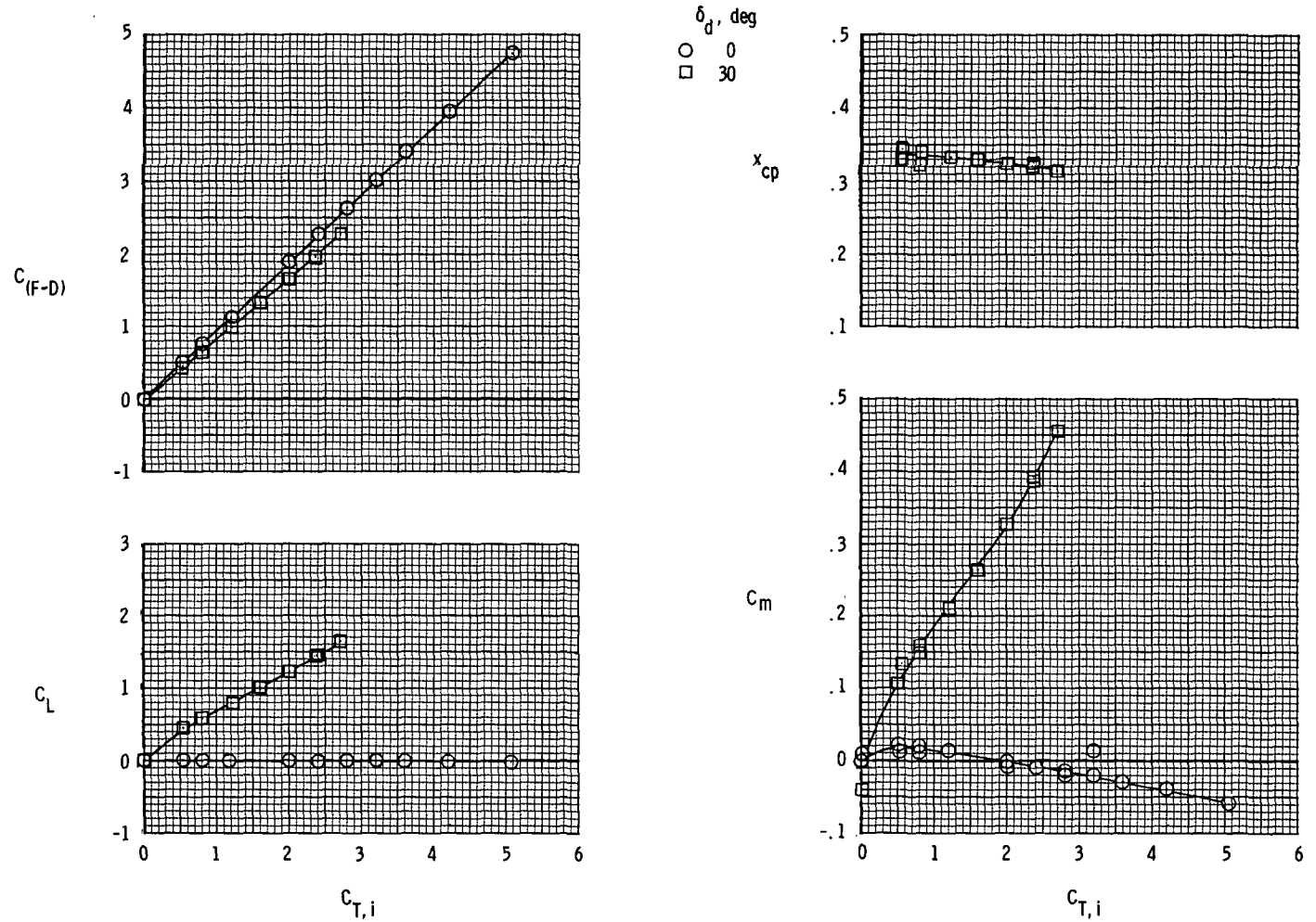

(a) M = 0.20.

Figure 17.- Variation of measured aerodynamic parameters with ideal gross thrust coefficient for model 2 with $i_w = -0.18^o$.

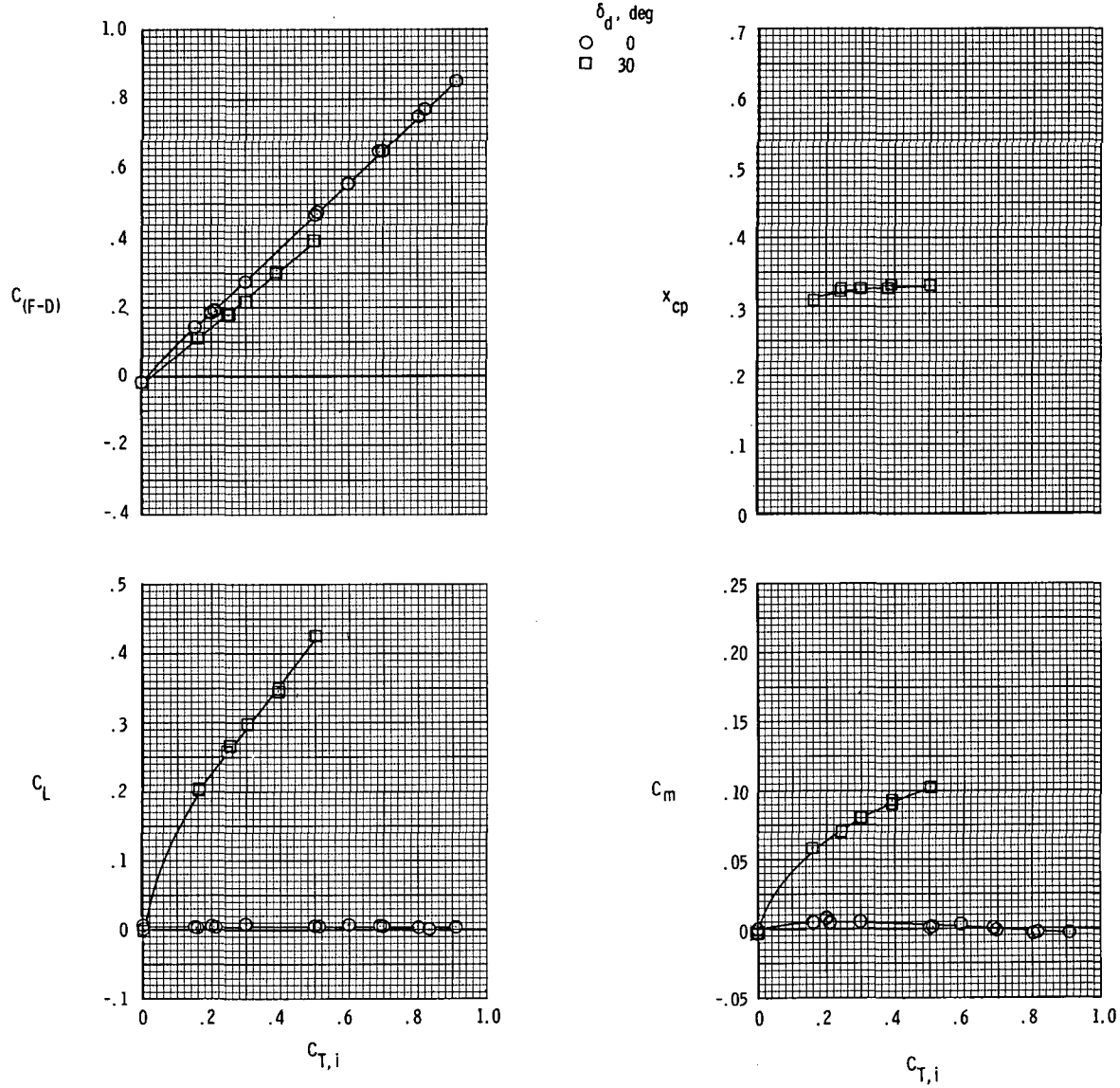

(b) M = 0.40.

Figure 17.- Continued.

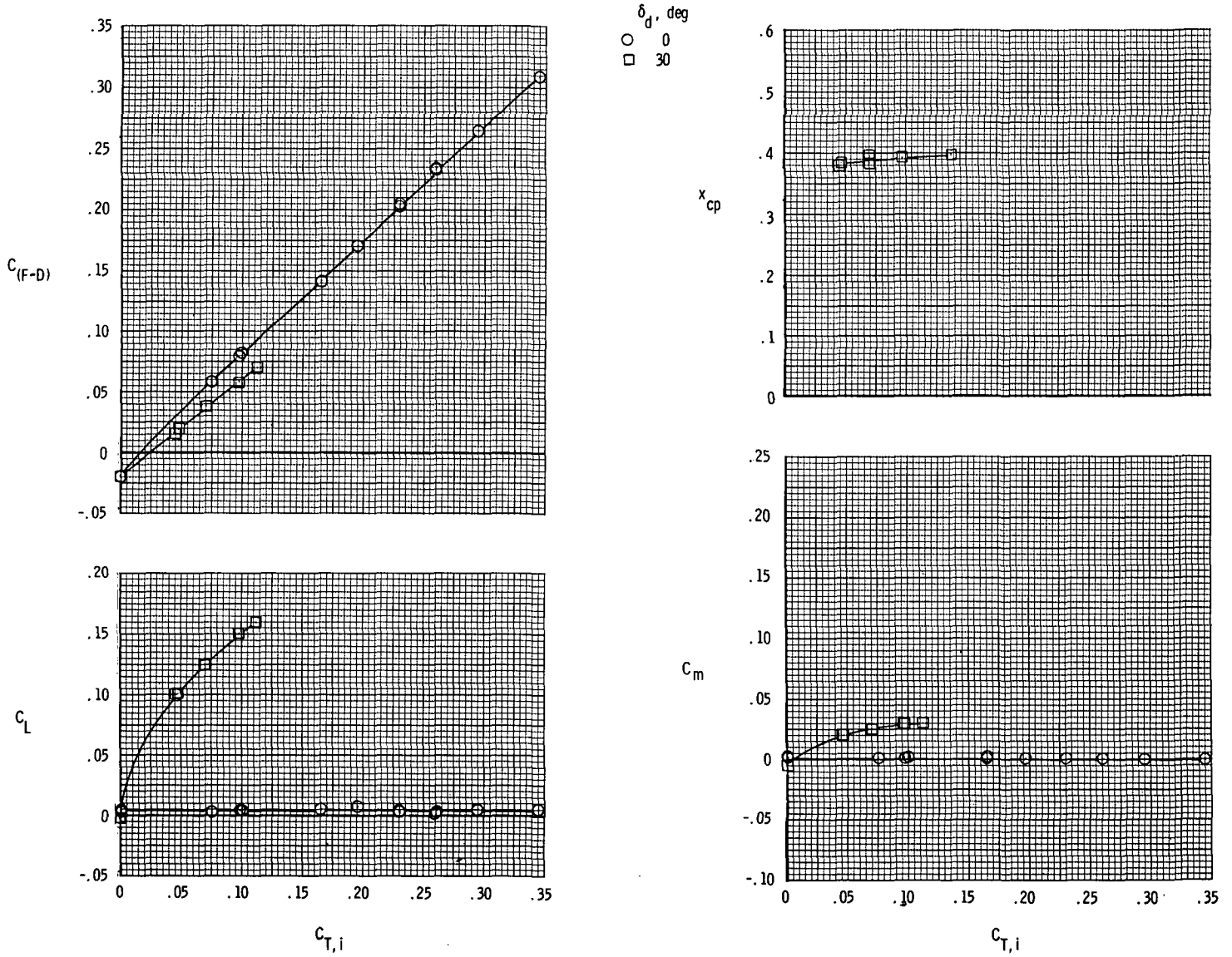

(c) M = 0.70.

Figure 17.- Continued.

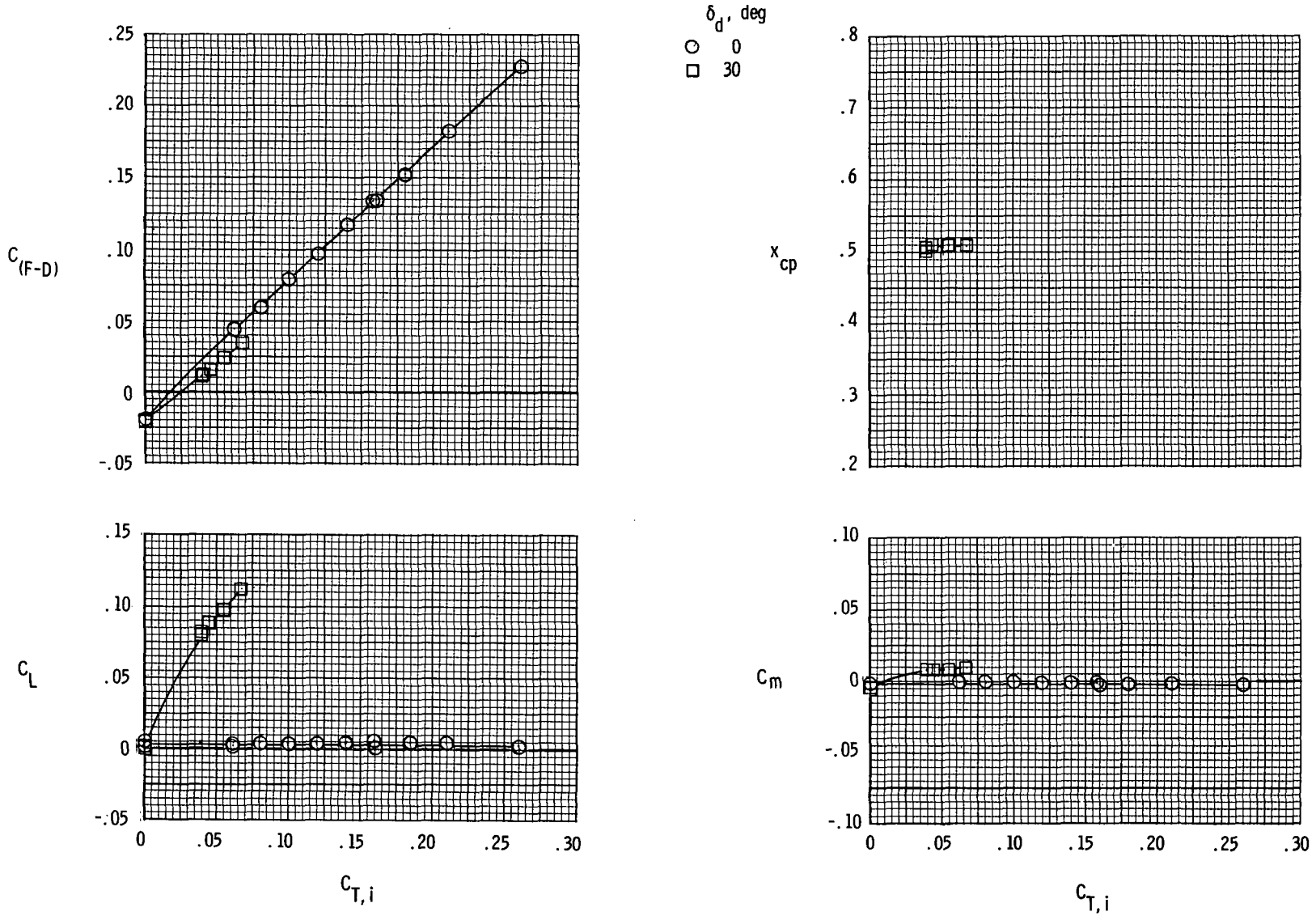

(d) M = 0.90.

Figure 17.- Continued.

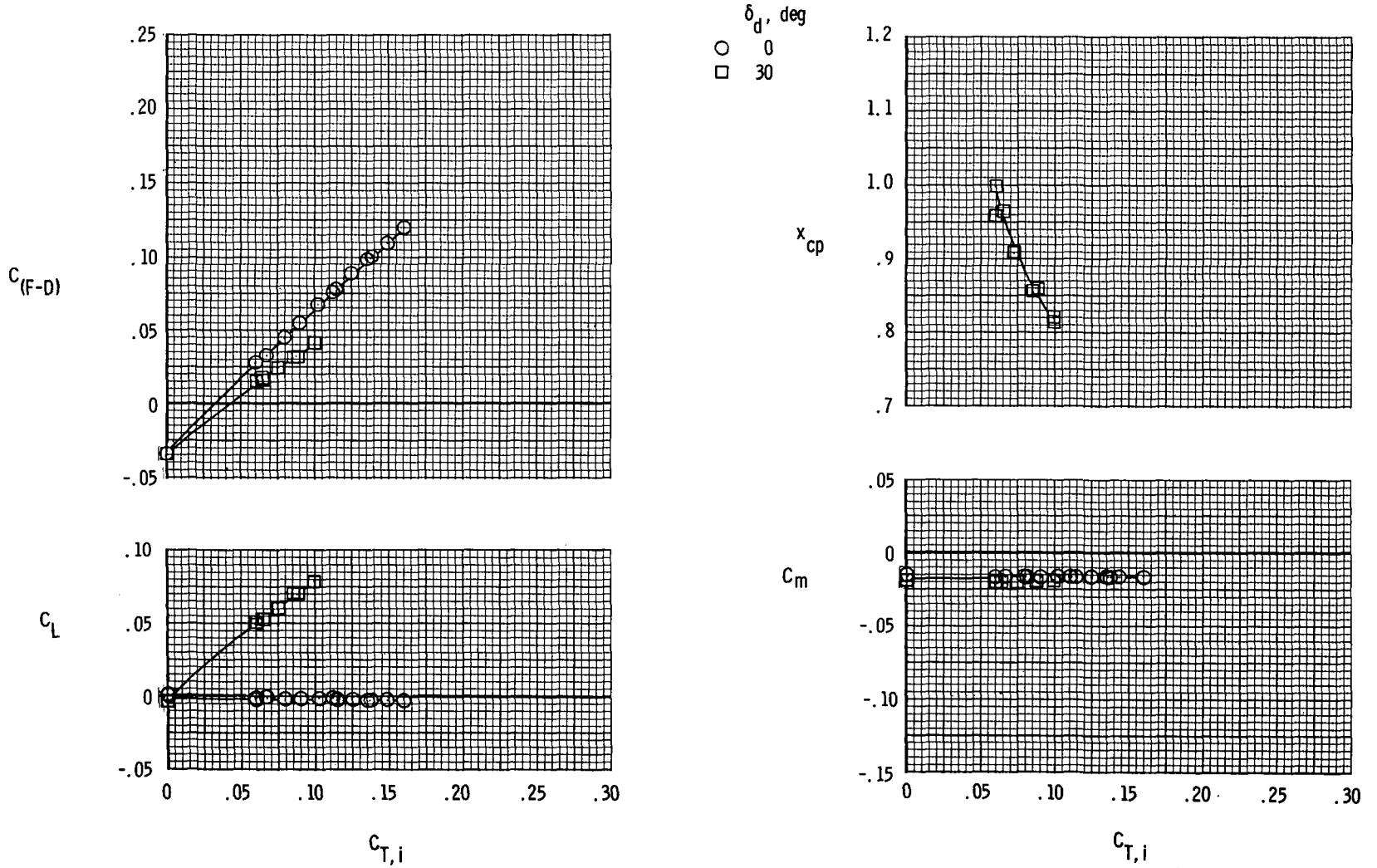

(e) M = 1.20.

Figure 17.- Continued.

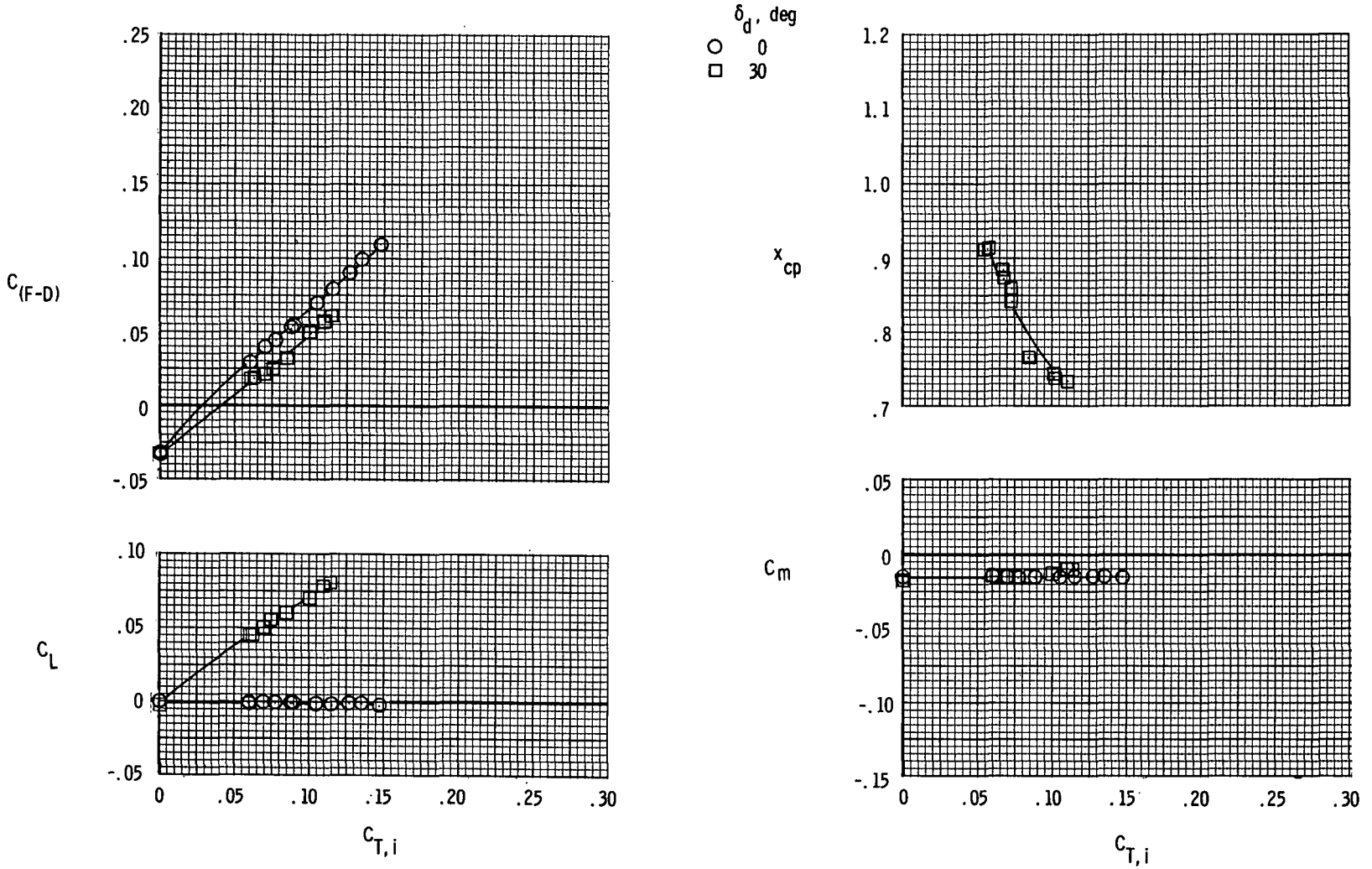

(f) M = 1.30.

Figure 17.- Concluded.

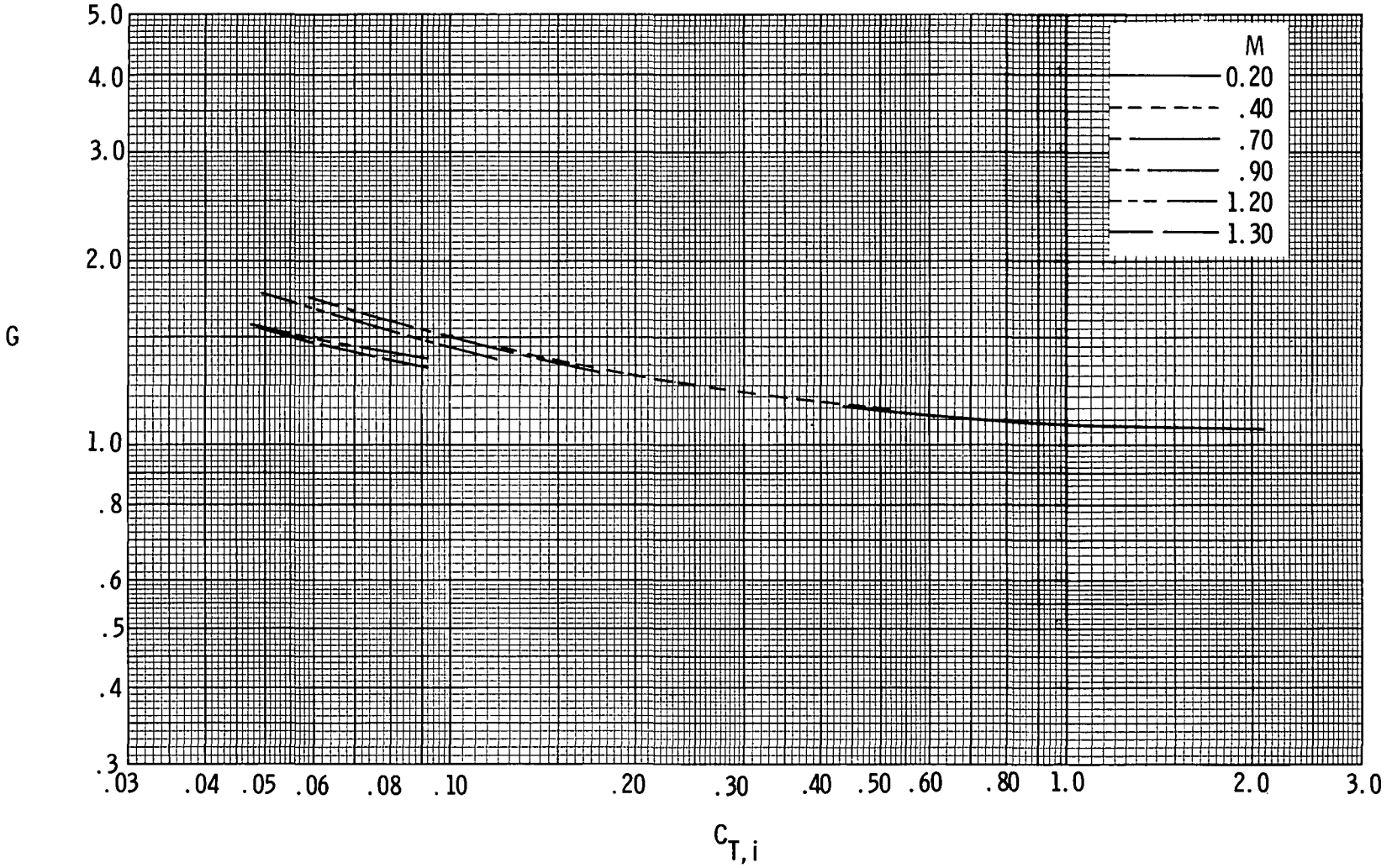

(a) Wings off.

Figure 18.- Variation of gain factor with ideal gross thrust coefficient for model 1.

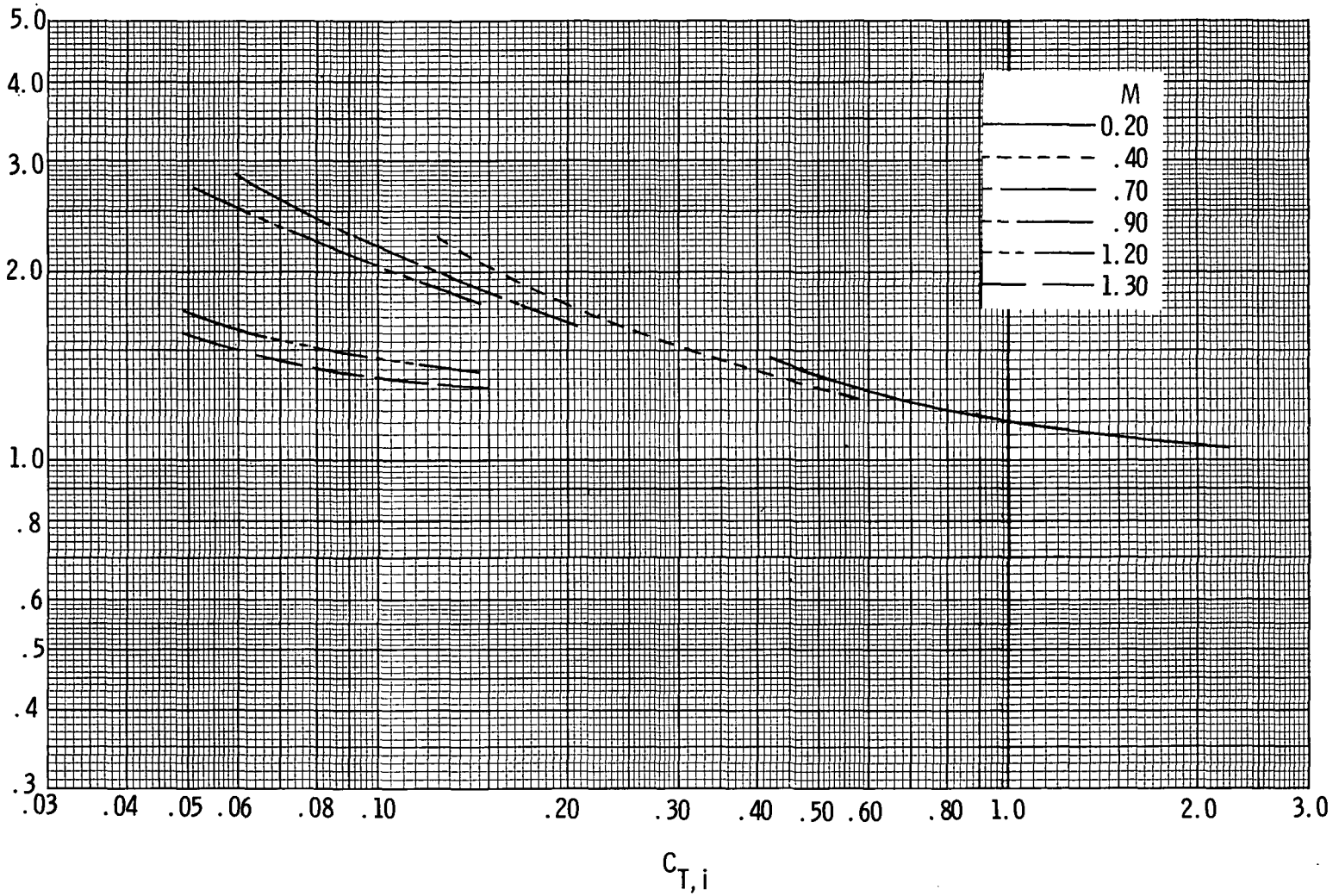

(b) $i_w = -2.26^o$.

Figure 18.- Continued.

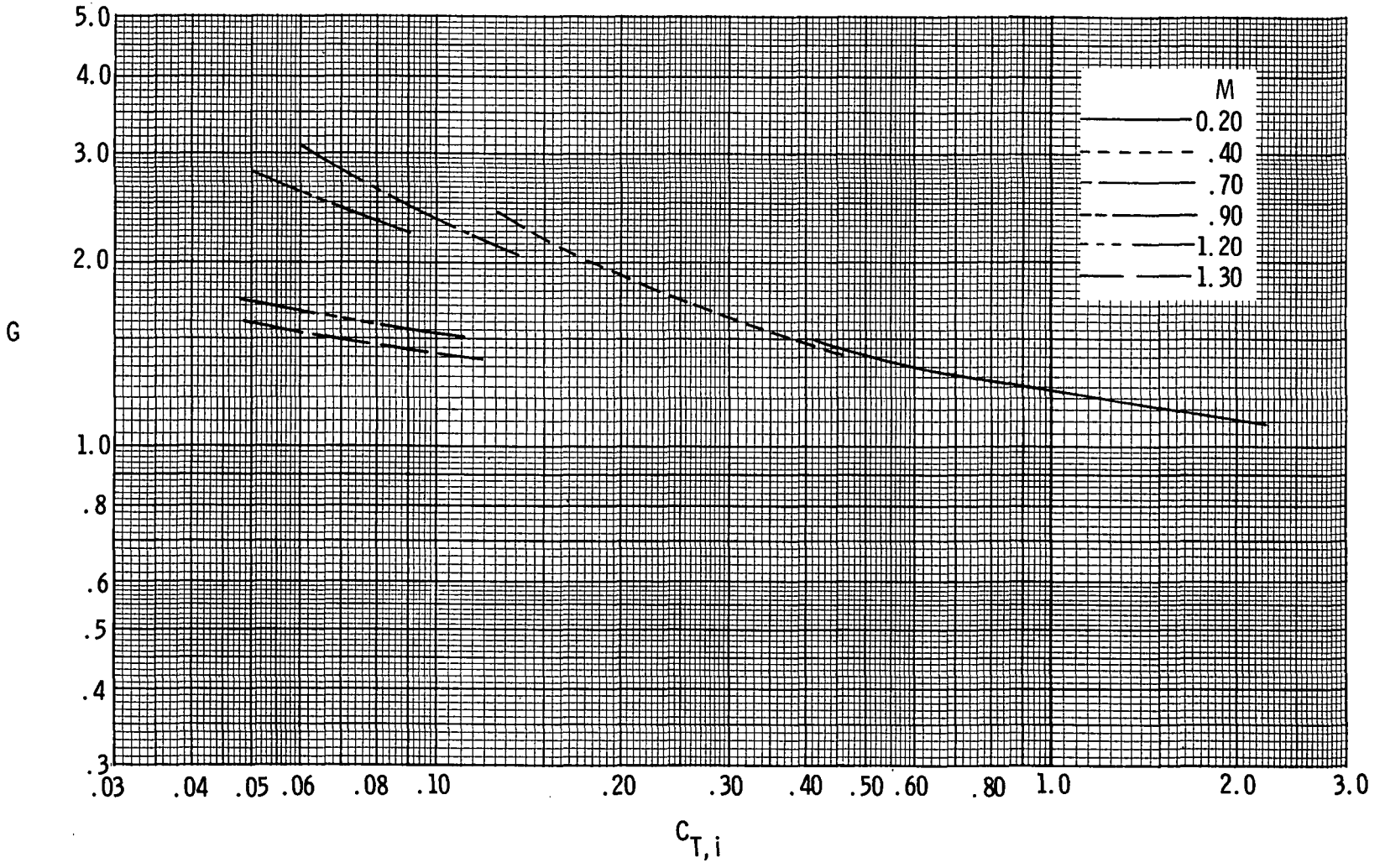

(c) $i_w = -1.38^o$.

Figure 18.- Continued.

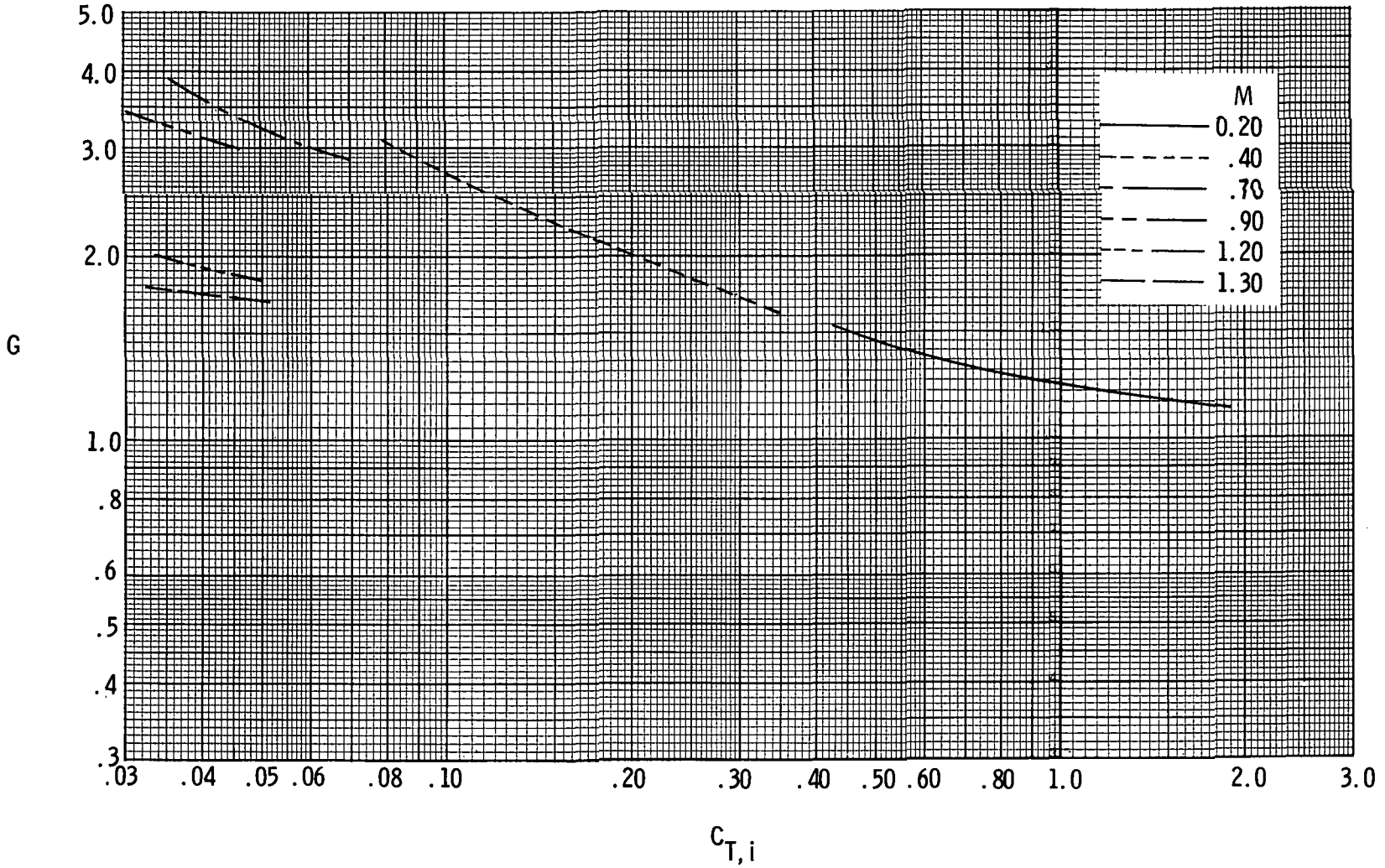

(d) $i_w = 0.62^o$.

Figure 18.- Concluded.

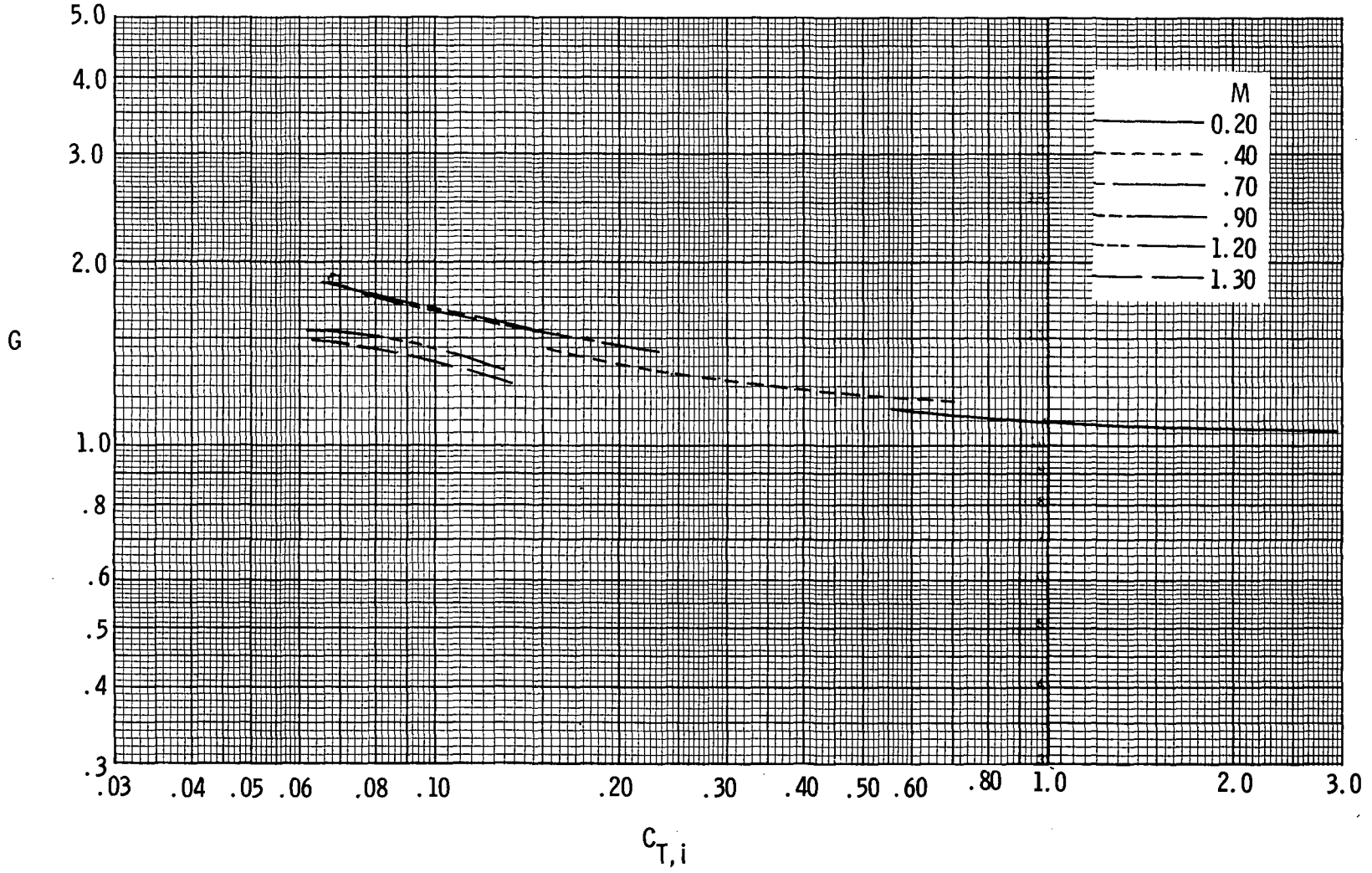

(a) Wings off.

Figure 19.- Variation of gain factor with ideal gross thrust coefficient for model 2.

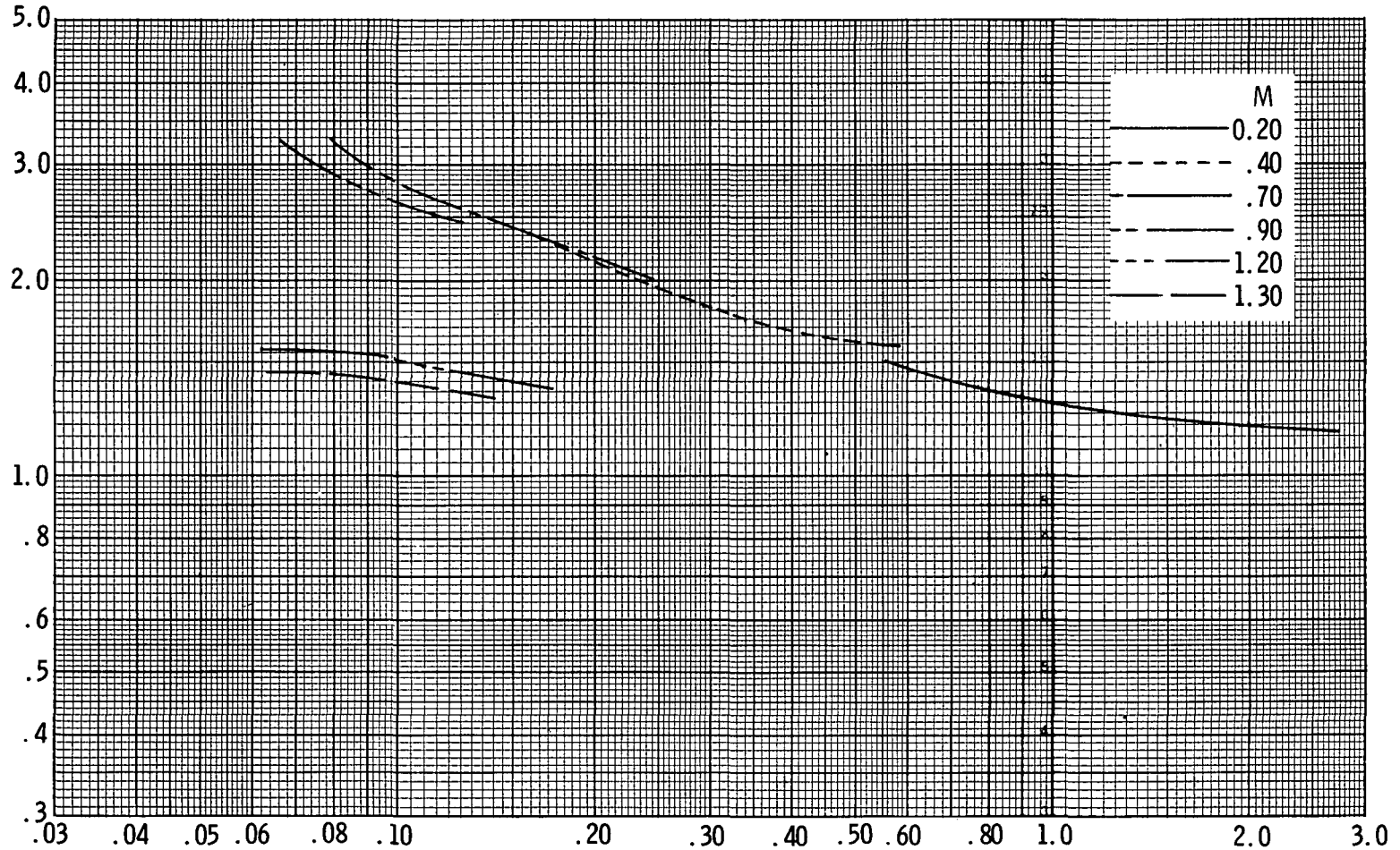

(b) $i_w = -2.04^o$.

Figure 19.- Continued.

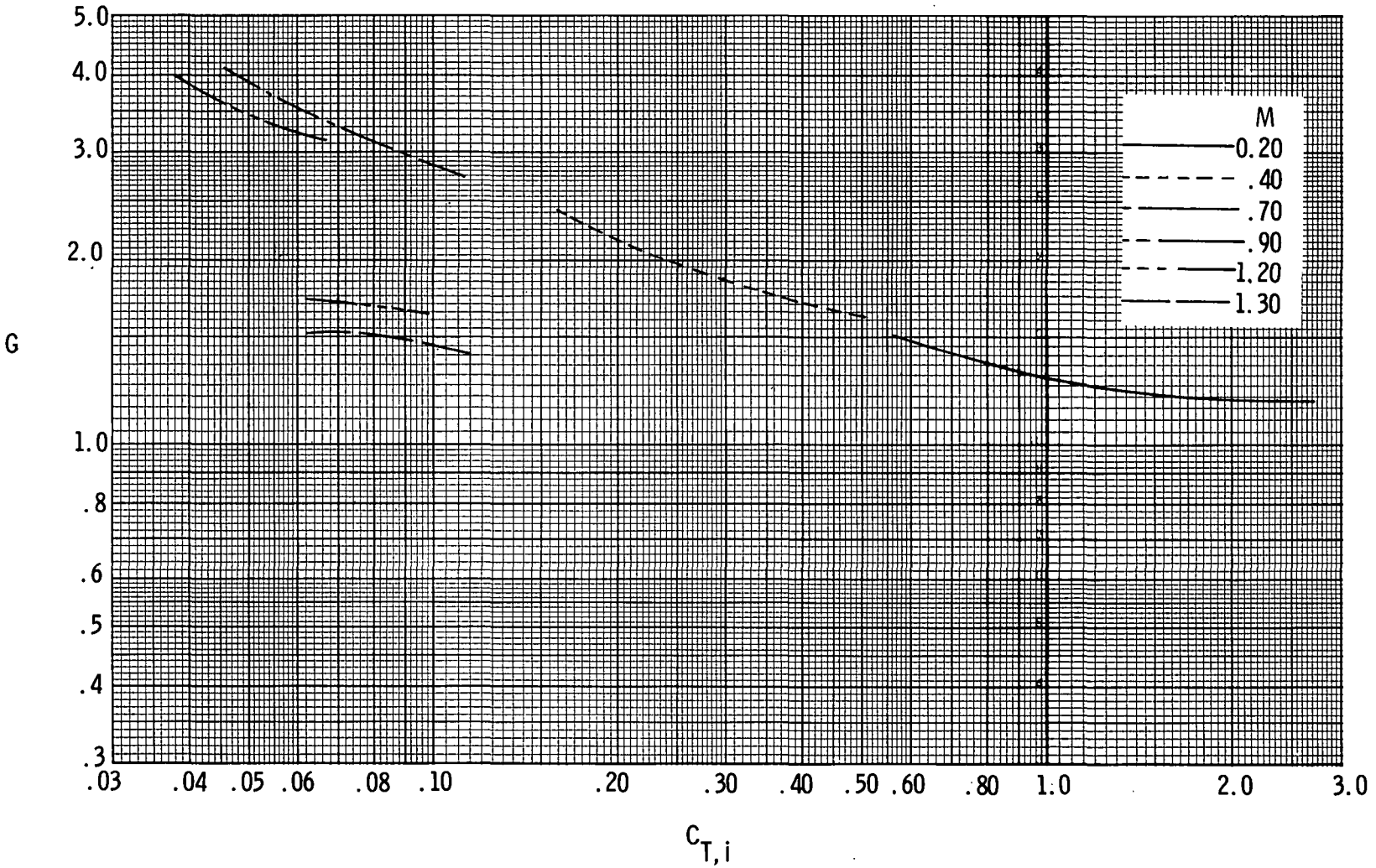

(c) $i_w = -0.18^o$.

Figure 19.- Concluded.

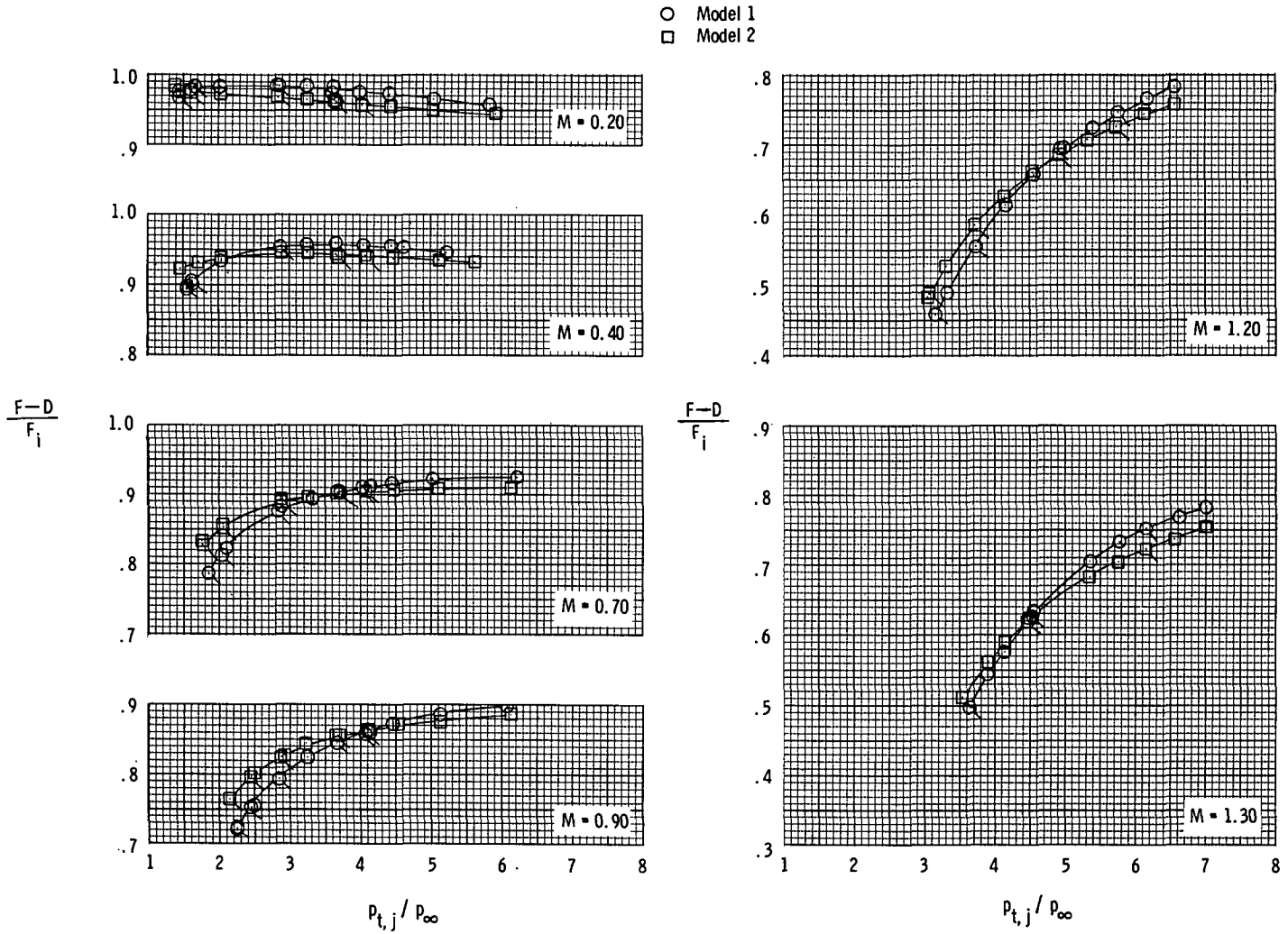

(a) $\delta_d = 0^o$.

Figure 20.- Variation of thrust-minus-drag ratio with jet total-pressure ratio for models 1 and 2 with wings off. Symbols with ticks represent values at decreasing jet total-pressure ratio.

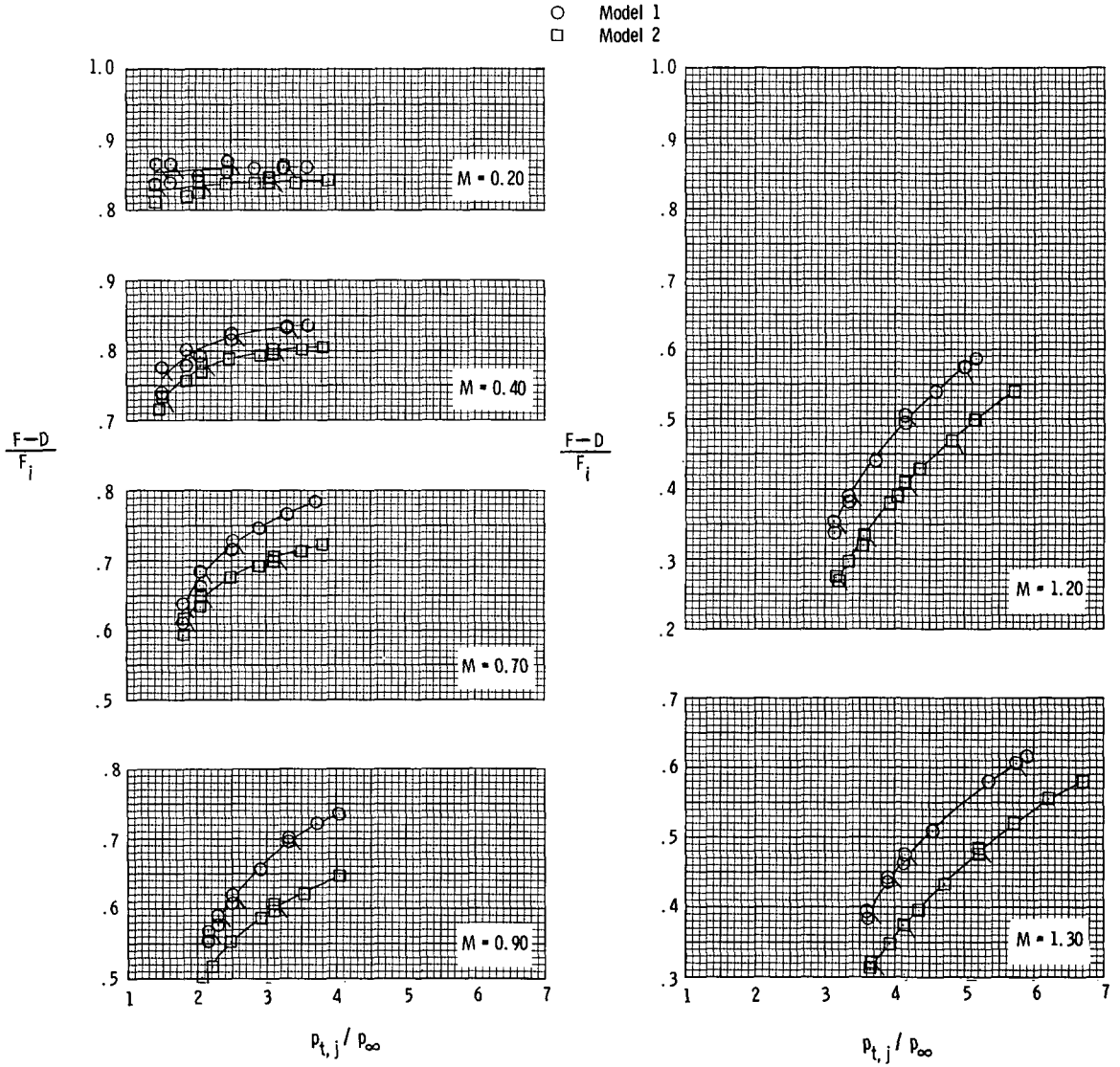

(b) $\delta_d = 30^o$.

Figure 20.- Concluded.

NATIONAL AERONAUTICS AND SPACE ADMISTRATION
WASHINGTON, D.C. 20546

OFFICIAL BUSINESS
PENALTY FOR PRIVATE USE $300

FIRST CLASS MAIL

POSTAGE AND FEES PAID
NATIONAL AERONAUTICS AND
SPACE ADMINISTRATION

U.S.MAIL

POSTMASTER: If Undeliverable (Section 1
Postal Manual) Do Not Ret

"The aeronautical and space activities of the United States shall be conducted so as to contribute . . . to the expansion of human knowledge of phenomena in the atmosphere and space. The Administration shall provide for the widest practicable and appropriate dissemination of information concerning its activities and the results thereof."

—NATIONAL AERONAUTICS AND SPACE ACT OF 1958

NASA SCIENTIFIC AND TECHNICAL PUBLICATIONS

TECHNICAL REPORTS: Scientific and technical information considered important, complete, and a lasting contribution to existing knowledge.

TECHNICAL NOTES: Information less broad in scope but nevertheless of importance as a contribution to existing knowledge.

TECHNICAL MEMORANDUMS: Information receiving limited distribution because of preliminary data, security classification, or other reasons.

CONTRACTOR REPORTS: Scientific and technical information generated under a NASA contract or grant and considered an important contribution to existing knowledge.

TECHNICAL TRANSLATIONS: Information published in a foreign language considered to merit NASA distribution in English.

SPECIAL PUBLICATIONS: Information derived from or of value to NASA activities. Publications include conference proceedings, monographs, data compilations, handbooks, sourcebooks, and special bibliographies.

TECHNOLOGY UTILIZATION PUBLICATIONS: Information on technology used by NASA that may be of particular interest in commercial and other non-aerospace applications. Publications include Tech Briefs, Technology Utilization Reports and Technology Surveys.

Details on the availability of these publications may be obtained from:

SCIENTIFIC AND TECHNICAL INFORMATION OFFICE

NATIONAL AERONAUTICS AND SPACE ADMINISTRATION

Washington, D.C. 20546